2020

Experimental Evaluation of Medium-Voltage Cascode Gallium Nitride (GaN) Devices for Bidirectional DC–DC Converters

Salah Salem H. Alharbi
University of Denver

Recommended Citation

Experimental Evaluation of Medium-Voltage Cascode Gallium Nitride (GaN)

Devices for Bidirectional DC–DC Converters

A Dissertation

Presented to

the Faculty of the Daniel Felix Ritchie School of Engineering and Computer Science

University of Denver

In Partial Fulfillment

of the Requirements for the Degree

Doctor of Philosophy

by

Salah Salem H. Alharbi

August 2020

Advisor: Dr. Mohammad Matin

Author: Salah Salem H. Alharbi
Title: Experimental Evaluation of Medium-Voltage Cascode Gallium Nitride (GaN)
Devices for Bidirectional DC–DC Converters
Advisors: Dr. Mohammad Matin
Degree Date: August 2020

Abstract

As renewable energy sources, such as photovoltaic (PV) cells and wind turbines, are rapidly implemented in DC microgrids, energy storage systems play an increasingly significant role in ensuring uninterrupted power supply and in supporting the reliability and stability of microgrid operations. Power electronics, especially bidirectional DC–DC converters, are essential parts in distributed energy storage and alternative energy systems because of their grid synchronization, DC power management, and bidirectional power flow capabilities. While there is increasing demand for more efficient, compact, and reliable power converters in numerous applications, most existing power converters are hindered by traditional silicon (Si) based semiconductors, which are reaching their theoretical and material limits as there is an insignificant possibility for further improvements. Wide bandgap (WBG) semiconductors, such as gallium nitride (GaN) and silicon carbide (SiC), exhibit superior physical properties and demonstrate great potential for replacing conventional Si semiconductors with WBG technology, pushing the boundaries of power devices to handle higher switching frequencies, output power levels, blocking voltages, and operating temperatures. However, tradeoffs in switching performance and converter efficiency when substituting GaN devices for Si and SiC counterparts are not well defined, especially in a cascode configuration. Additional research with further de-

tailed investigation and analysis is necessitated for medium-voltage GaN devices in power converter applications. Therefore, the objective of this research is to experimentally investigate the impact of emerging 650/900 V cascode GaN switching devices on bidirectional DC–DC converters that are suitable for energy storage and distributed renewable energy systems. Dynamic characteristics of Si, SiC, and cascode GaN power devices are examined through the double-pulse test (DPT) at different gate resistance values, device currents, and DC-bus voltages. Furthermore, the switching behavior and energy loss as well as the rate of voltage and current changes over the time are studied and analyzed at different operating conditions. A 500 W experimental converter prototype is designed and implemented to validate the benefits of cascode GaN devices on the converter operation and performance. Comprehensive analysis of the power losses and efficiency improvements for Si- based, SiC-based, and GaN-based converters are performed and evaluated as the switching frequency, working temperature, and output power level are increased. The experimental results reveal a significant improvement in switching performance and energy efficiency from cascode GaN power devices used in the bidirectional converters.

Acknowledgements

Table of Contents

List of Figures

ix

List of Tables

Chapter 1

Introduction

This chapter presents the background and challenges of bidirectional DC–DC power converters, especially for energy storage elements used in DC microgrids. Wide bandgap (WBG) semiconductor technology is examined in detail, with a discussion of its major advantages and its great benefits for power electric converters. It also addresses the research motivation and objective to perceive the importance of this dissertation. The main contributions are highlighted to identify this dissertation's originality, which is followed by the scope and outline of the research.

1.1   Research Background and Challenges

As concerns grow over climate changes and harmful environmental effects of burning fossil fuels, renewable energy sources such as wind turbines and solar panels are being deployed globally for sustainable and clean power generation systems [1–5]. Governments worldwide are taking aggressive actions to offset natural resource depletion, fossil fuel price instability, and electric power insecurity by in-

vesting in microgrid technologies [6–10]. Tremendous efforts have been devoted to merging DC microgrids into electric power distribution systems because they offer a significantly increased energy efficiency, reduced generation cost, and minimized system size compared with the AC microgrids [11–13]. The major benefits of DC microgrids are to increase the integration and penetration level of renewable sources as well as improve the reliability of electric grids in the distribution sector [14, 15]. Figure 1.1 presents a typical DC microgrid structure comprised of different distributed energy resources like small-scale wind turbines, PV arrays, fuel cells, energy storage elements, and plug-in hybrid electric vehicles (PHEVs), along with local loads and control devices connected to DC link through power electronics, as the voltage source inverter (VSI) linking the DC microgrid with the utility network [16, 17]. With the continuous increase in DC loads, such as laptops, computers, LED lights, and telecommunication centers, DC microgrids are considered as applicable and economic solutions for satisfying future smart energy demands since the most environmentally friendly distributed sources generate DC power [18, 19]. Therefore, DC microgrids are receiving growing interest both in academia and in practical power applications, resulting in extensive research for implementing microgrids in electric power systems.

The intermittency of distributed renewable generators poses crucial challenges in terms of the operation and control of DC microgrids [20–22]. Power fluctuations of renewable energy source cause instability in microgrid and inadequacy in accommodating continuously varying DC loads [23–27]. Among different distributed energy sources, energy storage systems such as batteries and ultracapacitors are essential parts in DC microgrids because they can effectively operate as a load or generator during charging or discharging mode, balancing the power flow
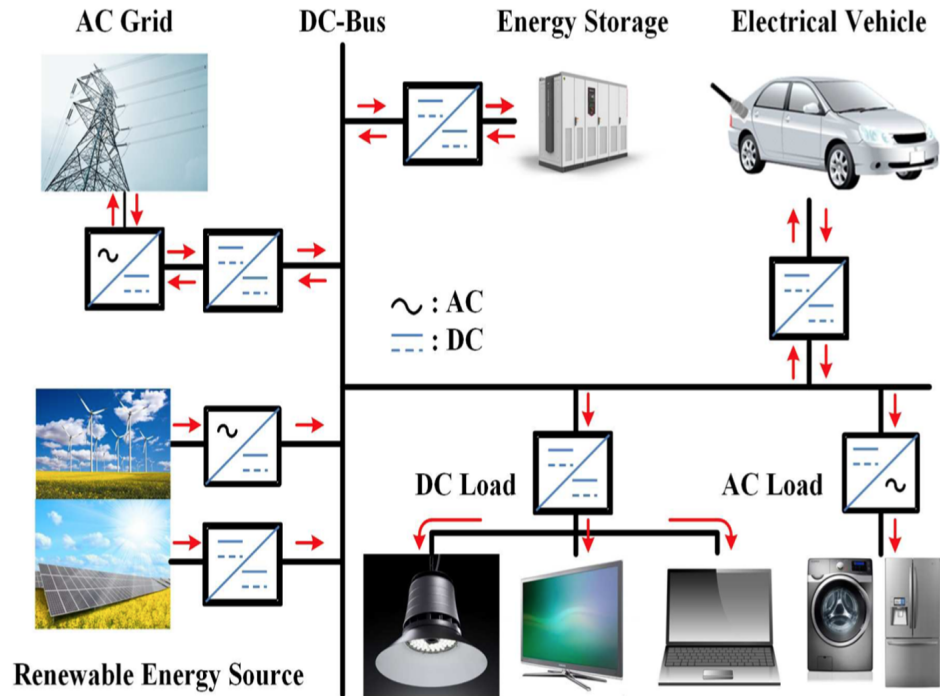
Figure 1.1: A typical DC microgrid system [16].

in the microgrid [28–30]. Energy storage elements are used to compensate the variability of alternative energy sources and maintain a smooth power flow to various DC loads [31–33]. They are also indispensable for energy management purposes and offering a backup power source for the DC microgrid when renewable energy sources are inadequate [23,34,35]. Batteries and ultra-capacitors improve the power quality of DC microgrid by operating as an uninterruptible power supply and enhancing the low voltage ride-through ability for distributed PV and wind power generation applications [36–39]. As a result, energy storage systems substantially support the DC microgrid operations in stability and reliability.

Power electronics, particularly bidirectional DC–DC power converters, play a pivotal role in interfacing energy storage systems with DC microgrids, where the power flow needs to be in both forward and reverse directions [5,40–42]. These con-

verters are not limited to energy storage elements but are also included in renewable energy systems, uninterruptable power supplies, electric vehicles, and other applications [43–46]. Based on the control systems, the bidirectional DC–DC converter operates as either a buck or boost type to regulate the current or voltage of the power system into a desired level. In terms of topology, bidirectional DC–DC converters are divided into two major categories, which are non-isolated and isolated configurations. Among those two topology configurations, transformer-less bidirectional converters are widely employed in DC microgrids due to their prominent advantages of increased efficiency, improved reliability, straightforward structure, uncomplicated control system, reduced size, and minimal cost [5, 47, 48].

However, these DC–DC bidirectional converters, especially buck-boost (half-bridge) power circuits, have major disadvantages of a limited voltage conversion ratio between input and output as well as a high voltage stress across switching devices leading to critical challenges in improving the reliability of the switches and the capability of the converter [5, 49–51]. Furthermore, most existing converters are suffering from intensive switching and conduction power losses under cruel operating conditions associated with power semiconductor devices, which are essential components of power electronics [5, 52–54]. Traditional silicon (Si) material is the most commonly semiconductor used in power switching devices [5]. The performance and efficiency of conventional bidirectional DC–DC converters are hindered by Si-based power devices, which are approaching their theoretical and physical limits [5, 27, 55–57]. Consequently, the restrictions of Si power switches are a rigid barrier to achieving major improvements in the converter efficiency and performance based on Si technology [5, 58].

1.2   Overview of Wide Bandgap Technology

Academic and industry researchers have devoted significant efforts and numerous resources to develop and fabricate alternative semiconductor materials with improved characteristics for next-generation power devices due to the limitations of Si devices and an acute global demand for power devices with higher operating capabilities [5, 59, 60]. Wide bandgap semiconductors, such as silicon carbide (SiC) and gallium nitride (GaN) offer superior material properties than conventional Si materials, enabling switching devices to operate effectively under harsh operating conditions [5, 61–63]. WGB materials offer outstanding physical properties such as a wider energy gap, better thermal conductivity, higher electron mobility, higher saturated drift velocity, and larger critical electric field [5, 64, 65]. The physical properties of different semiconductor materials are explained in Table 1.1.

Table 1.1: Key material properties of Si and WBG semiconductors [64, 65].

Material property	Unit	Si	6H-SiC	4H-SiC	GaN
Energy bandgap, E_g	[eV]	1.12	3.02	3.26	3.39
Thermal conductivity, λ	[W/cm·K]	1.5	4.9	4.9	1.3
Electron mobility, μ_n	[cm^2/ V·s]	1500	420	950	2000
Saturated drift velocity, v_{sat}	[$\times 10^7$ cm/s]	1	2	2	2.5
Critical electric field, E_c	[MV/cm]	0.23	2.5	2	3.8
Dielectric constant, ε_r	-	11.8	9.7	10	9

The higher saturation drift velocity and larger electron mobility of WBG materials allow power devices to operate at higher switching frequencies than comparable Si devices [66, 67]. WBG materials have better thermal conductivity, wider energy bandgap, and small intrinsic carrier concentrations. These features enable

them to sustain higher-operating temperatures without suffering excessive current leakage [68–70]. The wider energy bandgap and larger breakdown electric field of WGB materials permit power devices to perform more efficiently at high-blocking voltages. The higher electron mobility along with larger breakdown electric field of WBG materials yield power devices with much lower on-state resistance, contributing to a major reduction in the conduction loss. The considerable benefits of WBG materials enable power devices to work over a wide range of blocking voltages, junction temperatures, and switching frequencies with lower on-state resistance [71, 72]. These important operating characteristics of WBG devices significantly contribute to improved power density, reduced semiconductor loss, increased energy efficiency, decreased cool system and passive components, and minimize the size and cost of power converters. As a result, power converters with WBG semiconductor devices are the most promising solution to meet the growing demand for high-voltage, high-speed and high-temperature applications.

1.3   Dissertation Motivation and Objective

As discussed in the research background and challenge sub-sections, power electronics, especially bidirectional DC–DC converters in DC microgrid, are operationally limited by their Si-based devices and suffer from high voltage stress across these switching devices. Furthermore, these converters exhibit poor efficiency and low power density because of acute switching and conduction power losses from using Si devices at high-operating temperatures, high-blocking voltages, high-switching frequencies, and high-output power levels [58]. Since Si is indisputably approaching its theoretical and material limits, it would be very diffi-

cult to accomplish further improvements in Si-based converter efficiency and performance [58]. These issues pose critical challenges in meeting the high demand for more efficient, dense, compact, cost-effective, and reliable power converter for numerous applications.

Due to GaN superior physical properties, the GaN technology offers the most promising solution among other proposed ones for improving power electronic applications [5, 73, 74]. Although there is a limited research that evaluated 650 V cascode GaN power devices, most published works, such as [75, 76], have not comprehensively demonstrated the switching behavior of these devices at the medium-voltage level [5]. As previously mentioned, these works show inconsistent voltage level and device package, which play an important role in converter efficiency and performance due to different parasitic elements and gate circuit suitability [5]. Therefore, further investigations on 900/650 V cascode GaN-FETs used in power converters are needed to better understand the switching performance of these new devices and compared to existing Si switches at the same voltage rate within the same device package [5]. Additionally, none of the published research provides the necessary information and practical data to support using 900 V cascode GaN-FET devices integrated into power converters [5]. Although cascode GaN-FET devices were studied by some researchers, the tradeoffs in the switching performance, efficiency, size, and cost of the GaN-based converters are still unclear in the literature [5].

This research attempts to close this knowledge gap by comprehensively studying and evaluating 650 and 900 V GaN-FET devices integrated into the bidirectional DC–DC converters [5]. To facilitate this important research, Transphorm provided a sample of new 900 V cascode GaN-FET (TP90H050WS) in the TO-247 pack-

age [5]. This device is not yet commercially available, but it is expected to be released before the end of 2020 [5]. The motivation for this research is to provide the essential information and practical tools for incorporating cascode GaN-FET devices into power converters [5]. It includes a comprehensive dynamic characterization of GaN-FET devices, a comparative investigation on crucial impact factors in GaN-FET switching behavior compared to Si and SiC devices, and an evaluation of GaN-based converter performance under harsh operating conditions [5]. The aim is to obtain an efficient, uncomplicated, and cost-effective method to enhance the energy efficiency and switching operation of bidirectional DC–DC converters based on GaN technology. To achieve this aim, the effect of cascode GaN power devices on the converter's switching behavior and overall efficiency is tested and validated through experimental research and results.

1.4 Dissertation Scope, Contribution, and Outline

To realize the impacts of emerging cascode GaN-FET devices, GaN-based converters are designed and compared to widely used Si-based converters under identical switching speeds, working temperatures, blocking voltages, and output power levels [27]. This dissertation focuses particularly on cascode GaN power devices with blocking voltages of 650 and 900 V because these medium-voltage GaN devices are required by most distributed renewable sources, energy storage facilities, and electric vehicles in DC microgrids. The main contributions of this dissertation are identified as follows:

- A survey of the latest GaN power devices is carried out to understand their impact on converter performance, considering the blocking voltage, device package, and market availability of these devices.

- The methodology and tools are presented for experimentally evaluating both the switching characteristics of GaN-FETs in a cascode structure and the GaN-based converter.

- The switching behavior of cascode GaN-FETs is evaluated through the double-pulse test (DPT) to find the well-suited gate-driver circuit and gate-source voltage to these devices for achieving optimal switching performance.

- The effect of gate resistance in the control of cascode GaN-FETs during the turn-on and turn-off times is experimentally assessed at different operating points.

- The dynamic switching characterization of GaN devices is compared with commonly used Si devices under the same gate requirements to assess the switching performance when using cascode GaN-FETs.

- The rate of voltage (dv/dt) and current (di/dt) change over time along the energy loss in turn-on and turn-off events in GaN devices are experimentally tested and measured as the gate resistance, device current, and input voltage are increased to study their effects on the switching performance.

- The impact of GaN-FETs in a cascode configuration on converter level are experimentally evaluated at harsh operating conditions.

- A detailed analysis of power losses from the power devices, gate, passive compounds, and others loss in the circuit is conducted to obtain the highest converter efficiency.

- An accurate method of measuring the energy efficiency is demonstrated and justified to quantify the converter improvement based on the GaN technology.

To satisfy the objectives, this dissertation is structured as follows. Chapter 2 presents outstanding material properties of WBG semiconductor technology, especially GaN devices in a cascode configuration, as well as expresses appealing potential for replacing conventional Si counterparts. The relevant literature review of prior research along with the conducted survey of GaN power devices are demonstrated in this chapter. The unique advantages and main challenges of GaN devices are described while the GaN potential applications and markets are pointed out to provide a clear perspective of the merits of GaN technology.

In chapter 3, the DPT circuit is experimentally built in order to study the switching behavior of different power devices during turn-off and turn-on transitions. The switching energy losses and the rate of dv/dt and di/dt are computed and measured at different operating conditions. The power dissipation generated from semiconductor switching devices is calculated to evaluate the converter performance and efficiency at different operating conditions. This chapter also investigates optimal gate-source voltage, gate-driver circuit, and gate resistance for GaN power devices since these devices are most crucial elements in how power converter applications.

Chapter 4 assesses the switching characteristic and performance for cascode GaN-FETs and Si-MOSFET devices used in power converters. It also compares the dynamic characteristics of examined power devices in terms of switching per-

formance and energy loss. To realize the benefits of GaN devices, switching energy losses are determined at different gate resistance values, switch currents, junction temperatures, and DC-bus voltages. The experimental results are analyzed between the two GaN and Si power devices.

In chapter 5, the dynamic behavior investigation of Si-IGBT and SiC-MOSFET switches in terms of switching performance and energy loss is performed through the DPT circuit. The impacts of high gate resistance, switch current, and junction temperature, and DC-bus voltage on the switching behavior of the two tested devices are examined during the turn-on and turn-off events in order to integrate the most suitable semiconductor devices for high-power and high-switching converter applications. The experimental outcomes are assessed and compared between the two devices.

Chapter 6 provides the background description and state-of-the-art of bidirectional DC–DC converters to expound this research and its novelty. It starts with describing bidirectional DC–DC power converters, including isolated and non-isolated bidirectional topologies. Because of remarkable advantages and wide implementation of non-isolated bidirectional topologies in medium-voltage applications, this research fundamentally focuses on the non-isolated converters. Different topologies of non-isolated bidirectional DC–DC converters are evaluated and compared to determine a more compatible choice with power converters in DC microgrids, where energy storage and distributed renewable energy systems are widely implemented. The operation and analysis of the bidirectional DC–DC converter are illustrated in this chapter along with design considerations.

In chapter 7, the effects of merging various new semiconductor devices into power converters is aimed to be demonstrated at harsh operating conditions for

11

medium-voltage systems. The switching performance of cascode GaN-FETs, SiC-MOSFETs, and Si-MOSFETs implemented in the bidirectional buck-boost converter is tested with the same power converter layout. The semiconductor losses, including conduction and switching losses, occurred in power devices are calculated and compared as a function of increasing operating temperature and switching frequency. The GaN based converter is experimentally evaluated at various operating conditions and compared its performance to Si-based and SiC-based converters in terms of total power loss, overall efficiency, and cost in order to realize the benefits of using GaN technology.

Finally, chapter 8 summarizes the prime conclusions of this dissertation as well as presents an outlook for potential future work.

Chapter 2

GaN Semiconductor Technology

This chapter briefly introduces the unique properties of WBG semiconductor technology, particularly cascode GaN devices, showing great potential for replacing conventional Si counterparts. The literature review of prior research as well as the survey of GaN power devices are highlighted in this chapter. The remarkable advantages and major challenges of GaN devices are described and GaN potential applications are presented.

2.1   Wide Bandgap (WBG) Semiconductors

Recently, the benefits of WBG power devices have been well-promoted for power conversion systems. WBG-based power switches show great potential for enabling and implementing numerous applications that were previously impossible in the real-world [77–79]. WBG semiconductors exhibit superior material properties such as wider bandgap energy, higher saturated drift velocity, larger electron mobility, higher breakdown electric field, and reasonably better thermal conductiv-

ity [27]. These remarkable physical properties are enabling switching devices to work efficiently and effectively at high-blocking voltages, high-switching speeds, and high-operating temperatures [63, 80, 81]. Figure 2.1 presents the key electrical properties of the GaN material compared with SiC and Si materials [82, 83]. Thus, merging GaN semiconductor devices into power converters shows tremendous potentials in terms of improving power density and energy efficiency as well as reducing the cost and size power conversion applications.
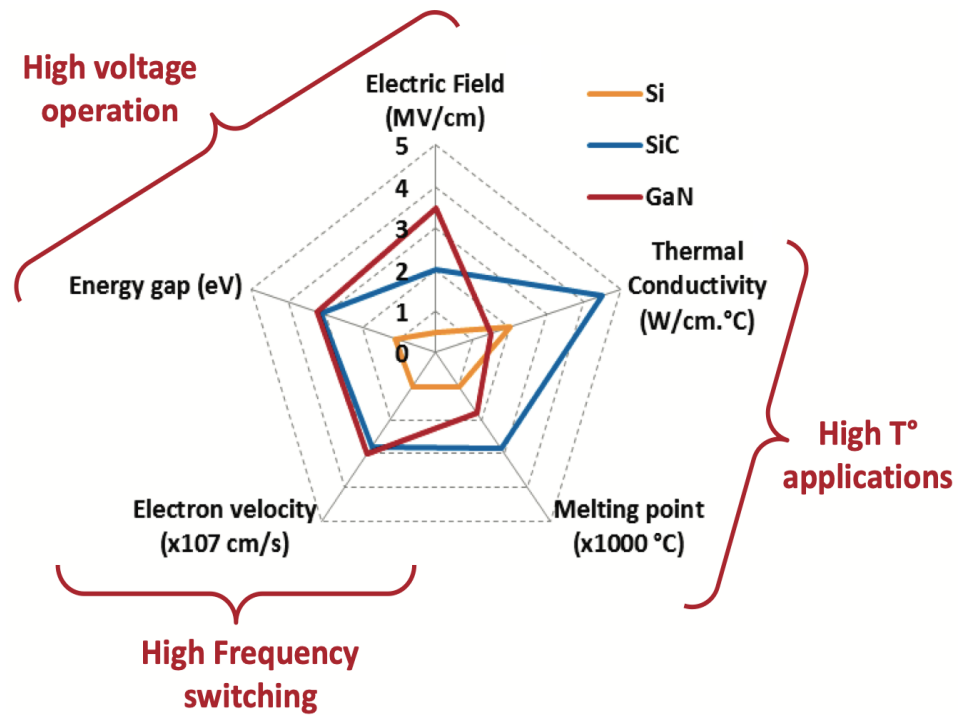
Figure 2.1: A comparative summary of Si, SiC, and GaN material properties [82].

2.2 Literature Review of GaN Power Devices

Due to the superior physical properties of GaN, worldwide academic and industrial researchers have spent considerable effort and resources studying GaN power

devices. It is essential to acknowledge the characteristics and the challenges of GaN power devices before integrating them into power electronics. A number of review and survey papers such as [84–86] reported on the characteristics of different WBG power devices, containing major advantages and design challenges. These papers demonstrated the WBG material properties and presented their great potential for power conversion system, identifying considerable benefits along with critical challenges. The background of GaN devices in power converters was described in [87–90]. These studies illustrate the recent development of GaN power devices and show how these devices can improve power converters.

Besides the background, characterization, and challenges of WBG technology, various prior publications [91–93] evaluated GaN power devices in terms of physical materials, device package, and gate drive circuits. For instance [94, 95], provide a detailed switching evaluation and converter assessment at different switching frequencies, operating temperatures, and output power levels. Other studies [96–98] covered gate driver requirements and switching performance for each technology as well as evaluated the power density and coveter efficiency.

Recent research [99–102] focused on the implementations of high-voltage GaN-FETs in a cascode configuration because of their highest operating capabilities for power converter applications. For example, different cascode GaN-FETs produced by Transphorm were integrated into a single-phase transformer-less PV inverter under hard-switching performance and the results showed that the inverter reached a peak efficiency of 99.18% at 1.3k W [103]. Transphorm also built and tested a 1 kW pole power-factor-correction converter with 99% efficiency at a switching frequency of 50 kHz [104].

Several studies [105–107] reported on cascode GaN-FET devices used in LLC resonant and buck converters with soft-switching techniques. Other published works [108–110] reported on implementing Transphorm cascode GaN-FET devices into an uninterruptible power supply (UPS), an isolated switched capacitor DC–DC converter, and a switched capacitor three-port inverter application. The comparison between GaN, SiC, and Si devices presented in these papers show a lack of consistency in voltage level and device package, which are critical factors on converter efficiency and performance due to the difference of parasitic element between these devices.

To accurately measure energy efficiency and evaluate converter performance, the design and prototype of WGB- and Si-based converters must be considered due to the layout effect along with parasitic inductance and capacitance in the power circuit. Additionally, the gate circuit plays a significant role in driving and controlling power devices, which can greatly impact converter performance in terms of switching behavior and energy loss.

2.3   GaN Power Devices

GaN power devices are gaining considerable attention for next-generation power electronic converters because these devices exhibit physical properties superior to those of traditional Si materials, providing great potential for power conversion systems [5]. As semiconductor switching devices are the main elements of power converters, it is important to understand their switching characteristics and performance in order to employ cascode GaN devices in converter designs [5].

2.3.1 Vertical and Lateral GaN Devices

Compared to other WBG semiconductors, GaN-based power devices possess faster switching speeds and lower semiconductor losses, making them attractive to the energy industry for high-frequency, high-density, high-efficiency, and high-reliability converter applications [111,112]. The lateral GaN heterojunction field effect transistor (HFET), which is called the high-electron mobility transistor (HEMT), was lately released and is commercially available at voltage levels above 600 V. GaN HEMT devices are classified into vertical and lateral structures. Vertical GaN HEMTs have yet to be commercially produced; therefore, most current literature focuses on GaN HEMTs in a lateral configuration [96, 113]. The depletion-mode of GaN HEMT is normally-on so it can be difficult to employ these devices in power conversion systems where normally-off switches are preferred due to operational safety and gate-driver circuitry simplicity. However, a cascode structure is adopted to overcome this issue, resulting in a normally-off device [114, 115]. This dissertation focuses on GaN HEMTs in a cascode configuration as there is already ongoing research on developing normally-off lateral GaN HEMTs through various approaches.

2.3.2 Depletion-Mode and Enhancement-Mode GaN Devices

Based on different structures of the gate terminal, GaN HEMTs can be fabricated and constructed in depletion-mode or enhancement-mode, which is determined by the internal material structure and layout during the production process [5, 116, 117]. Figure 2.2 shows different modes of GaN devices, which are depletion-mode and enhancement-mode [5, 118]. Depletion-mode of GaN HEMTs

17

is normally-on so it can be difficult to incorporate these devices into high-power conversion systems where normally-off switches are more suitable due to operational safety considerations and gate-driver circuitry simplicity [5]. However, the cascode structure, which is basically adding another transistor in a series way, overcomes this issue, resulting in a normally-off device [5]. Though this structure has the disadvantage of increasing on-state resistance, this issue becomes insignificant at high-voltage levels since the on-resistance of the high-voltage GaN device is not greatly affected through combining a low-voltage Si transistor into the device [5].
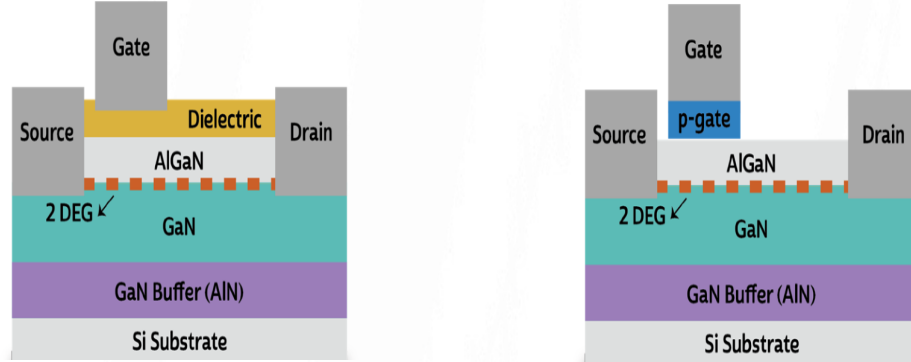
Figure 2.2: The cascode depletion-mode (left) and enhancement-mode (right) of GaN power devices [118].

The cascode GaN-FET consists of a low-voltage normally-off Si-MOSFET along with a high-voltage normally-on GaN-HEMT in a series configuration [5, 27]. The cascode GaN device structure is shown in Figure 2.3 [5]. The combination of Si-MOSFET and GaN-HEMT is packaged in a cascode configuration and acts as one single transistor, which is called a cascode GaN-FET device [5]. The two switching devices are linked together so that the output drain-source voltage of the Si-MOSFET controls the input gate-source voltage of the GaN-HEMT [5]. In this package, the current flows through the Si-MOSFET and GaN-HEMT during the

on-state event while the blocking voltage is shared between the two devices during the off-state event [5]. The main advantages of cascode GaN-FETs are very low reverse recovery charge and gate charge along with a small crossover loss [5]. Among others GaN switches, these devices are more robust and reliable in terms of a wide gate safety margin, high-transient over-voltage capability, and intrinsic lifetime test [5]. Operationally, cascode GaN-FETs offer higher safety and simpler gate-driver circuit along with lower ringing behavior of the switching device [5].
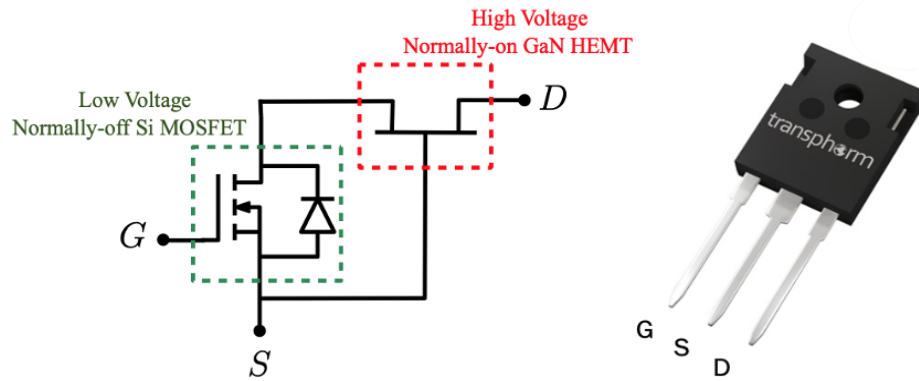
Figure 2.3: GaN-HEMT power device in a cascode configuration.

On the other hand, GaN-HEMTs in enhancement-mode feature normally-off devices without the additional transistor or cascode structure. They exhibit a lower on-state resistance and zero reverse recovery loss, causing better switching performance. The main disadvantages of the enhancement-mode of GaN HEMTs are that these devices require very complicated gate-driver circuits and contain a low threshold voltage, making the devices very susceptible to ringing effect. Due to these issues, GaN-HEMTs in the enhancement-mode are undesirable for high-power DC–DC converter applications. Therefore, this research focuses on cascode GaN-FETs since they offer the highest blocking voltage rates in different packages that are currently available on the market.

2.4 Survey of GaN Devices

Due to unique material advantages and high operating capabilities of GaN semiconductors, GaN-based power devices have been attracting a considerable deal of interest in power converter applications. Worldwide academic and industrial researchers are actively involved in conducting tremendous research and effort on the development of GaN technology. Figure 2.4 describes GaN power device landscape, including a large number of government laboratories and universities as well as main GaN semiconductor manufacturers and GaN integrators. The first commercial GaN transistors with a maximum voltage level of 200 V were released by Efficient Power Conversion Corporation (EPC) in 2010. Intensive work and research were conducted on implementing these GaN devices in point-of-load, power-amplifier, and radio-frequency applications [119, 120]. Multiple semiconductor manufacturers have announced new GaN power devices including MicroGaN, GaN Systems, Transphorm, Nexperia, HRL Laboratories, NXP semiconductor, Panasonic, Fujitsu, International Rectifier, STMicroelectronics, Microsemi, On Semiconductor, Infineon, Texas Instruments, and VisIC.

A detailed survey of GaN power devices is carried out to find the most compatible GaN devices for high operating applications. The core factors that contribute to this survey are commercially available GaN power devices, voltage rating, current rating, and device packaging. Table 2.1 summaries the existing semiconductor manufacturers that are continuously producing commercially available GaN power devices.

GaN System and Transphorm are gaining significant attentions for high operating applications because they are the only two semiconductor manufacturers

20
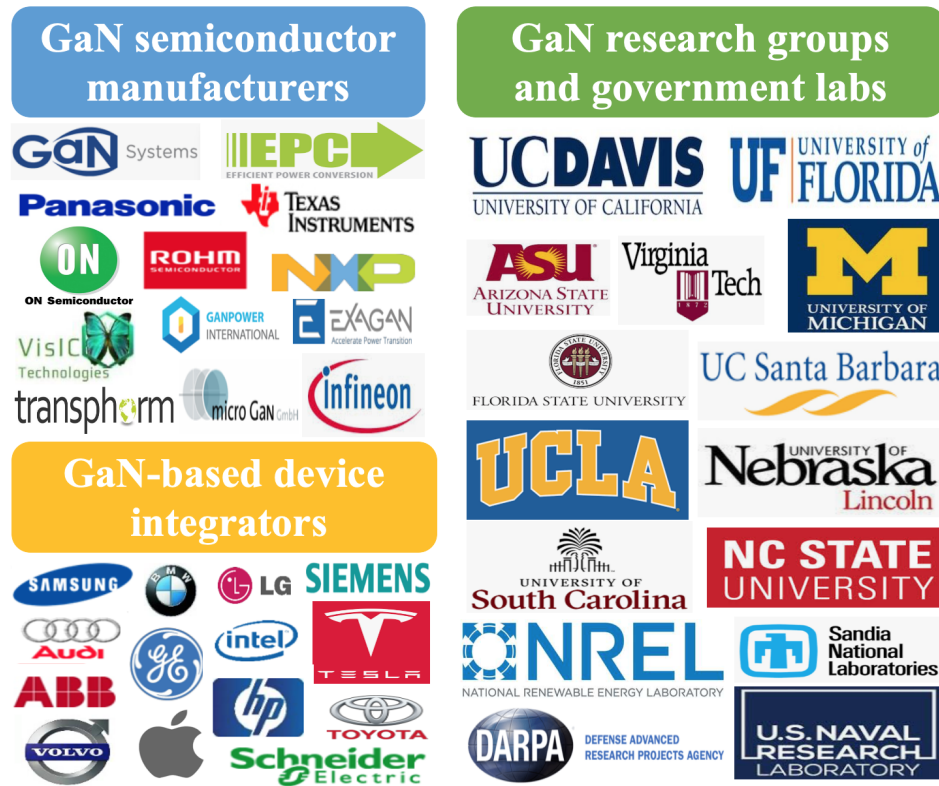
Figure 2.4: GaN power device landscape.

that continuously manufacture above 600 V GaN power devices. Among other GaN devices, the GaN-field effect transistor (FET) in a cascode structure, manufactured by Transphorm, is becoming increasingly attractive for power electronic applications. Transphorm is the only vender manufacturing the highest-voltage GaN power devices with the most commonly used device packages, which are 220 and 247 transistor outlines (TO). The main advantages of these cascode GaN-FETs are higher switching frequency, smaller on-state resistance value, lower reverse recovery charge, and smaller leakage current [72]. The GaN-FET switch in a cascode structure is composed of a low-voltage normally-off Si Metal Oxide Semiconductor Field Effect Transistor (MOSFET) and a high-voltage normally-on GaN High Electron Mobility Transistor (HEMT) in a series configuration [27]. Re-

cently, Transphorm released 650 V cascode GaN-FETs with different high current rates that feature higher operating capability, lower gate charge, smaller crossover loss, and more suitable device package with simple gate driving requirements. Transphorm is expected to release a new 900 V cascode GaN-FETs with TO-247 packaging in the beginning of 2020. As mentioned previously, the GaN HEMT devices are classified into vertical and lateral configurations. Since vertical GaN HEMTs have yet to be produced on a commercial level, this research focuses on GaN HEMTs in a lateral structure.

Table 2.1: The survey of commercially available GaN power devices.

Manufacturer	Voltage rating (V)	Current rating (A)	Package
Transphorm	600, 650, 900	6.5, 9, 15, 16, 17, 20, 25, 27, 34, 35, 36, 46.5, 47.2, 50	TO-220-3, TO-247-3, Power DFN
On Semiconductor	600	9, 17	TO-220-3
Panasonic	600	13, 26	DFN-8
Nexperia USA Inc.	650	34.5	TO-247-3
Infineon Techologies	600	12.5, 15, 31	PG-DSO-20, PG-HSOF-8, PG-LSON-8
EPC	15, 30, 40, 60, 65, 80, 100, 150, 200	1, 2, 6, 10, 18, 22, 31, 34, 48, 53, 60, 90	Die
GaN Systems	100, 650	3.5, 7.5, 8, 11, 15, 22.5, 30, 38, 60, 90	Die, PDFN-6, GaNPX

2.5   GaN Power Devices Applications and Markets

Due to outstanding material properties of WBG devices, engineers and designers are attracted to adopt GaN and SiC devices into power electronics and system designs to achieve next-level improvements in converter performance and system level [121]. Figure 2.5 schematically points out main potential applications of GaN and SiC switching devices utilized in power converters at high, medium, low voltage ranges [122]. Although GaN-based power devices theoretically exhibit better performance than Si and SiC counterparts, the lack of high-quality free-standing GaN layers hinders the rapid development of GaN switches with higher voltage levels. Thus, GaN power devices are being tailored for low-to-medium voltage power electronics.

As the market reported recently by numerous semiconductor manufacturers and analysts, GaN switching devices are more suitable for the low voltage range from 200 up to 600 V, which contains a big number of the consumer device electronics, such as power correction factors (PCFs), power supplies, and audio-amplifiers [123]. In the high voltage range above 1.2 kV, SiC switching devices remain so far the desirable choice for electric grids, rail transportations, and industrial applications, owing to the excellent crystalline material quality and device performance reliability. The medium voltage range, especially between 600 and 900V, is considered to crucially strategic because it covers a wide scale of power converters for energy storage, electric vehicle/hybrid electric vehicle (EV/HEV) applications, and distributed renewable energy systems. Due to the rapid development and increased availability of GaN devices above 600 V in the market, GaN power switches are highly expected to be in competition and coexistence with SiC and Si counterparts

in this medium voltage range. Therefore, this dissertation is focusing on the GaN devices at the medium voltage level.
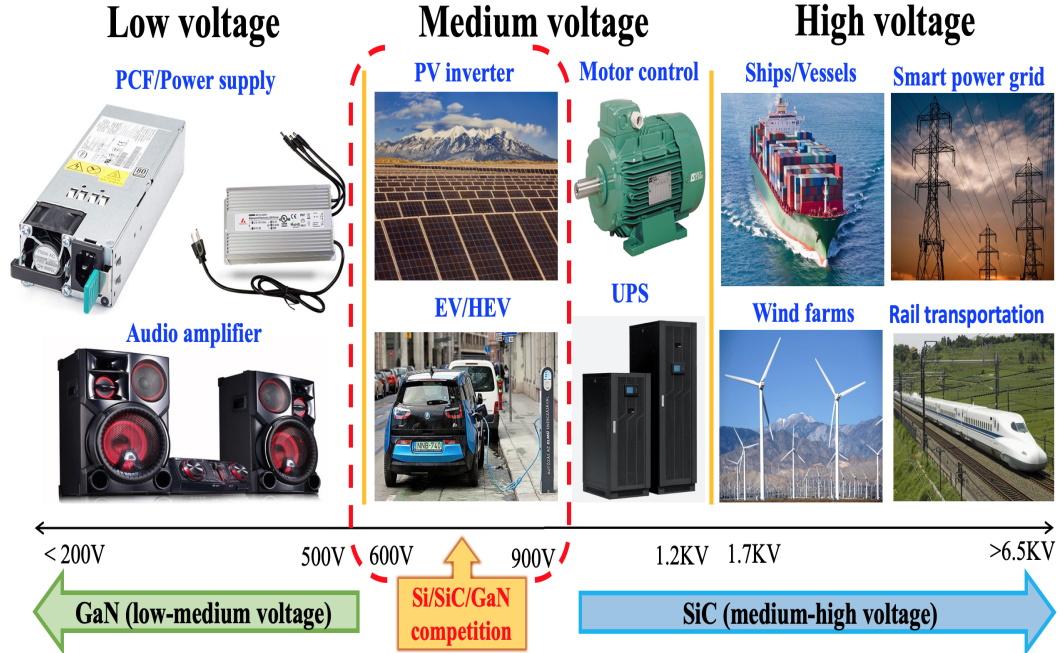
Figure 2.5: Key potential applications of GaN and SiC devices used in power converters as a function of voltage range [122].

Despite of the GaN physical quality and long-term reliability, GaN devices are becoming increasingly integrated into high-power and high-speed converters due to their significant operating capabilities, leading to improved energy conversion system. Figure 2.6 is envisaged the expected trajectory for GaN switching transistor market, which is anticipated to exceed $450 million US dollars by 2022 [124]. Obviously, the adaptation of GaN power devices is significantly going to be widespread in various power converter applications, such as power supply, EV/HEV, wireless and data communication, and uninterruptible power supply (UPS) systems. The high operating capabilities of GaN devices provide considerable potential for improving power converters in terms of increase efficiency and

enhanced power density along with reduced size and minimized cost. Recently, Apple and Tesla have recently announced that they are incorporating GaN semiconductors in order to achieve more efficient, compact, and robust features in their new products. Consequently, it is very promising for GaN devices to be widely adopted and implemented in high-speed and high-power conversion systems in the future.
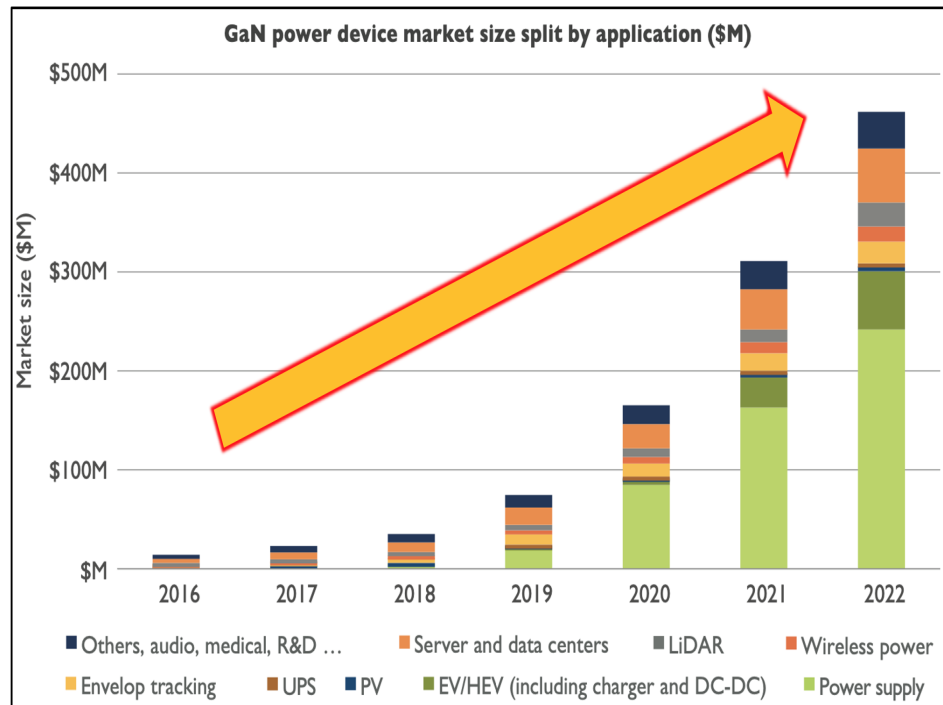
Figure 2.6: The growth of GaN power device market [124].

2.6 Power Device Comparison

The electrical characteristic and switching behavior of power devices play a significant role in the conversion system since semiconductor switching devices are major elements in power converter electronics [5]. GaN and SiC power de-

vices are the most mature WBG semiconductors and they are well established and commercially available [5]. These devices can withstand high operating temperatures and switching frequencies, allowing for smaller cooling systems and passive components [5, 58]. They also exhibit lower on-state resistance, leading to reduce conduction loss [5,58]. In order to investigate the effect of various semiconductor switching devices on the converter level, cascode GaN-FET, SiC-MOSFET, Si-IGBT, Si-MOSFET are integrated individually into the power converter to compare and assess their performance in terms of switching behavior and energy efficiency [5,58].

	Cascode GaN-FET	Si MOSFET	SiC MOSFET	Si IGBT
	transphorm	infineon	CREE	International IOR Rectifier
Part number	TP90H050WS	IPW90R120C3	C3M0065090D	IRG4PF50WDPbF
Voltage & Current	900 V, 34 A	900 V, 36 A	900 V, 36 A	900 V, 51 A
On-state resistance/ Saturation voltage	50 mΩ (25°C)	120 mΩ (25°C)	65 mΩ (25°C)	2.25 V (25°C)
Device package	TO-247-3	TO-247-3	TO-247-3	TO-247-3

Figure 2.7: key parameters of implemented devices in the power converter.

Table 2.7 provides the key parameters of each semiconductor device employed in the converter performance comparison [5]. The aforementioned power devices are chosen based on their similarity in electrical characteristics and compatibility with the power converter operation [5,63]. The methodology that adopted for here is to have an equal comparison between different device technologies [5]. This can

be obtained by selecting the identical voltage rate and device package as well as the same on-state resistance and current rate for each device if it is possible [5]. Figure 2.8 illustrates the main factors for selecting the different power devices.
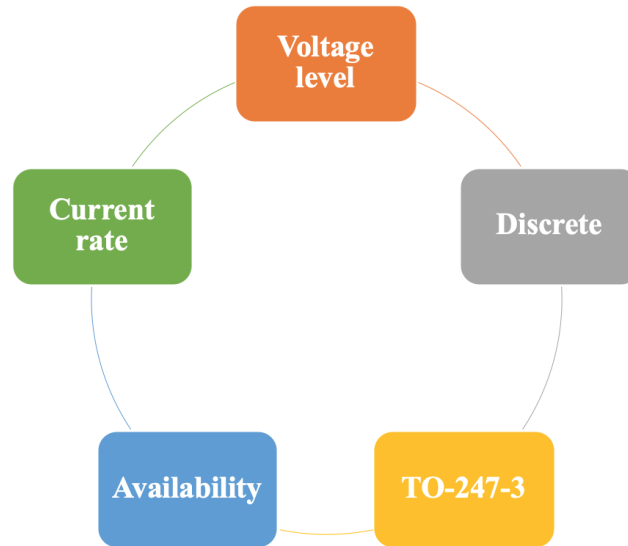
Figure 2.8: Main factors of power device selection.

2.7 Summary

In this chapter, unique material advantages and benefits of WBG semiconductors are demonstrated while the latest and current research on GaN power device is reviewed. The fundamental configurations and characteristics of GaN transistors are addressed, including vertical and lateral semiconductors and enhancement-mode as well as depletion-mode and enhancement-mode GaN devices. A survey of the recent GaN power devices is carried out and summarized to obtain the most suitable GaN devices for power converters along with their commercial status and specifications, considering the blocking voltage, device package, and market availability of these devices. Due high operating capabilities of GaN technology, GaN-

based power applications and markets are highlighted to express the increased level of GaN device adaptation and implementation in commercial and industrial sectors.

Chapter 3

Switching Performance Methodology and Characterization

A double-pulse test (DPT) is experimentally designed and constructed to obtain and examine the switching behavior of semiconductor devices during turn-on and turn-off transitions. The equipment and instruments used in DPT circuit are described with their specifications. In order to achieve accurate results, the procedure of aligning current and voltage waveforms is illustrated in this chapter. The switching energy losses along with the rate of voltage and current changes are calculated and measured at high operating conditions. The power loss resulted from semiconductor switching devices is determined to evaluate the converter performance and energy efficiency at different switching speeds, operating temperatures, and blocking voltages. The impacts of gate source voltage, gate driver circuit, and gate resistance on GaN power devices are investigated to find optimal gate parameters for a better power converter operation.

3.1   Double-Pulse Test (DPT) Circuit

A double-pulse test (DPT) circuit is a very essential step to characterize the switching behavior of various devices; therefore, this circuit is implemented to evaluate the switching performance during turn-on and turn-off transitions as well as determine the optimal gate requirements for each device [5]. Figure 3.1 simplifies the built DPT circuit for the switching behavior evaluation [5]. The turn-on and turn-off energy losses of each power device are obtained through the DPT circuit [5]. The double-pulse signal is generated from the DC dual-channel function generator (Keysight 33500B) to apply to the gate driver (Infineon 1EDI60I12AH) for controlling and turning on/off the device [5]. The width of each pulse plays a substantial role in controlling the current flowing in the inductive load [5]. Thus, the width and magnitude of first and second pulses should be set up very carefully in order to reach to the desired value of device current [5].
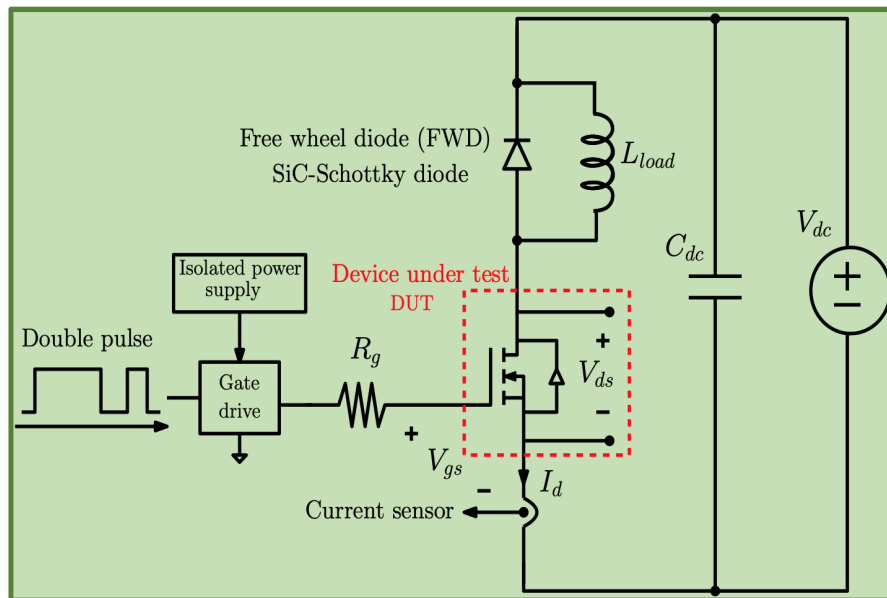
Figure 3.1: The DPT circuit schematic for switching evaluation.

30
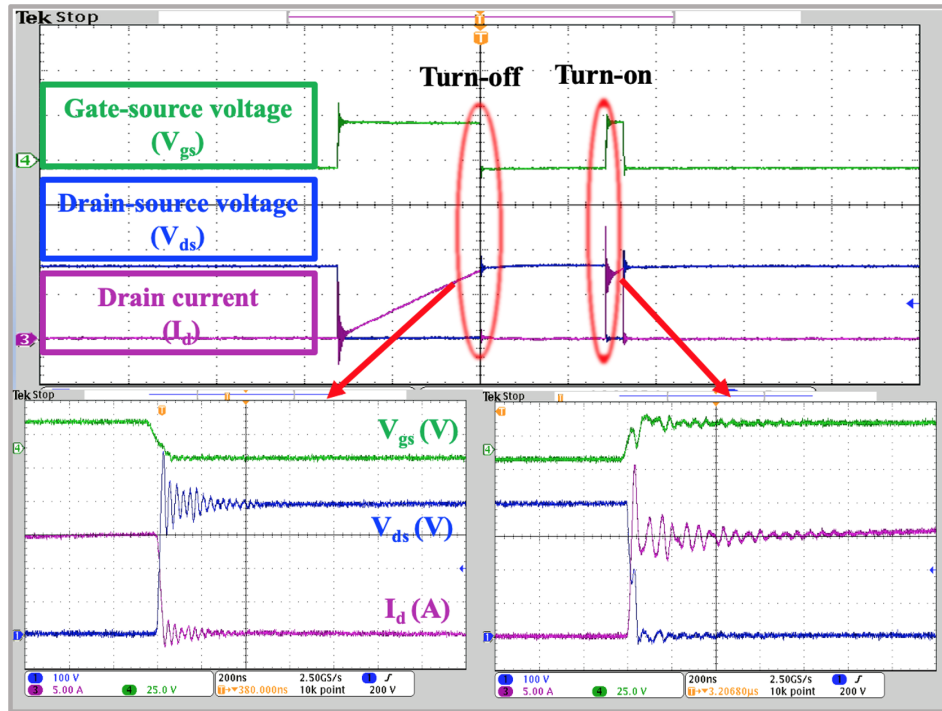
Figure 3.2: Drain-source voltage, gate-source voltage, and drain current waveforms under the double-pulse operation during the turn-off and turn-on transitions.

Figure 3.2 presents the expected waveforms of drain-source voltage, gate-source voltage, gate under the double-pulse operation during the turn-off and turn-on transitions [5]. These waveforms are captured by a 4-channl digital oscilloscope (Tektronix DPO3014) obtains waveform data and switching characteristics [5]. In the meantime, the high-voltage differential probes (Tektronix P5200A) are utilized to measure the drain-source voltage and gate-source voltages as the current sensor (Pearson 2877) is utilized to measure the current passing through the power device [5]. As the device is conducting, the inductor current is increased linearly as shown in Figure 3.2 [5]. This current is reached to the set-up current value once the device is turned-on at the end of the first pulse by applying negative gate-source voltage [5]. In the switching investigation, the turn-off behavior and energy loss
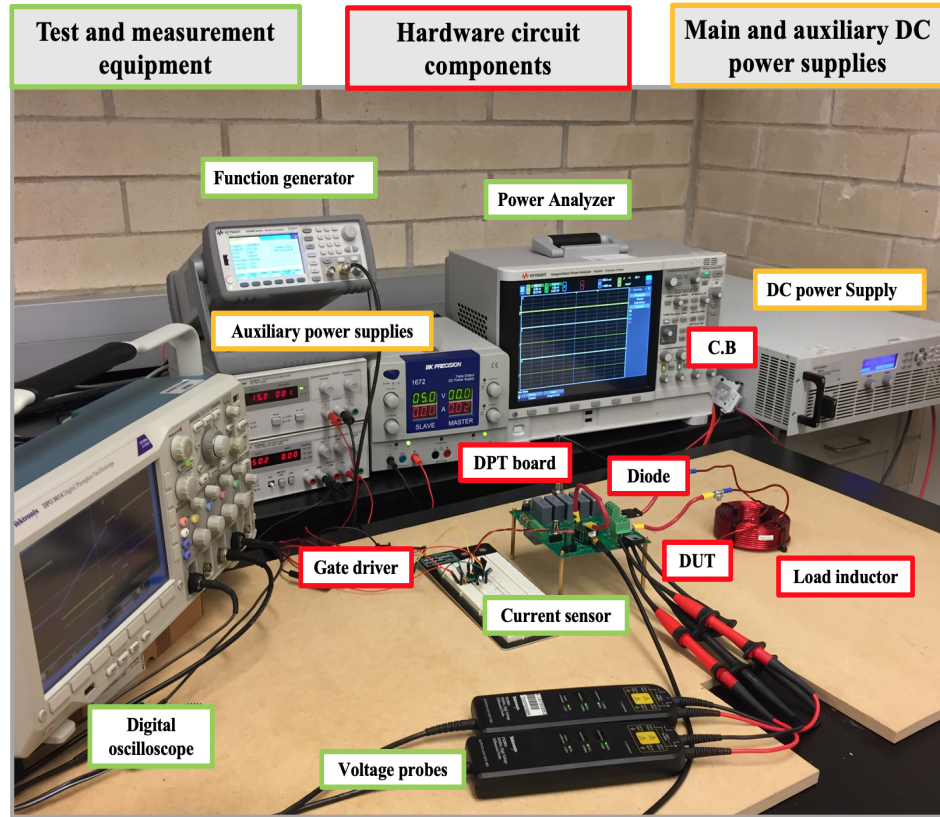
Figure 3.3: The experimental DPT circuit.

Table 3.1: Key equipment and instruments for the DPT circuit.

Component	Type/value	Deskew
DC-power supply (Keysight N8937A)	15 kW	–
Function generator (Keysight 33500B)	30 MHz, 2 channels	–
Inductive load (Air core)	450μH	–
DC capacitor (R75PR4100AA30K)	20μF	–
Digital oscilloscope (DPO3014)	100 MHz, 4 channels	–
High-voltage-differential probe (P5200A)	50 MHz, 50X/500X	11.6 ns
Pearson current sensor (2878)	1 Volt/Ampere +1/-0%	0 ns
Digital hot-plate magnetic (MS300)	up to 300°C	–

of each power device are specified at the end of the first pulse while the turn-on behavior and energy loss of each power device are identified at the beginning of the second pulse [5, 72].

3.2   Equipment and Instruments of DPT Circuit

The DPT components are presented to examine switching behavior of different power devices and compared their performance at different operating conditions [5]. Table 3.1 addresses the main equipment and instruments of DPT circuit that are used for evaluating the switching characterization of each device [5]. Due to virtually zero reverse-recovery effects, the SiC-Schottky diode (C3D16065D1) is utilized in the DPT circuit to offer a freewheeling path for the inductor current as well as to enhance the switching behavior of the two power devices during the turn-on and turn-off transitions [5, 27]. The four tested semiconductor devices, which are Si-MOSFET, Si-IGBT, SiC-MOSFET, and cascode GaN-FET, are individually assessed through the DPT circuit with the implemented SiC-Schottky diode [5]. Figure 3.3 shows the experimental DPT hardware with test instruments, circuit components, and DC power supplies [5].

3.3   Alignment of Voltage and Current Waveforms

In order to achieve correct and accurate and results, the current and voltage waveforms should be aligning. To do that, the voltage and current probes are deskewed to align their waveforms. This procedure is very important to get rid of measurement delay and distortion occurred between the voltage and current chan-

nels, obtaining accurate measurements for switching behavior and loss evaluations of each device [72]. The procedure of de-skewing voltage abd current waveforms is presented, as follows:

- The signal path compensation (SPC) calibrates the digital oscilloscope after the oscilloscope has been operated for at least 10 minutes.

- In the oscilloscope, the signal path compensation (SPC) is chosen to calibrate the digital cope after it has been working for more than ten or fifteen minutes.

- A built circuit of a small voltage source and a fixed resistive load is used to adjust the waveforms.

- DC offset of the probe is set-up at zero for each mode of attenuation settings before utilizing the voltage and current probes.

- In the oscilloscope, the delay time is measured between the current and voltage waveforms.

- The voltage waveform is shifted by adding measured delay time in order to be aligned with the current waveform.

3.4   Power Loss Analysis

The power dissipation occurred in semiconductor switching devices is important to be analyzed to evaluate the converter performance and efficiency at different operating conditions [5]. Switching devices are generally responsible for the largest power loss because these devices are major elements in power converters [5]. The

main power consumption in semiconductor devices can be divided into conduction and switching power losses [5].

3.4.1 Conduction Loss of Power Devices

Conduction loss (P_{con}) is occurred when the current is flowing through the power device [5, 72]. This loss depends on the static on-state resistance value and device current [5]. Thus, the conduction loss for power devices such as Si-MOSFET, SiC-MOSFET, and cascode GaN-FET, is expressed as [5]

$$P_{con} = I_{rms}^2 \, R_{ds(on)} \tag{3.1}$$

where I_{rms} and $R_{ds(on)}$ are the room-mean-square of switch current and drain-source on-state resistance of the switch [5]. For Si-IGBT and diode, the conduction loss is determined by [5]

$$P_{con} = V_f \, I_{avg} + I_{rms}^2 \, r_{(on)} \tag{3.2}$$

where V_f, I_{avg}, I_{rms}, and r_{on} are the forward voltage drop, average and room-mean-square values of the device current, and dynamic on-state resistance of the power device, respectively [5]. From Table 2.7, the conduction loss for Si-MOSFET, Si-IGBT, SiC-MOSFET, and cascode GaN-FET is calculated at various switch currents [5]. Table 3.2 highlights a comparison of the conduction loss for these devices at a switching frequency of 50 kHz as the switch current is increasing from 4 to 12 A [5]. Clearly, cascode GaN-FET offers a significantly lower conductions loss among different power devices due to its smaller on-state resistance [5]. Figure 3.4 shows that conduction loss of all devices is evaluated at two junction tempera-

35

Table 3.2: Conduction loss of different power devices.

Switch current (A)	Conduction loss (W)			
	Si MOSFET	Si IGBT	SiC MOSFET	Cascode GaN-FET
4	1.9	9.3	1.1	0.8
6	4.3	13.6	2.3	1.6
8	7.7	18.5	4.2	3.2
10	12	23	6.5	5
12	17.3	28.2	9.4	7.2

tures (T_j) of 25 and 125°C while the switching frequency is 50 kHz [5]. It noticed that the conduction loss for Si-MOSFET and Si-IGBT is drastically increased at higher junction temperature while the conduction loss for SiC-MOSFET and cascode GaN-FET is increased slightly because WBG devices feature considerably larger electric field and higher thermal conductivity compared to Si devices [5].
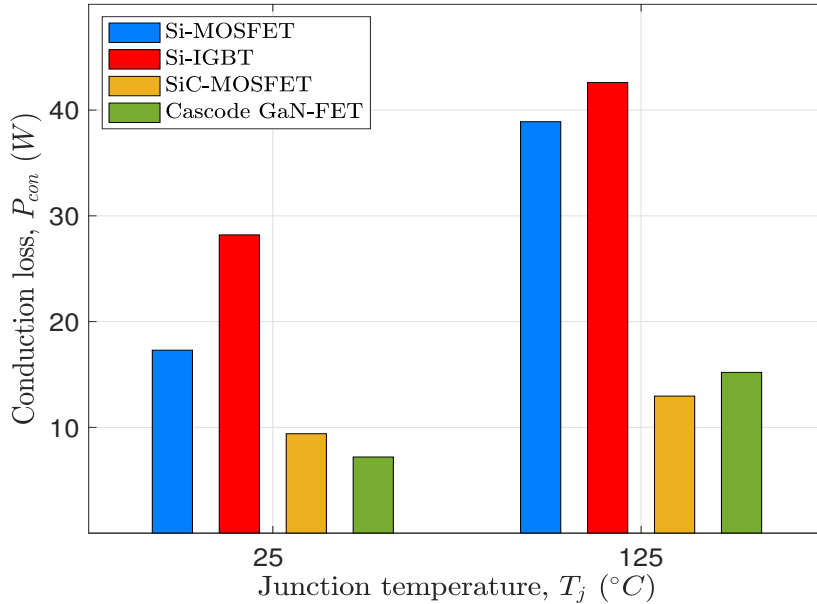
Figure 3.4: Conduction loss of different devices at two junction temperatures.

3.4.2   Switching Loss of Power Devices

Switching loss virtually contributes to a large amount of the total power loss in energy conversion systems [5]. Therefore, this loss is very important to be computed in this section in order to assess the impact of using Si-MOSFET, Si-IGBT, SiC-MOSFET, and cascode GaN-FET devices [5]. The switching energy loss for different semiconductor devices used in power converters is obtained and assessed and through the DPT circuit at various operating conditions [5]. Energy loss is calculated by integrating the product of the measured drain-source voltage (v_{ds}) and drain current (i_d) waveforms during turn-on (t_{on}) and turn-off (t_{off}) times whereas the total switching energy loss (E_{total}) is the sum of the turn-on (E_{on}) and turn-off (E_{off}) energy losses [5, 27]. The switching power loss (P_{sw}) is obtained by multiplying the total switching energy loss of each device by switching frequency [5, 58], as described by

$$E_{on} = \int_{ton} v_{ds}(t)i_d(t)dt \tag{3.3}$$

$$E_{off} = \int_{toff} v_{ds}(t)i_d(t)dt \tag{3.4}$$

$$E_{total} = E_{on} + E_{off} \tag{3.5}$$

$$P_{sw} = E_{total}\ f_{sw} \tag{3.6}$$

In Table 3.3, the switching power loss for Si-MOSFET, Si-IGBT, SiC-MOSFET, and cascode GaN-FET is calculated at various junction temperatures while the switch current is 12 A [5]. Figure 3.5 presents that the switching loss for these de-

Table 3.3: Switching loss of various semiconductor devices.

Junction temperature	Switching power loss (W)			
	Si MOSFET	Si IGBT	SiC MOSFET	Cascode GaN-FET
$T_j = 25°C$	21.5	24.9	10.5	9
$T_j = 125°C$	42.3	49.4	15	17.4

vices is evaluated at the junction temperature of 25°C when the switching frequency is increased from 50 to 150 kHz [5]. It is noticed that cascode GaN-FET along with SiC-MOSFET exhibit a significantly lower switching power loss compared to Si-MOSFET and Si-IGBT at a higher junction temperature and higher switching frequency [5]. This major reduction in loss results from a small delay time and a low rate of the dv/dt and di/dt during turn-on and turn-off transitions [5]. Table
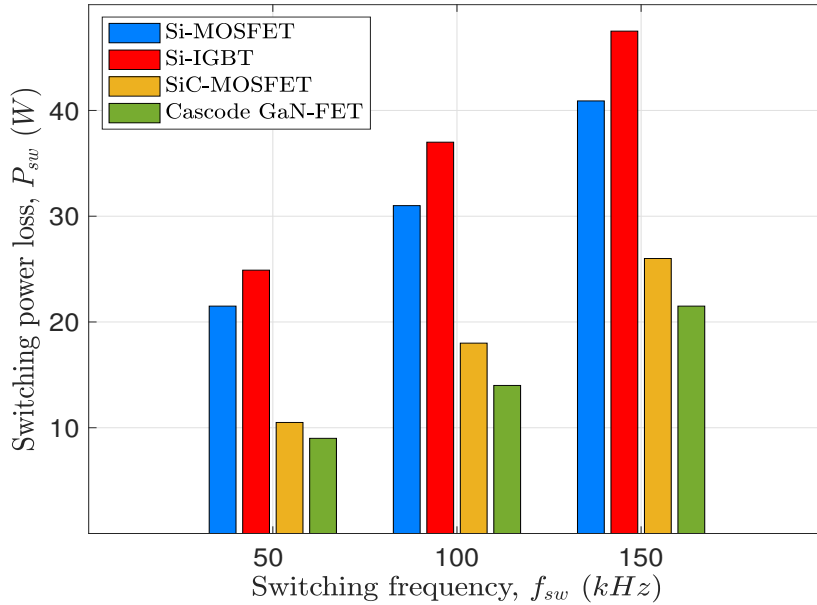
Figure 3.5: Switching power loss for different power devices as the switching frequency is increased from 50 to 150 kHz and the switch current is 12 A.

Table 3.4: Conduction and switching power losses for different power devices.

Semiconductor device	Loss	$T_j = 25°C$	$T_j = 125°C$
Si-MOSFET	P_{con}	17.3 W	38.9 W
	P_{sw}	21.5 W	42.3 W
Si-IGBT	P_{con}	28.2 W	42.6 W
	P_{sw}	24.9 W	49.4 W
SiC-MOSFET	P_{con}	9.4 W	12.9 W
	P_{sw}	10.5 W	15 W
Cascode GaN-FET	P_{con}	7.2 W	15.2 W
	P_{sw}	9 W	17.4 W

3.4 shows a comparative evaluation of conduction and switching power losses for all devices at two junction temperatures of 25 and 125°C while the switch current is 12 A and the switching frequency is 50 kHz [5]. Obviously, cascode GaN-FET and SiC-MOSFET provide higher operating capabilities with remarkably lower conduction and switching losses among other devices [5].

3.5   Different Electrical Gate Parameters

Gate-source voltage, gate-driver circuit, and gate resistance are critical factors in how power devices operate and switch efficiently because their switching behavior relies upon these factors. The switching performance of the cascode GaN-FET is assessed at different gate-driver circuits, gate source voltages, and gate resistance values in order to find the optimal values of gate requirements.

3.5.1   Gate Source Voltage

According to the device's datasheet, the gate-source of the cascode GaN-FET switches between –20 and +20 V, which is unrealistic to obtain a low switching energy loss during turn-on and turn-off transitions with this wide gate-source range. This device is very sensitive to negative gate voltage due to GaN material properties. The cascode GaN-FET is examined at different gate-source voltages through the DPT experiment. It achieves better switching behavior, especially in drain-source voltage, with a lower energy loss at the gate-source voltage of –5 and +15 V. Figure 3.6 and Figure 3.7 show the cascode GaN-FET switching waveforms with two different ranges of the gate-source voltage, which are –7/+18 V and –5/+15 V, during the turn-on transition. As a result, it is important to carefully tailor the gate-source voltage in order to improve switching performance.
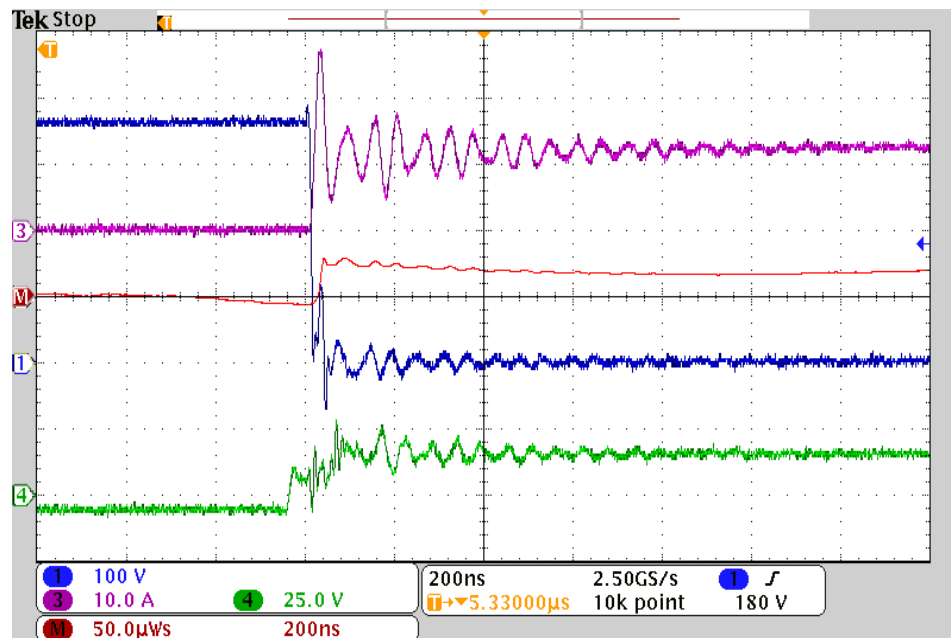
Figure 3.6: Turn-on waveforms with gate-source voltage of –7/+18 V at V_{ds} = 360 V, I_d = 12 A, and T_j = 25°C.
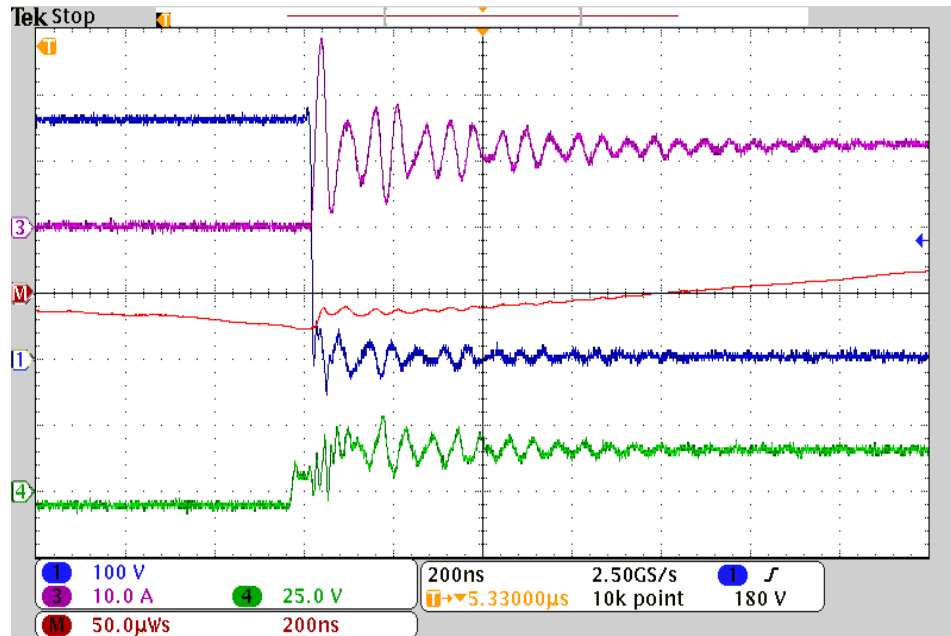
Figure 3.7: Turn-on waveforms with gate-source voltage of –5/+15 V at V_{ds} = 360 V, I_d = 12 A, and T_j = 25°C.

3.5.2 Gate Driver Circuit

The characteristics of cascode GaN-FETs are studied to determine the most suitable gate driver circuit for driving these devices. To achieve the greatest potential from GaN devices, the gate drivers must provide a wide range of gate-source voltages and protect power devices from the avalanche current flowing into the gate and the gate over-voltage. The Infineon (1EDI60I12AH) and Texas Instruments (UCC5350SBD) drivers are the most compatible gate driver circuits with GaN devices based on the characteristics in the device datasheet. Figure 3.8 and Figure 3.9 present the cascode GaN-FET switching waveforms at two different gate driver circuits during the turn-on transition. Therefore, the selection of gate-driver circuits has a clear impact on the switching behavior of GaN devices.
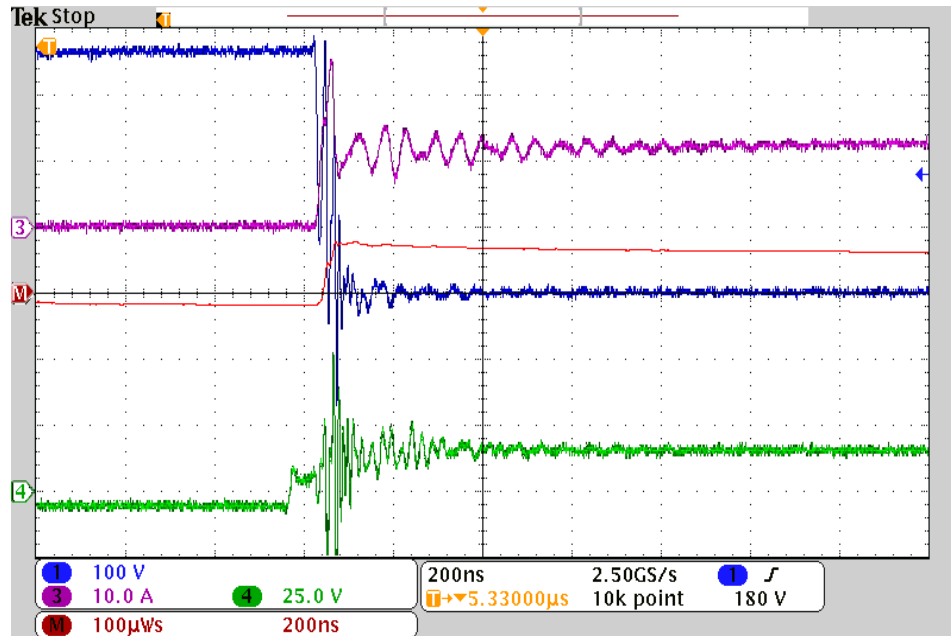
Figure 3.8: Turn-on waveforms with Texas Instruments UCC5350SBD driver at V_{ds} = 360 V and I_d = 12 A.
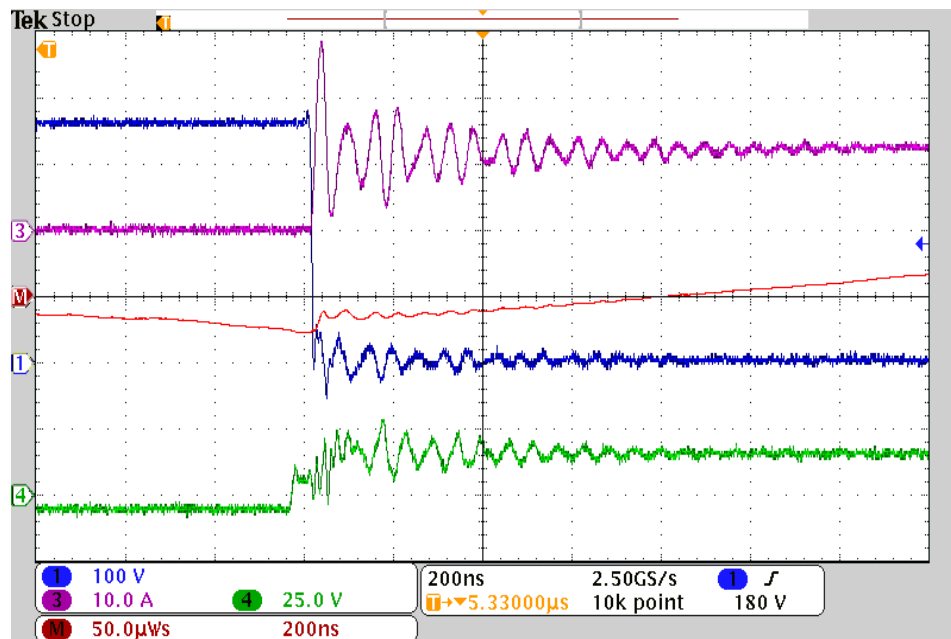
Figure 3.9: Turn-on waveforms with Infineon 1EDI60I12AH driver at V_{ds} = 360 V and I_d = 12 A.

3.5.3 Gate Resistance Value

Similarly, gate resistance value plays a significant role in the switching performance of GaN devices. Increasing gate resistance increases the switching energy loss. However, a higher value of gate resistance can greatly mitigate the overshoot and reduce the oscillation resulting from the high current and voltage transients. Figure 3.10 and Figure 3.11 show the turn-on waveforms of the cascode GaN-FET at two different gate resistances of 5 and 20 Ω. Importantly, the choice of gate resistance is critical for the proper switching operation of cascode GaN-FET devices.
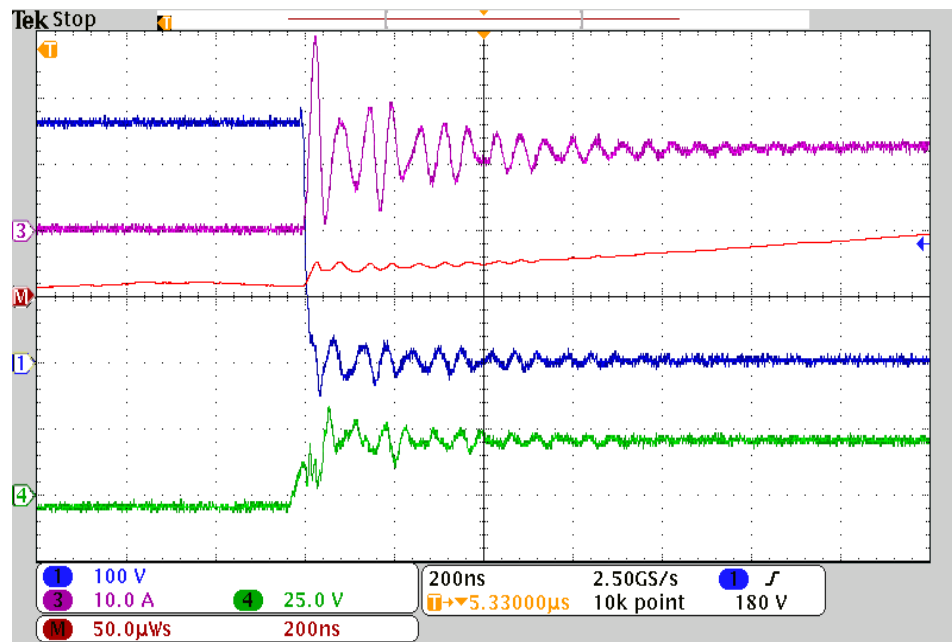
Figure 3.10: Turn-on waveforms at gate resistances of 5 Ω at $V_{ds} = 360$ V and $I_d = 12$ A.
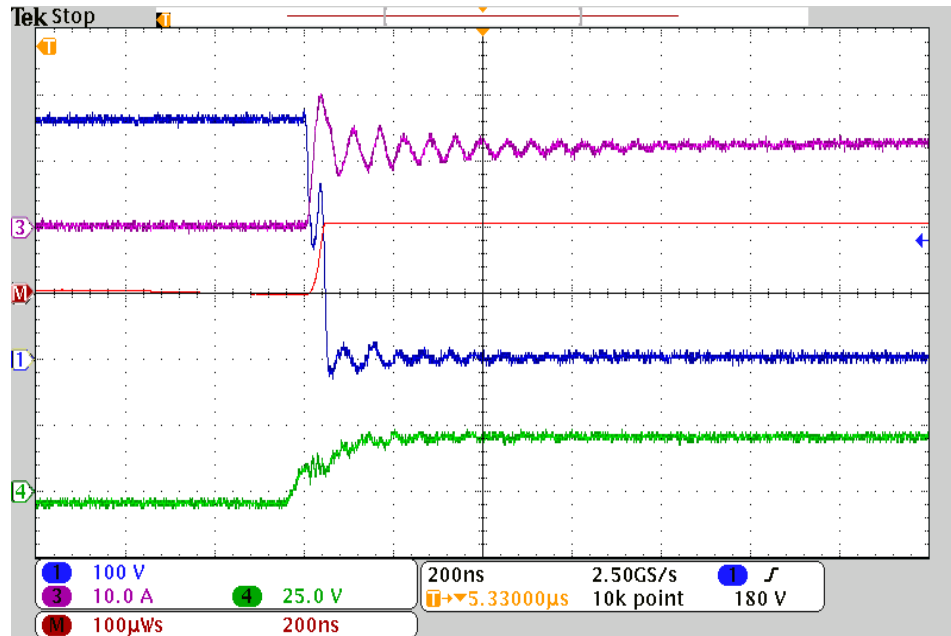
Figure 3.11: Turn-on waveforms at gate resistances of 20 Ω at V_{ds} = 360 V and I_d = 12 A.

3.6   Summary

In this chapter, the DPT circuit, including the gate-driver circuit, load inductor, and DC capacitor along with the measurement requirements, such as voltage and current probes, for the switching characterization is discussed to study the switching performance of each power device during turn-off and turn-on transitions. The components implemented in the DPT circuit are explained with their specifications. From DPT board, the switching energy losses and the rate of dv/dt and di/dt are computed at different operating conditions as well as the power dissipation from semiconductor switching devices is analyzed to evaluate the converter performance and efficiency at different operating conditions. Compared to Si and SiC power devices, the results showed that cascode GaN-FET provides a significantly lower

44

semiconductor losses due to their smaller on-state resistance and shorter switching times. Gate-source voltage, gate-driver circuit, and gate resistance considered to be the most crucial factors in how power devices operate and switch efficiently because their switching behavior are depending on these factors. As cascode GaN-FET assessed experimentally, the gate-driver (1EDI60I12AH), from Infineon, is used for driving operations while the turn-on and turn-off gate resistance values are set-up as to15 and 5 Ω. In the meantime, the gate-source voltage is selected to be –5/+15 To achieve better performance for GaN devices.

Chapter 4

Cascode GaN-FET Switching Characterization over Si-MOSFET

It is important to understand the device switching characteristic and performance in order to employ different semiconductor devices in power converters [5]. So, this chapter assesses and compares the dynamic characteristics of the cascode GaN-FET and Si-MOSFET in terms of switching performance and energy loss [5]. The impacts of operating conditions such as gate resistance, switch current, junction temperature, and DC-bus voltage on the switching device behavior are evaluated in terms of energy losses [5]. The experimental results are analyzed and compared between the two devices [5].

4.1   Switching Performance Evaluation

The switching performance of Si-MOSFET and cascode GaN-FET devices are investigated and characterized under the hard-switching condition through the stan-

dard inductive-clamped load test circuit, which is known as a double-pulse test (DPT) [5, 63]. Table 4.1 lists the main parameters of two different power devices that are examined under the same junction temperature, switch current, and input voltage [5, 63]. These devices have the same package structures to ensure that they contain exact parasitic inductance and capacitance effects [5, 63]. The gate-source voltage and gate resistance of the used power devices provided in the manufacturer's datasheet are taken into consideration for the evaluation [5, 63]. Because of the nearly zero reverse-recovery effects, the SiC-Schottky diode is employed in the DPT circuit to provide a freewheeling path for the inductor current as well as to improve the switching behavior of the two power devices during the turn-on and turn-off events [5, 125, 126].

Table 4.1: Core parameters of the two power devices examined.

Semiconductor device	Cascode GaN-FET	Si-MOSFET
Manufacturer	Transphorm	On Semiconductor
Part number	TP65H035WS	NTHL082N65S3F
Blocking voltage	650 V	650 V
Rating current	46.5 A	40 A
Max junction temperature	150°C	150°C
Package	TO-247	TO-247

4.1.1 Si-MOSFET Switching Waveforms

The drain-source voltage (V_{ds}) and drain current (I_d) of the Si-MOSFET is studied to evaluate its switching behavior during the turn-on and turn-off transitions at the input voltage of 360 V, switch current of 12 A, and operating temperature of 25°C [5]. The 650 V, 40 A Si-MOSFET device is tested with a gate-source (V_{gs})

voltage of –5 to +15 V for the turn-on and turn-off transitions while the turn-on ($R_{g(on)}$) and turn-off ($R_{g(off)}$) gate resistance values are 15 and 5 Ω to achieve an optimal lower switching energy loss and smaller overshoot [5, 63]. This device shows fast switching frequencies with relatively lower on-state resistance [5,63].

Figure 4.1 and Figure 4.2 show the drain-source voltage, drain current, gate-source voltage, and energy loss waveforms of the Si-MOSFET during the turn-on and turn-off events [5]. The drain current waveform exhibits a high overshoot of 11 A along with a clear ringing in current and voltage waveforms during the turn-on transition due to the capacitance of the diode [5, 72]. In this event, the time-on is 80 ns while the dv/dt and di/dt are 6.9 kV/μs and 0.9 kA/μs, respectively [5, 63]. During the turn-off transition, there is a considerable overshoot of 132 V along with a large ringing in both the current and voltage waveforms due to the
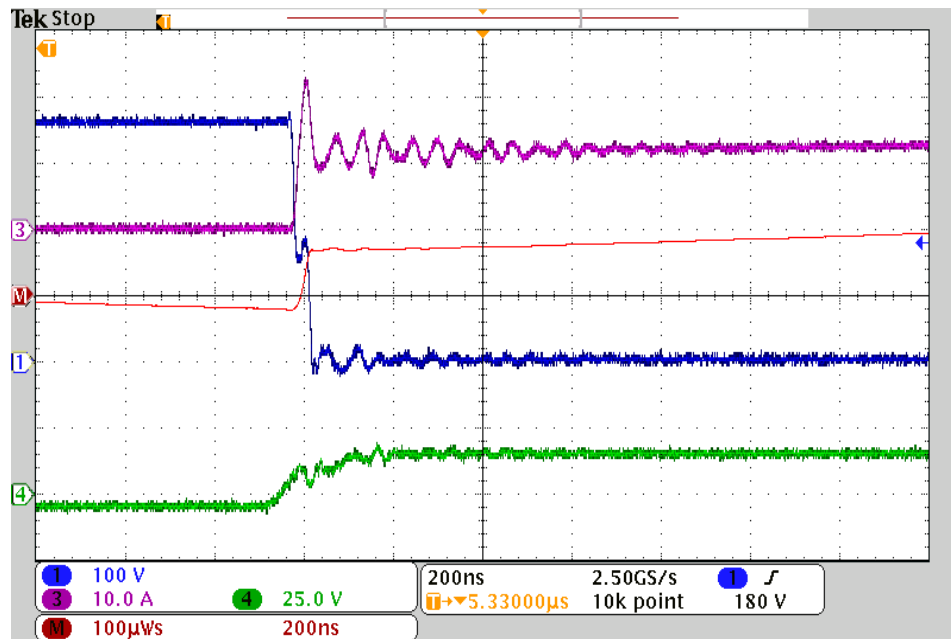
Figure 4.1: Turn-on waveforms of Si-MOSFET with V_{gs} = –5/+15 V, $R_{g(on)}$ = 15 Ω, and $R_{g(off)}$ = 5 Ω when V_{ds} = 360 V, I_d = 12 A, and T_j = 25°C.
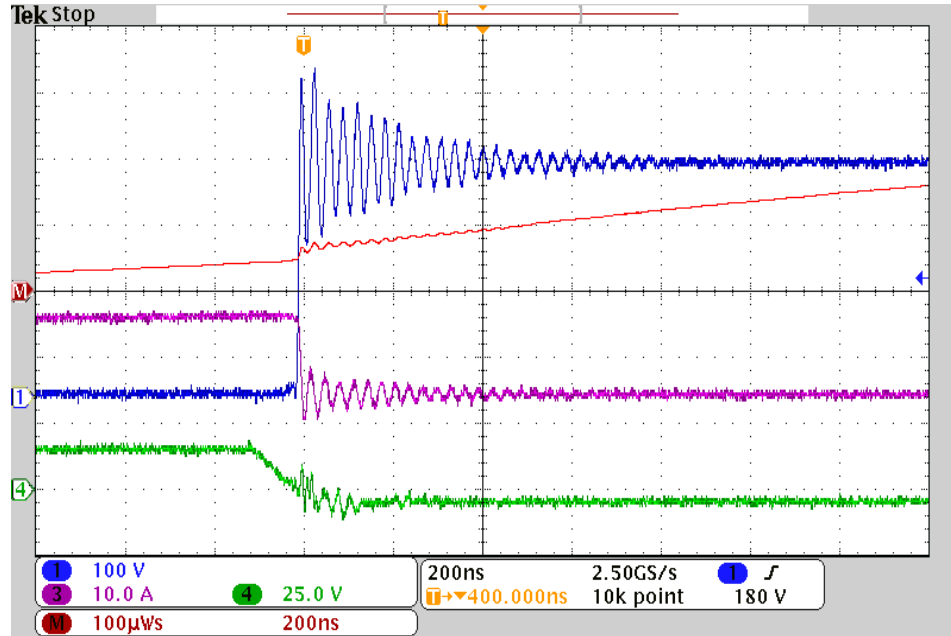
Figure 4.2: Turn-off waveforms of Si-MOSFET with V_{gs} = –5/+15 V, $R_{g(on)}$ = 15 Ω, and $R_{g(off)}$ = 5 Ω when V_{ds} = 360 V, I_d = 12 A, and T_j = 25°C.

stray inductance, which can be reduced by controlling the current commutation loop [5, 58]. In this event, the time-off is 92.8 ns while the dv/dt and di/dt are 48 kV/μs and 1.5 kA/μs, respectively [5]. The measured turn-on and turn-off energy losses are 94 and 30 μJ, respectively [5, 63].

4.1.2   Cascode GaN-FET Switching Waveforms

The drain current and drain-source voltage of the cascode GaN-FET is examined to assess its switching behavior during the turn-on and turn-off transitions at the input voltage of 360 V, switch current of 12 A, and operating temperature of 25°C [5]. The 650 V, 46.5 A cascode GaN-FET device operates at a gate-source voltage of –5 to +15 V for the turn-on and turn-off events while the turn-on and turn-off gate resistance values are 15 and 5 Ω to minimize energy losses and en-

49

hance switching behavior [5]. The main advantages of this device are low on-state resistance, high-switching speed, and small-intrinsic capacitance with ultra-low reverse recovery charge [5, 27].

Figure 4.3 and Figure 4.4 depict the drain-source voltage, drain current, gate-source voltage, and energy loss waveforms of the cascode GaN-FET during the turn-on and turn-off events [5]. Noteworthy, the drain current waveform shows a large overshoot of 15 A along with a major ringing in current and voltage waveforms during the turn-on transition because the reverse recovery charge of the internal body diode for the low voltage Si-MOSFET is embedded inside the cascode GaN power device as well as the high Miller effects [5, 107]. In this event, the time-on is 50 ns while the dv/dt and di/dt are 48 kV/μs and 1.3 kA/μs, respectively [5]. In the turn-off transition, there is a small overshoot of 36 V along with a very small
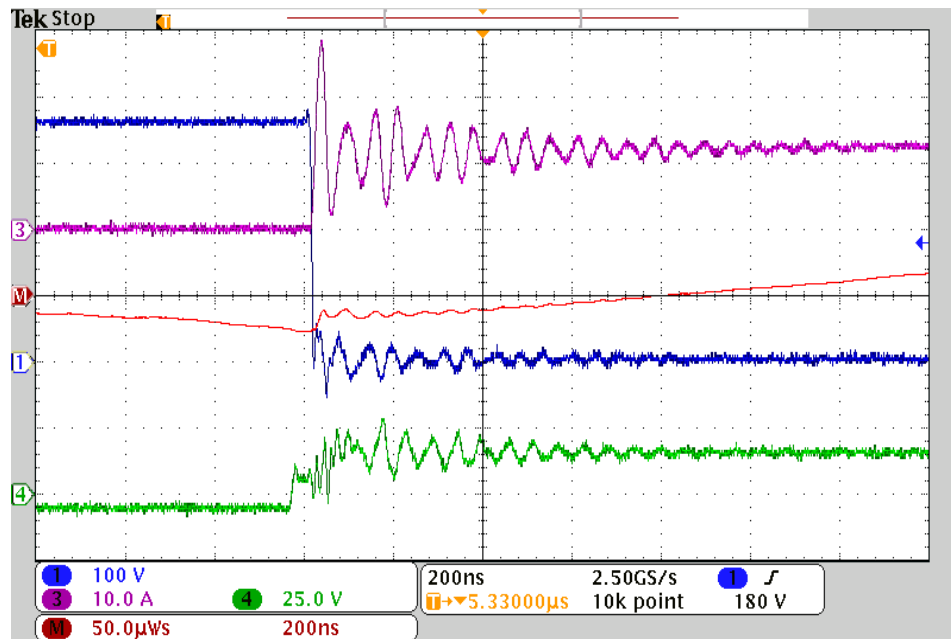
Figure 4.3: Turn-on waveforms of cascode GaN-FET with V_{gs} = –5/+15 V, $R_{g(on)}$ = 15 Ω, and $R_{g(off)}$ = 5 Ω when V_{ds} = 360 V, I_d = 12 A, and T_j = 25°C.
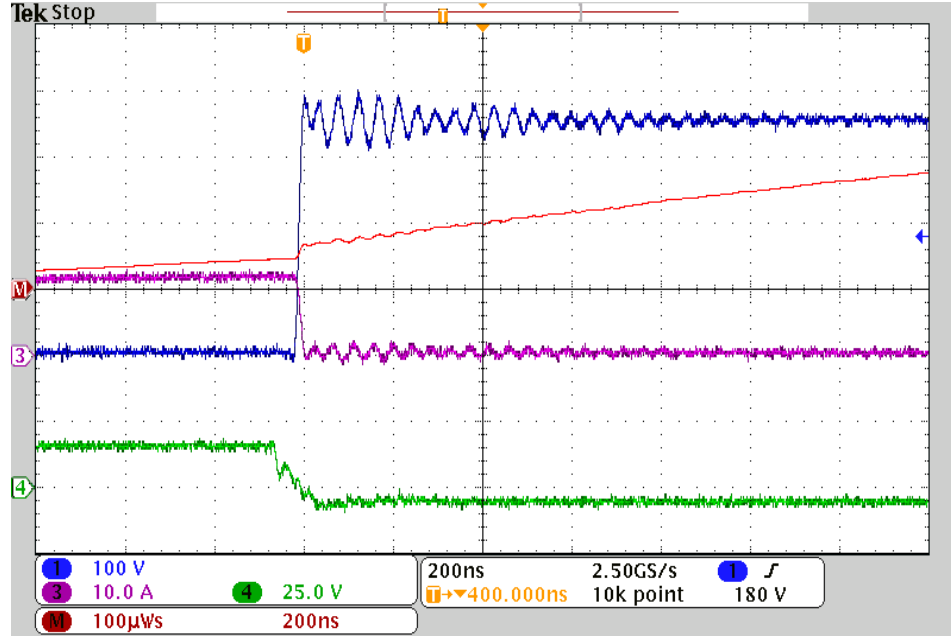
Figure 4.4: Turn-off waveforms of cascode GaN-FET with V_{gs} = –5/+15 V, $R_{g(on)}$ = 15 Ω, and $R_{g(off)}$ = 5 Ω when V_{ds} = 360 V, I_d = 12 A, and T_j = 25°C.

ringing in both the drain current and drain-source voltage waveforms due to the cascode configuration and capacitance charge [5, 72, 127]. In this event, the time-off is 60 ns while the dv/dt and di/dt are 23.2 kV/μs and 0.7 kA/μs, respectively [5]. The measured turn-on and turn-off energy losses are 29 and 22 μJ, respectively [5].

4.2   Switching Performance Comparison

Based on the experimental results, the cascode GaN-FET exhibits considerably reduced energy losses compared to the Si-MOSFET because the switching time during the turn-on and turn-off events is much shorter than the Si device [5]. Though the overshoot and ringing effects in the cascode GaN-FET are notable due to high dv/dt and di/dt across the parasitic elements during the turn-on, the Si-MOSFET shows a very large overshoot and ringing phenomenon in both the drain current and

drain-source voltage waveforms during the turn-off [5, 27]. In the turn-off event, the dv/dt and di/dt of the Si-MOSFET are larger than those in the cascode GaN-FET device [5]. Table 4.2 summarizes the switching performance results of the Si-MOSFET and cascode GaN-FET in turn-on and turn-off events.

Table 4.2: Switching behavior comparison between Si-MOSFET and cascode GaN-FET devices.

	Turn-on transition		Turn-off transition	
	Si-MOSFET	GaN-FET	Si-MOSFET	GaN-FET
Switching loss (μJ)	94	29	30	22
dv/dt (kV/μs)	6.9	48	48	23.2
di/dt (kA/μs)	0.9	1.3	1.5	0.7
Switching time (ns)	80	50	92.8	60

4.3   Switching Energy Loss Assessment

The switching energy losses of Si-MOSFET and cascode GaN-FET are evaluated at different operating conditions of gate resistance values, switch currents, junction temperatures, and DC-bus voltages [5]. As previously discussed in chapter 3, the two devices are examined at the same gate requirements to distinguish their switching performance [5]. In the meantime, the gate-driver circuit (1EDI60I12AH) is used for driving each device as the gate-source voltage is –5/+15 V [5].

4.3.1   Different Gate Resistance Values

Gate resistance has a significant impact on the switching performance of devices [5]. The energy loss considerably increases at higher gate resistance so low-

ering gate resistance reduces the transient time of the switching device [5, 63]. This process can help to minimize the energy loss; nevertheless, a smaller gate resistance can increase the overshoot and ringing of device current and voltage during turn-on and turn-off times [5, 63]. The choice of gate resistance is a critical factor for the proper switching operation of power devices [5]. Therefore, Si-MOSFET and cascode GaN-FET are examined at different gate resistance values and each device is operated at 360 V and 12 A [5].
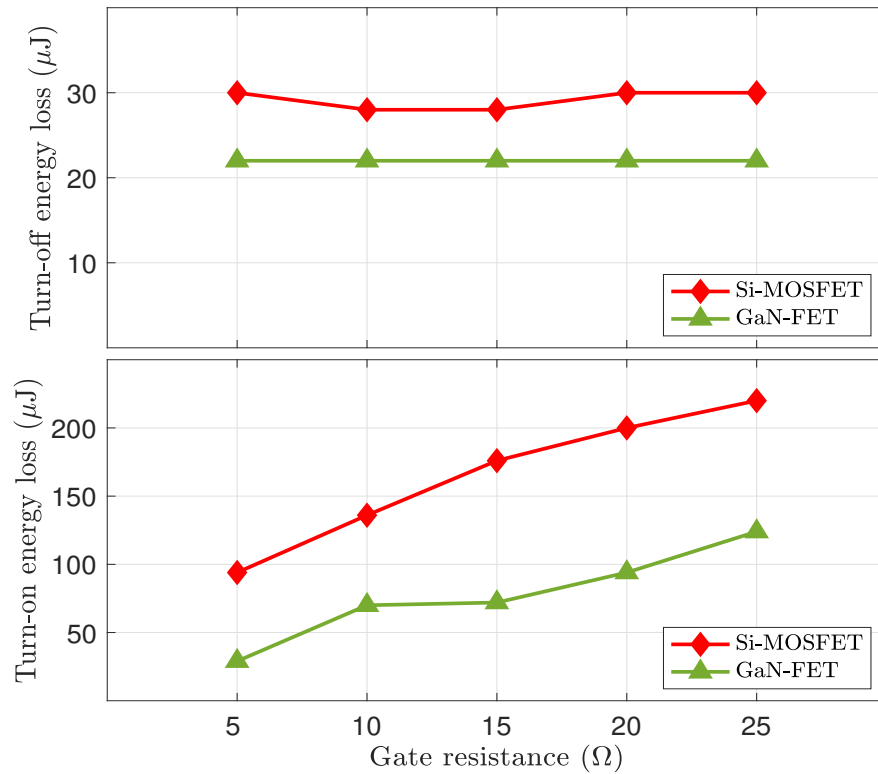
Figure 4.5: Turn-off and turn-on energy losses of Si-MOSFET and cascode GaN-FET as the gate resistance is increased from 5 to 25 Ω.

The turn-off gate resistance is elevated from 5 to 25 Ω while the turn-on gate resistance stays at a fixed value of 5 Ω [5]. The top Figure 4.5 illustrates that the turn-off energy losses for both devices are nearly constant as increasing the turn-off

gate resistance value [5]. At the turn-off gate resistance of 25 Ω, turn-off losses of Si-MOSFET and cascode GaN-FET are 30 and 22 μJ, respectively [5]. The bottom Figure 4.5 shows a major increase in turn-on losses for the Si-MOSFET and cascode GaN-FET as the turn-on gate resistance is increased from 5 to 25 Ω while the turn-off gate resistance remains fixed at 5 Ω [5]. However, the turn-on loss of the cascode GaN-FET increases slightly with increasing the turn-on gate resistance [5]. Turn-on losses of Si-MOSFET and cascode GaN-FET are 220 and 124 μJ, respectively, at the turn-on gate resistance of 25 Ω [5]. The cascode GaN-FET obtains 43.6% reduction in the energy loss at a higher turn-on gate resistance compared to the Si-MOSFET during the turn-on event [5]. This means that the changing gate resistance value showa a major impact only on the turn-on energy losses for both devices [5]. Table 4.3 shows the total energy loss comparison for both devices at various gate resistances [5].

Table 4.3: Total energy loss of Si-MOSFET and cascode GaN-FET at different gate resistance values.

Gate resistance (Ω)	Total switching energy losses (μJ)	
	Si-MOSFET	Cascode GaN-FET
5	124	51
10	164	92
15	204	94
20	230	116
25	250	146

The effect of changing gate resistances on each switching device is evaluated through the DPT circuit during turn-off and turn-on times [5]. The results show that the turn-on loss for the Si-MOSFET is almost two times higher than the turn-on loss for the cascode GaN-FET at the higher gate resistance value [5]. Therefore,

different gate resistances have a notable influence on both switching performance and energy loss of power devices during the two switching transitions [5]. Reducing the turn-off and turn-on gate resistances can decrease the switching time and loss, causing high the dv/dt and di/dt rates with large oscillation and overshoot in the device voltage and current waveforms [5].
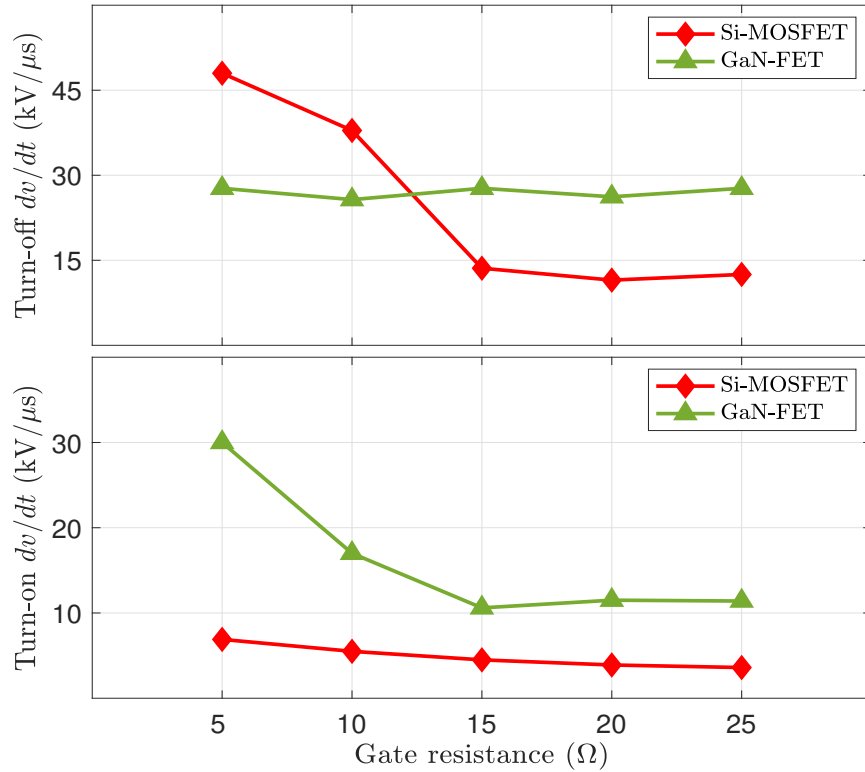
Figure 4.6: Turn-off and turn-on dv/dt of Si-MOSFET and cascode GaN-FET as the gate resistance is increased from 5 to 25 Ω.

Figure 4.6 and Figure 4.7 show dv/dt and di/dt rates of each device at various gate resistances during the turn-off and turn-on events [5]. The dv/dt and di/dt rates for Si-MOSFET and cascode GaN-FET are reduced by increasing gate resistance values [5]. The cascode GaN-FET exhibits higher rates because of high stray parasitic elements and faster switching frequency compared to the Si-MOSFET [5].

55

To mitigate the high dv/dt and di/dt rates in the switching performance of the cascode GaN-FET, the gate resistance during the turn-off and turn-on events should be increased [5]. Thus, it is crucially important to obtain the optimal gate resistance value for each semiconductor device employed in the power converter design [5].
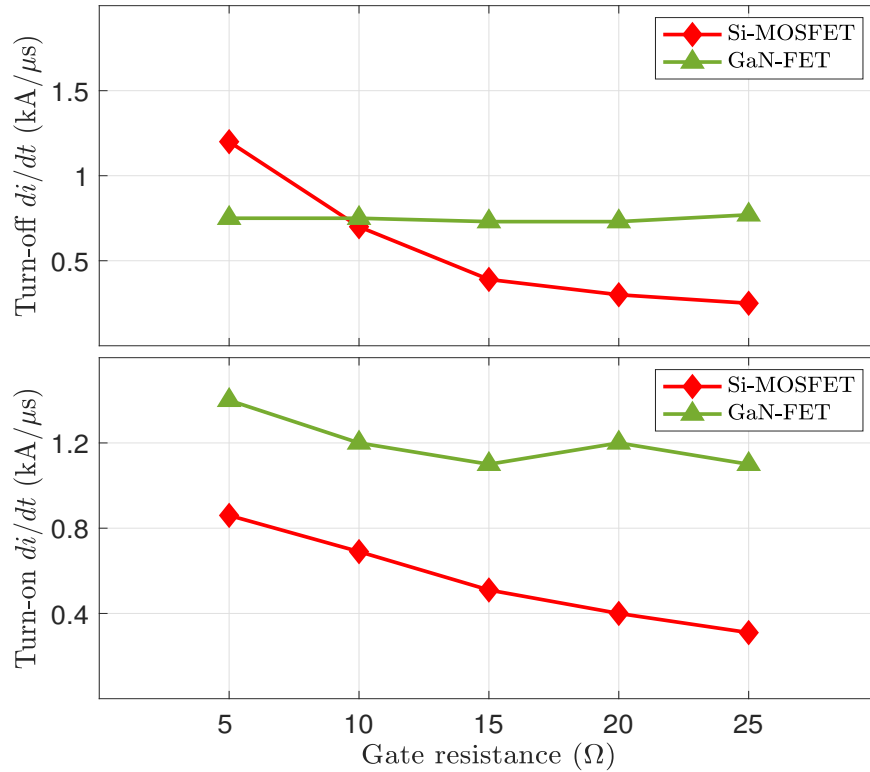
Figure 4.7: Turn-off and turn-on di/dt of Si-MOSFET and cascode GaN-FET as the gate resistance is increased from 5 to 25 Ω.

4.3.2 Different Switch Currents

Si-MOSFET and cascode GaN-FET are performed under the input voltage of 360 V and junction temperature of 25°C as the switch current is increased from 4 to 12 A [5, 27]. Table 4.4 highlights turn-on and turn-off energy losses of the two devices at different switch currents [5]. The switching energy losses of the Si-

MOSFET, especially turn-on loss, are drastically high due to Miller current effect [5, 27]. Although the turn-off loss of the two devices is quite similar, the turn-

Table 4.4: Comparison of turn-on and turn-off energy losses between Si-MOSFET and cascode GaN-FET at different switch currents.

Current (A)	Si-MOSFET		Cascode GaN-FET	
	E_{on} (μJ)	E_{off} (μJ)	E_{on} (μJ)	E_{off} (μJ)
4	39	20	8	26
6	49	21	10	27
8	62	25	14	28
10	75	27	18	29
12	98	31	24	30
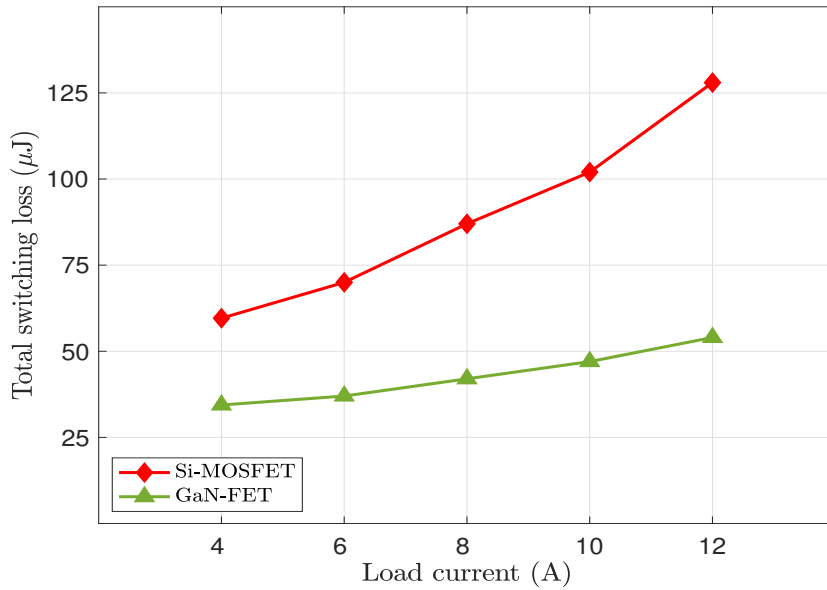
Figure 4.8: Total switching energy loss of Si-MOSFET and cascode GaN-FET as the switch current is increased from 4 to 12 A.

on loss of the Si-MOSFET is two times more than the turn-on loss of the GaN-FET, particularly after the switch current is exceed 6 A [5]. Figure 4.8 illustrates

the total switching energy loss for Si-MOSFET and cascode GaN-FET at different switch currents, showing their effects on the total energy loss [5]. As the switch current increases, the total energy loss of the two devices increases linearly [5, 27]. However, the total energy loss of the cascode GaN-FET is outstandingly reduced by 57.8% compared to the loss of Si-MOSFET at the switch current of 12 A [5, 27]. Thus, GaN is capable of operating at a higher current with lower energy loss [5].

4.3.3 Different Junction Temperatures

To investigate the effect of different operating temperatures, the hotplate is used to heat only the device under test (DUT) while the entire DPT circuit is placed in the room temperatures [5]. Figure 4.9 shows that the turn-on, turn-off, and total energy losses of each device increase as the junction temperature is increased from 50 to 150°C [5]. It is clear that the total energy loss of each device increases significantly with increasing junction temperature [5], as shown in Table 4.5. However, the cascode GaN-FET achieves remarkably lower total energy loss compared to Si-MOSFET throughout different junction temperatures [5]. At the temperature of 100°C, Figure 4.10 illustrates that the switching energy loss of the cascode GaN-

Table 4.5: Total energy loss of two tested devices at different junction temperatures.

Device technology	Total energy loss at different temperatures		
	50°C	100°C	150°C
Si-MOSFET	114μJ	204μJ	250μJ
Cascode GaN-FET	60μJ	130μJ	208μJ
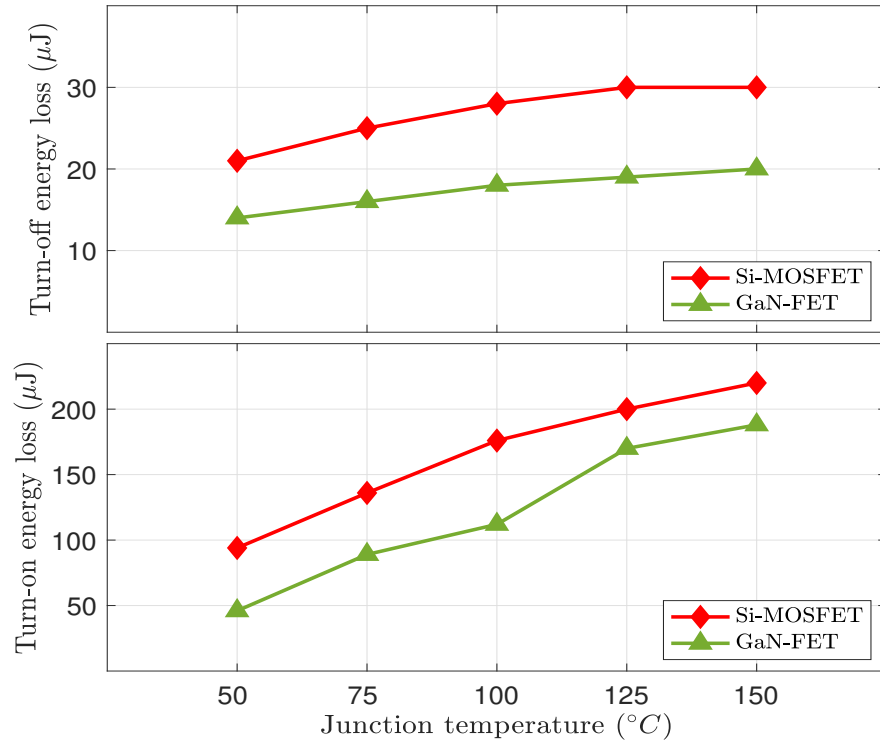
Figure 4.9: Turn-on and turn-off energy losses of Si-MOSFET and cascode GaN-FET as the junction temperature is increased from 25 to 150°C.

FET reduced by 36.3% compared to Si-MOSFET [5]. It means that GaN exhibits excellent switching performance with lower losses at higher temperatures [5].
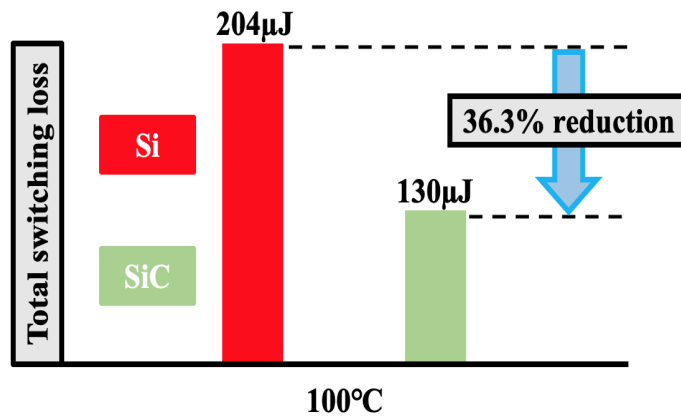
Figure 4.10: Total energy loss of Si-MOSFET and cascode GaN-FET at the junction temperature of 100°C.

4.3.4 Different DC-bus Voltages

The switching energy losses of Si-MOSFET and cascode GaN-FET are assessed at the switch current of 10 A and junction temperature of 25°C as a function of increasing DC-bus voltage [5, 27]. Table 4.6 shows a comparison of the total energy losses as the DC-bus voltage is increased from 200 to 360 V [5]. The switching energy losses are measured by integrating the instantaneous power during a commuted interval [5,58], as the previously mentioned. The energy losses for Si-MOSFET and cascode GaN-FET increases in conjunction with increasing the DC-bus voltage [5], as shown in Figure 4.11. However, the cascode GaN-FET provides a lower total energy loss as the DC-bus voltage increases [5, 58]. At the DC-bus voltage of 360 V and switch current of 10 A, the cascode GaN-FET reduces the total energy loss by nearly 60% compared to the Si-MOSFET [5, 58]. Thus, GaN device provides improved switching performance along with considerably reduced energy losses at a higher voltage [5].

Table 4.6: Comparison of turn-on and turn-off energy losses between Si-MOSFET and cascode GaN-FET at different DC-bus voltages.

DC-bus voltage (V)	Si-MOSFET		Cascode GaN-FET	
	E_{on} (μJ)	E_{off} (μJ)	E_{on} (μJ)	E_{off} (μJ)
200	10	18	2	12
240	23	20	4	14
280	39	22	6	16
320	56	24	8	22
360	75	27	15	26
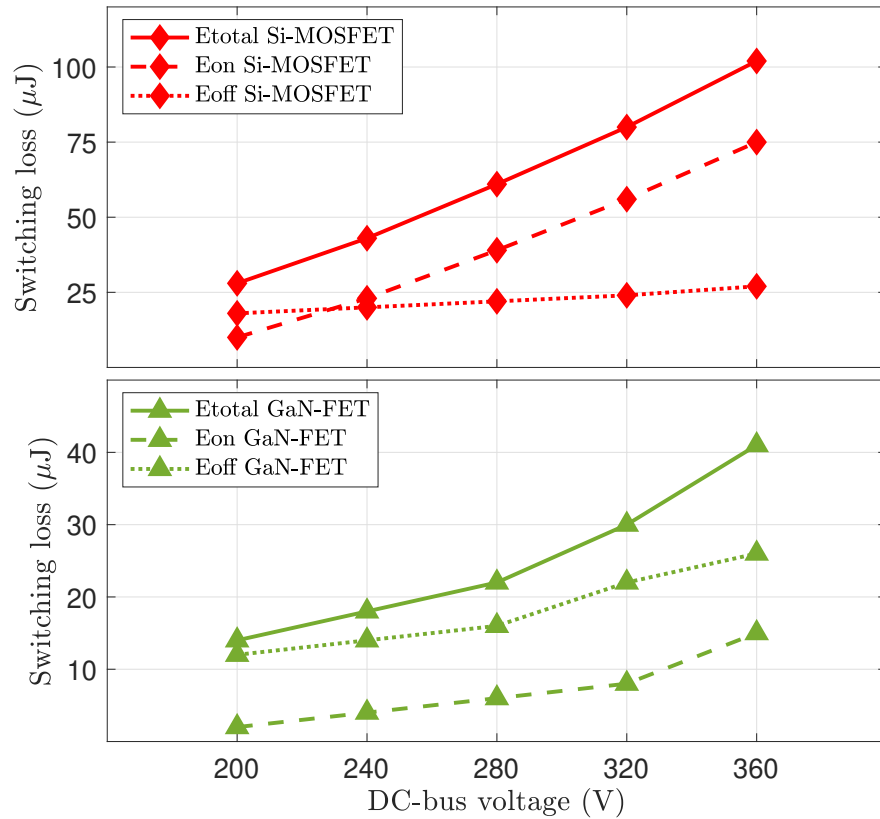
Figure 4.11: Turn-on, turn-off, and total energy losses of Si-MOSFET and cascode GaN-FET at switch current of 10 A as the voltage increased from 200 to 360 V.

4.4 Summary

The switching behavior and switching energy loss of Si-MOSFET and cascode GaN-FET are analyzed and assessed through the DPT circuit. The turn-on and turn-off, total energy losses of the two tested devices are evaluated at various operating points of a gate resistance value, switch current, junction temperature, and DC-bus voltage because these high operating capabilities of the GaN device are major advantages and benefits over the traditional Si device. The cascode GaN-FET offers a major reduction in total energy loss compared to the Si-MOSFET as a function of

61

increasing operating conditions. Compared to the Si-MOSFET, the cascode GaN-FET exhibits excellent switching characteristics along with very low energy losses. Therefore, GaN power device considerably enhances the switching performance of the converter.

Chapter 5

SiC-MOSFET Switching Characterization over Si-IGBT

This chapter evaluates the dynamic behavior of Si-IGBT and SiC-MOSFET power devices in terms of switching performance and energy loss. The effects of a high gate resistance, switch current, and junction temperature, and DC-bus voltage on the switching performance of the two tested power devices are examined in order to implement the most suitable semiconductor devices for high-power and high-switching converter applications. The experimental outcomes are assessed and compared between the two devices.

5.1   Switching Performance Evaluation

The dynamic switching performance of the Si-IGBT and SiC-MOSFET power devices is evaluated through DPT circuit during the turn-on and turn-off times. The switching behavior of each device is captured at the DC-bus voltage of 360 V and

switch current of 12 A as well as analyzed their performance in terms of current and voltage overshoots, dv/dt and di/dt, switching times, and switching energy losses. Table 5.1 provides the main parameters of Si-IGBT and SiC-MOSFET power devices used in the switching performance investigation. For a fair comparison, the two different power devices are examined under identical junction temperatures and the same device package to maintain the exact parasitic inductance and capacitance effects along with avoiding inconsistency between switching results [63]. Nevertheless, the gate-source voltage and gate resistance of the two tested devices are chosen based on the optical switching performance that can be archived, taking the datasheet of each device into consideration [63].

Table 5.1: Fundamental parameters of the two power devices tested.

Semiconductor device	SiC-MOSFET	Si-IGBT
Manufacturer	ROHM	Infineon
Part number	SCT3060AL	IKW30N65H5
Blocking voltage	650 V	650 V
Rating current	39 A	55 A
Max junction temperature	175°C	175°C
Package	TO-247	TO-247

5.1.1 Si-IGBT Switching Waveforms

The switching behavior of the collector-emitter voltage (V_{ce}) and collector current (I_c) of the Si-IGBT is assessed during the turn-on and turn-off transitions at the input voltage of 360 V, switch current of 12 A, and operating temperature of 25°C. The 650 V, 55 A Si-IGBT device is examined with a gate-emitter (V_{ge}) voltage of –5 to +15 V for the turn-on and turn-off events when the turn-on and turn-off

gate resistance values are 15 and 5 Ω to have a lower energy loss and a smaller overshoot in switching waveforms [63]. This device has a high current capability and low saturation voltage with a relatively faster switching speed compared to the other IGBTs [27].

Figure 5.1 and Figure 5.2 show the collector-emitter voltage, collector current, gate-emitter voltage, and energy loss waveforms of the Si-IGBT during the turn-on and turn-off events. The collector current waveform exhibits a high overshoot of 10 A along with a small ringing in current and voltage waveforms during the turn-on event because of the commutation loop inductance [27]. In this event, the time-on is 84.5 ns while the dv/dt and di/dt are 6.4 kV/μs and 0.96 kA/μs respectively. During the turn-off event, there is a major overshoot of 98 V along with a large ringing in the collector current and collector-emitter voltage waveforms due to the
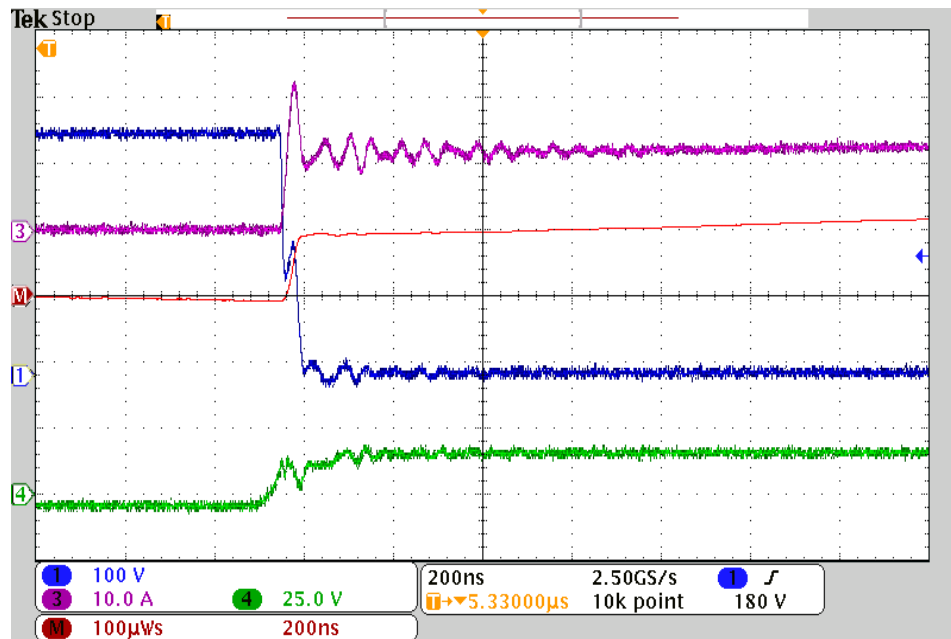
Figure 5.1: Turn-on waveforms of Si-IGBT with V_{ge} = –5/+15 V, $R_{g(on)}$ = 15 Ω, and $R_{g(off)}$ = 5 Ω when V_{ce} = 360 V, I_c = 12 A, and T_j = 25°C.
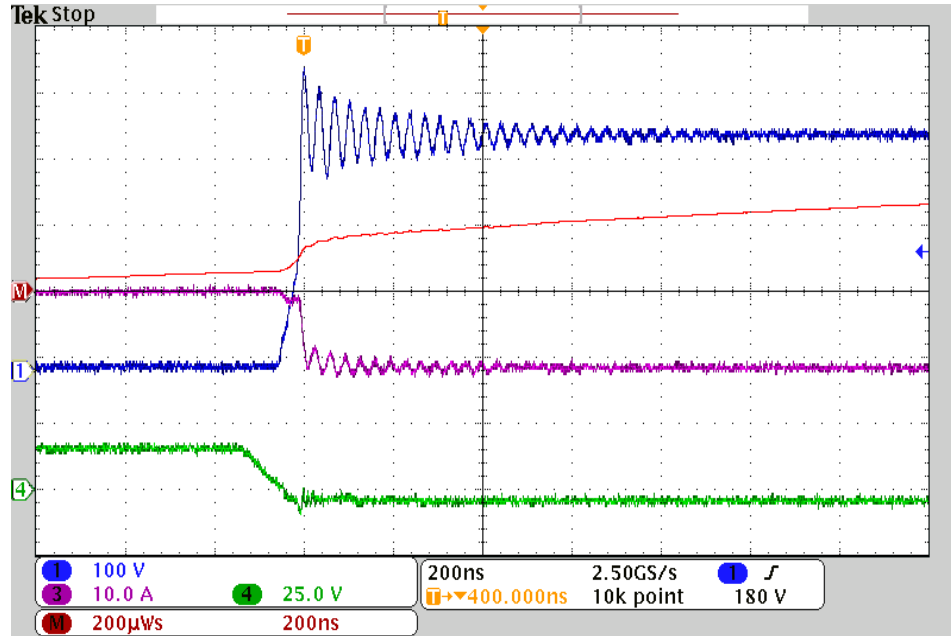
Figure 5.2: Turn-off waveforms of Si-IGBT with $V_{ge} = -5/+15$ V, $R_{g(on)} = 15$ Ω, and $R_{g(off)} = 5$ Ω when $V_{ce} = 360$ V, $I_c = 12$ A, and $T_j = 25°$C.

tailing current effect [27, 128, 129]. In this event, the time-off is 120 ns when the dv/dt and di/dt are 6.7 kV/μs and 0.21 kA/μs, respectively. The measured turn-on and turn-off energy losses are 102 and 108 μJ, respectively.

5.1.2 SiC-MOSFET Switching Waveforms

The drain current and drain-source voltage waveforms of the SiC-MOSFET is tested to evaluate its switching behavior during the turn-on and turn-off events at the input voltage of 360 V, switch current of 12 A, and operating temperature of 25°C [5]. The 650 V, 39 A SiC-MOSFET device operates at a gate-source voltage of –5 to +15 V for the turn-on and turn-off switching times when the turn-on and turn-off gate resistance values are set at 15 and 5 Ω to decrease energy losses and improve switching performance [5, 63]. The prime advantages of this device are a

66

low on-state resistance, small gate charge, and high switching frequency with fast reverse recovery [5, 72].

Figure 5.3 and Figure 5.4 show the drain-source voltage, drain current, gate-source voltage, and energy loss waveforms of the SiC-MOSFET during the turn-on and turn-off events [5]. The drain current waveform shows a small overshoot of 6 A along with a very slight ringing in current waveform during the turn-on event because of the reverse recovery charge of the body diode [5, 72]. In this event, the time-on is 82 ns when the dv/dt and di/dt are 3.5 kV/μs and 0.4 kA/μs, respectively [5]. During the turn-off event, there is a large overshoot of 112 V along with a considerable ringing in the drain current and drain-source voltage waveforms due to the parasitic effects [5, 63, 130, 131]. In this event, the time-off is 54 ns when
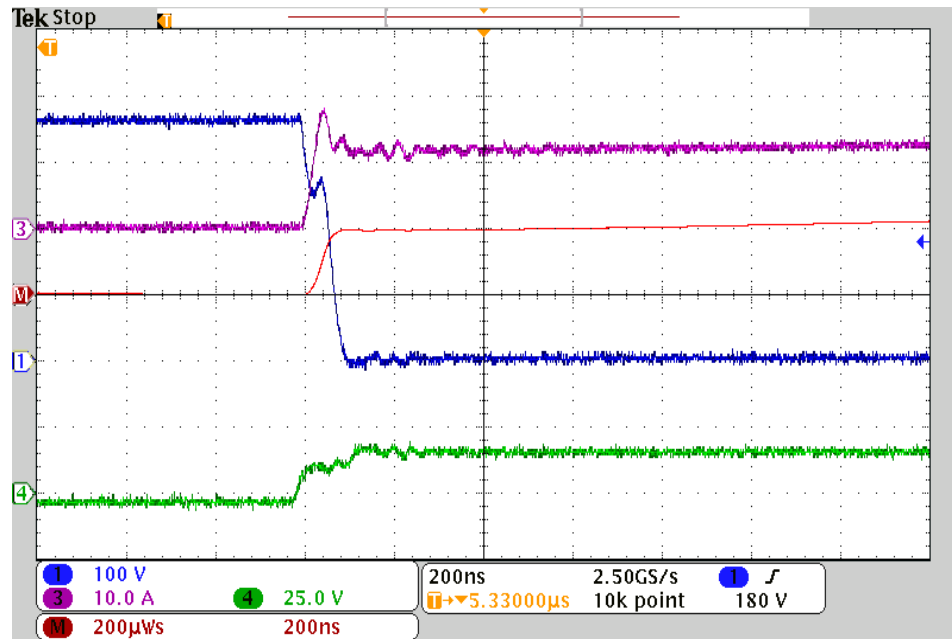
Figure 5.3: Turn-on waveforms of SiC-MOSFET with V_{gs} = –5/+15 V, $R_{g(on)}$ = 15 Ω, and $R_{g(off)}$ = 5 Ω when V_{ds} = 360 V, I_d = 12 A, and T_j = 25°C.
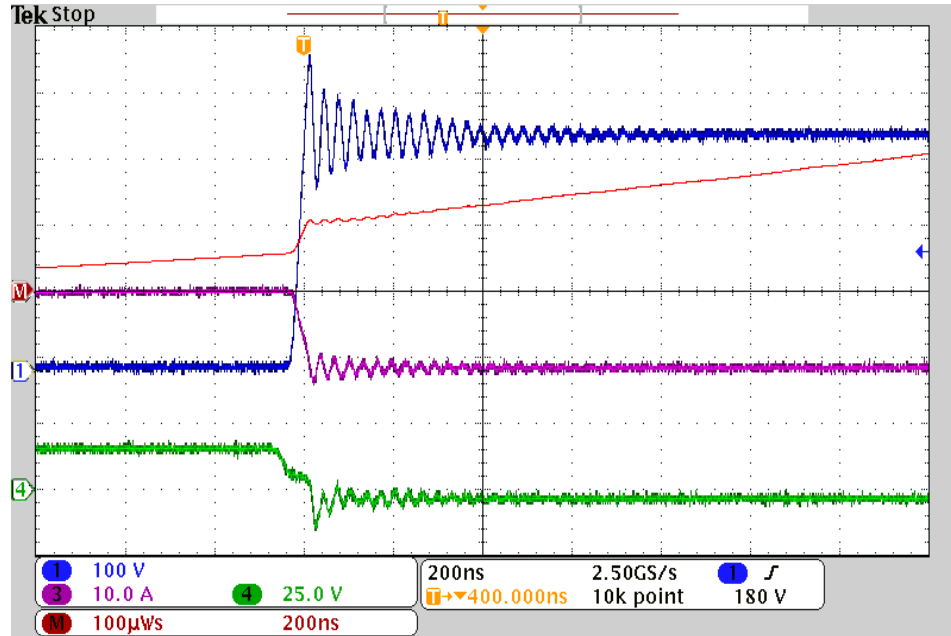
Figure 5.4: Turn-off waveforms of SiC-MOSFET with V_{gs} = –5/+15 V, $R_{g(on)}$ = 15 Ω, and $R_{g(off)}$ = 5 Ω when V_{ds} = 360 V, I_d = 12 A, and T_j = 25°C.

the dv/dt and di/dt are 11.1 kA/μs and 0.3 kA/μs, respectively [5]. The measured turn-on and turn-off energy losses are 96 and 52 μJ, respectively [5].

5.2   Switching Performance Comparison

According to the experimental results, the SiC-MOSFET show a major improvement in the overall switching performance. The SiC-MOSFET offers a significant reduction in switching energy losses compared to the Si-IGBT because the switching time is smaller than the Si device during the turn-on and turn-off events. Though the overshoot and ringing effects in both Si-IGBT and SiC-MOSFET are notable due to high dv/dt and di/dt during the turn-off time, the Si-IGBT shows a very larger overshoot and ringing phenomenon in the drain-source voltage and drain current waveforms during the turn-off event [27]. In the turn-on event, the dv/dt

and di/dt of the Si-IGBT are larger than those in the SiC-MOSFET device. Table 5.2 sums up the switching performance results of the SiC-MOSFET and Si-IGBT in turn-on and turn-off events.

Table 5.2: Switching behavior comparison between Si-IGBT and SiC-MOSFET devices.

	Turn-on event		Turn-off event	
	Si-IGBT	SiC-MOSFET	Si-IGBT	SiC-MOSFET
Switching loss (μJ)	102	96	108	52
dv/dt (kV/μs)	6.4	3.5	6.7	11.1
di/dt (kA/μs)	0.96	0.4	0.21	0.3
Switching time (ns)	84.5	82	120	54

5.3   Switching Energy Loss Assessment

The turn-on and turn-off energy losses of Si-IGBT and SiC-MOSFET are assessed as the gate resistance value, switch current, junction temperature, and DC-bus voltage are increased. The two power devices are tested at the same gate requirements to investigate their switching performance. The gate-driver of Infineon (1EDI60I12AH) is used for driving SiC-MOSFET while the gate-driver of Infineon (1EDI60H12AH) is employed for driving Si-IGBT as the gate-source voltage is –5/+15 V for both devices.

5.3.1   Various Gate Resistance Values

Gate resistance plays a major role in improving the switching performance of power devices because energy loss considerably increases with a high gate resis-

tance and reducing gate resistance can minimize the transient time of the switching device. Although lowering gate resistance can help to decrease the energy loss, the small gate resistance can cause a large overshoot along with a major ringing in the device voltage and current during turn-on and turn-off transitions [27]. The value of gate resistance should be chosen very careful in order to obtain the proper switching operation for power devices. Thus, Si-IGBT and SiC-MOSFET devices are investigated at different gate resistance values.

Table 5.3: Comparison of turn-on and turn-off energy losses between Si-IGBT and SiC-MOSFET at various gate resistance values.

	Turn-on energy loss (μJ)		Turn-off energy loss (μJ)	
Gate resistance	Si-IGBT	SiC-MOSFET	Si-IGBT	SiC-MOSFET
5 Ω	39	20	8	26
10 Ω	49	21	10	27
15 Ω	62	25	14	28
20 Ω	75	27	18	29
25 Ω	98	31	24	30

The Si and SiC semiconductor devices are evaluated at the input voltage of 360 V and switch current of 12 A with increasing gate resistance value, as show in Table 5.3. The turn-on energy losses for the two tested devices are calculated as the turn-on gate resistance increased from 5 to 25 Ω and the turn-off gate resistance is fixed at 5 Ω. At the turn-on gate resistance of 25 Ω, turn-on energy losses of Si-IGBT and SiC-MOSFET are 98 and 31 μ, respectively. On the other hand, the turn-off energy losses for both devices are computed when the turn-off gate resistance is elevated from 5 to 25 Ω and the turn-on gate resistance stays at a fixed value of 5 Ω. At the turn-off gate resistance of 25 Ω, turn-off energy losses of Si-IGBT and SiC-MOSFET are 24 and 30 μ, respectively.
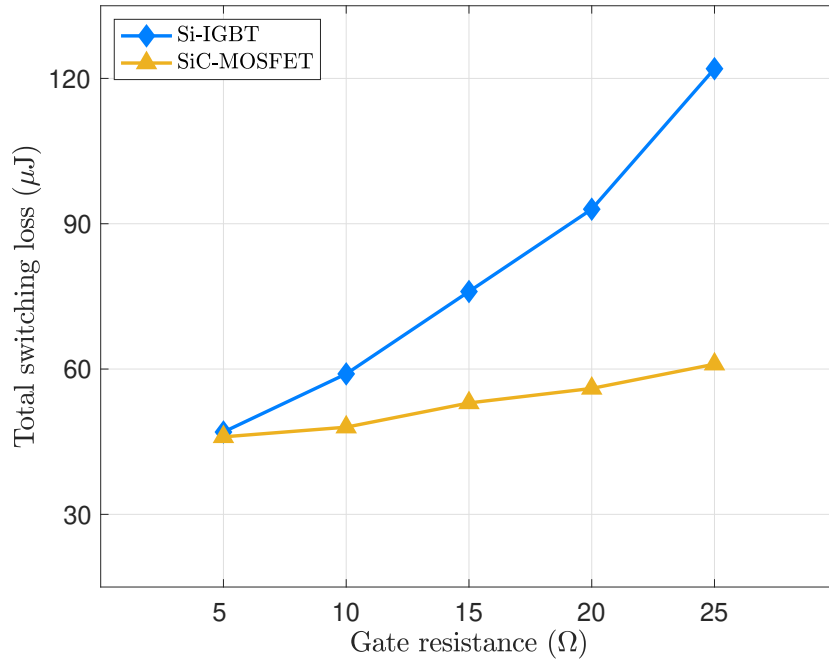
Figure 5.5: Total energy loss of Si-IGBT and SiC-MOSFET as the gate resistance is increased from 5 to 25 V.

Though the turn-off energy losses for both devices are relatively similar, there in a big difference in the turn-on energy losses between the Si and SiC devices at a higher gate resistance value. It is obvious that the SiC-MOSFET achieves 68.4% reduction in the turn-on energy loss compared to the Si-MOSFET at the turn-on gate resistance of 25 Ω. Figure 5.5 shows the total energy loss comparison for both devices at various gate resistances. Therefore, the changing gate resistance value has a significant impact only on the turn-on energy losses for both devices, where SiC-MOSFET provides a lower switching loss throughout different gate resistance values.

Figure 5.6 and Figure 5.7 show dv/dt and di/dt rates for Si and SiC devices during the turn-off and turn-on events when the gate resistance value is increased from

71
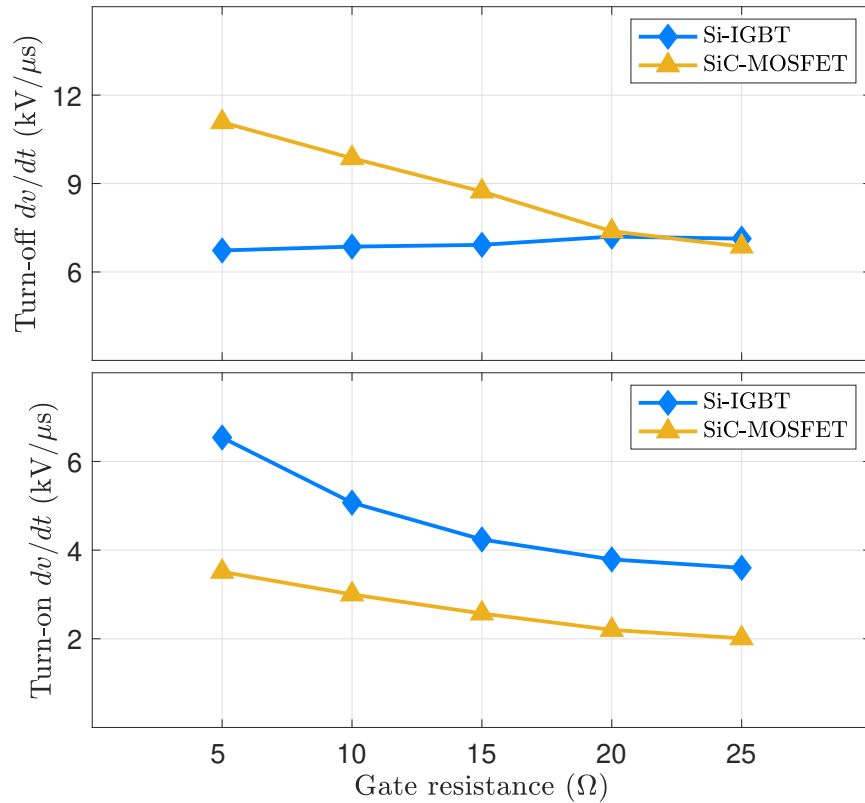
Figure 5.6: Turn-off and turn-on dv/dt of Si-IGBT and SiC-MOSFET as the gate resistance is increased from 5 to 25 Ω.

5 to 25 Ω. It is noted that dv/dt and di/dt rates for Si-IGBT and SiC-MOSFET are reduced by increasing gate resistance value. The SiC-MOSFET exhibits higher dv/dt and di/dt rates during the turn-off transitions because of higher stray parasitic elements and faster switching frequency compared to the Si-IGBT. To reduce the high rates of dv/dt and di/dt for the SiC-MOSFET, the gate resistance during the turn-off and turn-on times should be increased to gain a better switching performance, leading to improved power converters.
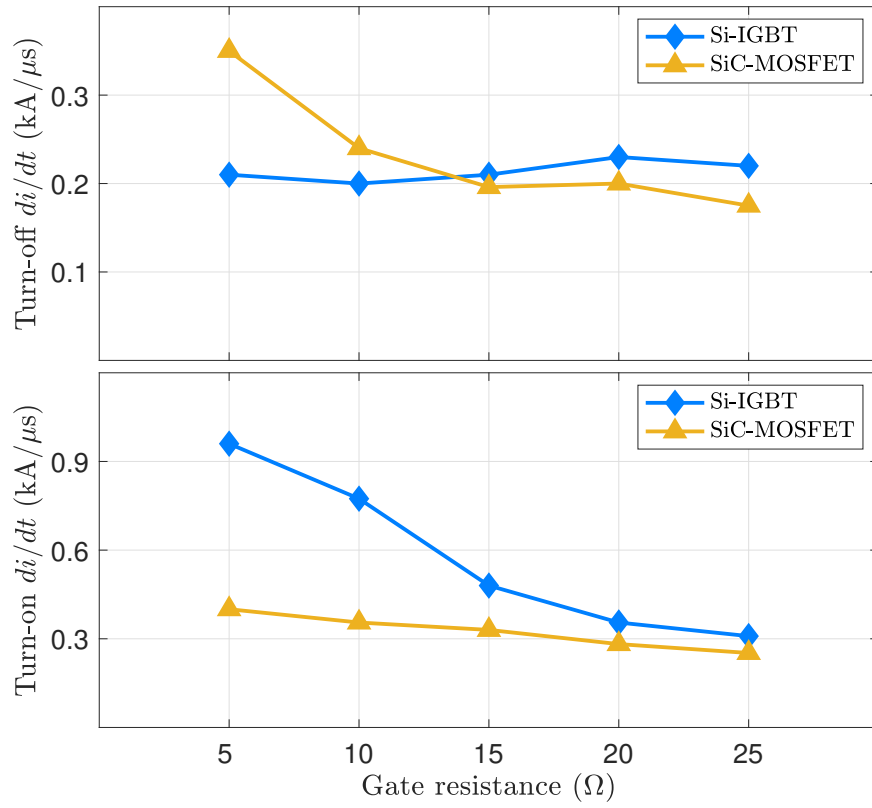
Figure 5.7: Turn-off and turn-on di/dt of Si-IGBT and SiC-MOSFET as the gate resistance increased from 5 to 25 Ω.

5.3.2 Various Switch Currents

Si-IGBT and SiC-MOSFET are performed and tested through DPT circuit under the input voltage of 360 V and junction temperature of 25°C as the switch current is increased from 4 to 12 A [63]. The turn-on and turn-off gate resistance values for each device are selected to be 5 and 15 Ω. Figure 5.8 illustrates that turn-on and turn-off energy losses for Si and SiC devices are increased in conjunction with increasing switch current. Although the turn-on energy loss of two tested devices is quite similar, the turn-off energy loss of the Si-IGBT is significantly higher than

the turn-off loss of the SiC-MOSFET, particularly after the switch current is exceed 6 A.
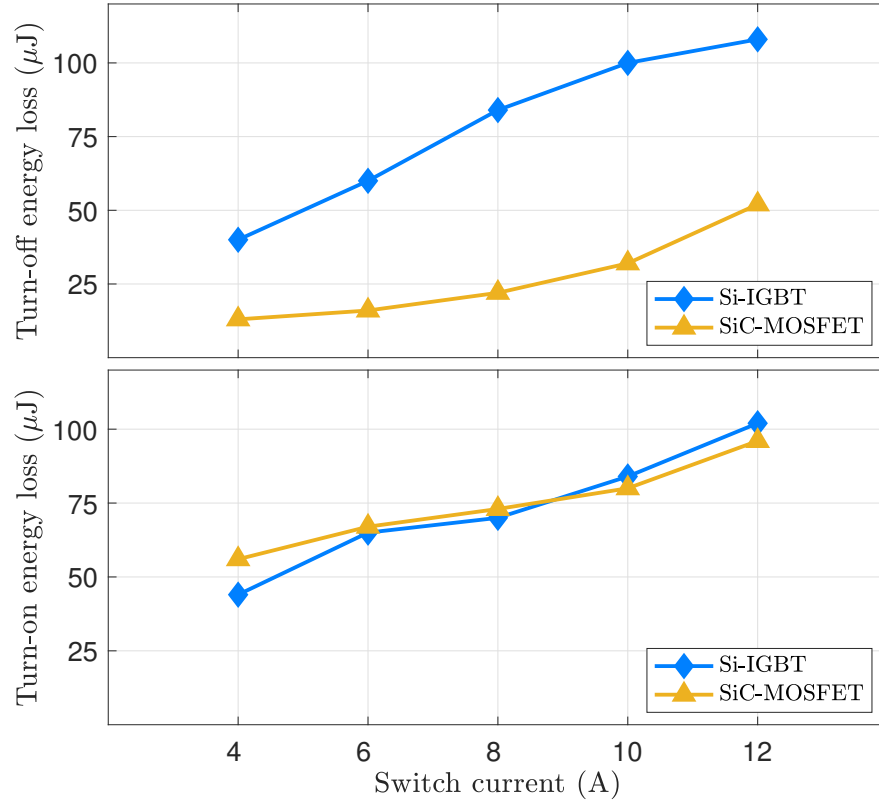
Figure 5.8: Turn-off and turn-on energy losses of Si-IGBT and SiC-MOSFET as the switch current is increased from 4 to 12 A.

Table 5.4 highlights a comparison of total switching energy loss of the two devices at different switch currents, which can have a major impact on the energy loss. As the switch current increases, the total energy loss of the two devices increases linearly [27]. Nevertheless, the total energy loss of the SiC-MOSFET is remarkably reduced by 29.5% compared to the total energy loss of the Si-MOSFET at the switch current of 12 A [63]. The high reduction in the total loss of the SiC-MOSFET results from its lower internal gate resistances and smaller input capaci-

tance. Therefore, SiC device is enabling power converter to work at a higher current with much lower energy loss.

Table 5.4: Total energy loss of Si-IGBT and SiC-MOSFET at various switch currents.

	Total switching energy loss (μJ)	
Switch current	Si-IGBT	SiC-MOSFET
4 A	84	69
6 A	125	82
8 A	154	95
10 A	184	112
12 A	210	148

5.3.3 Various Junction Temperatures

The effect of raising operating temperatures on switching total energy losses for Si and SiC power switches is investigated through the hotplate utilizing to heat only the device under test while the entire DPT circuit is placed in the room temperatures. For the safe operation, the heat sink of the tested device is connected to the hot plate by an external heat sink in order to increase the operation temperature. Figure 5.9 presents the turn-on, turn-off, and total energy losses of each device increase as function of increasing junction temperature from 50 to 150°C. It is obvious that switching energy losses of Si-IGBT and SiC-MOSFET increase significantly as the junction temperature is raised. However, the SiC-MOSFET provides smaller switching energy losses compared to the Si-MOSFET throughout different junction temperatures. Figure 5.10 illustrates that the total loss of the SiC-MOSFET is reduced by 35.4% compared to the Si-IGBT at the temperature of 150°C. Thus, SiC

device shows an excellent switching performance with remarkably lower energy losses at higher operating temperatures.
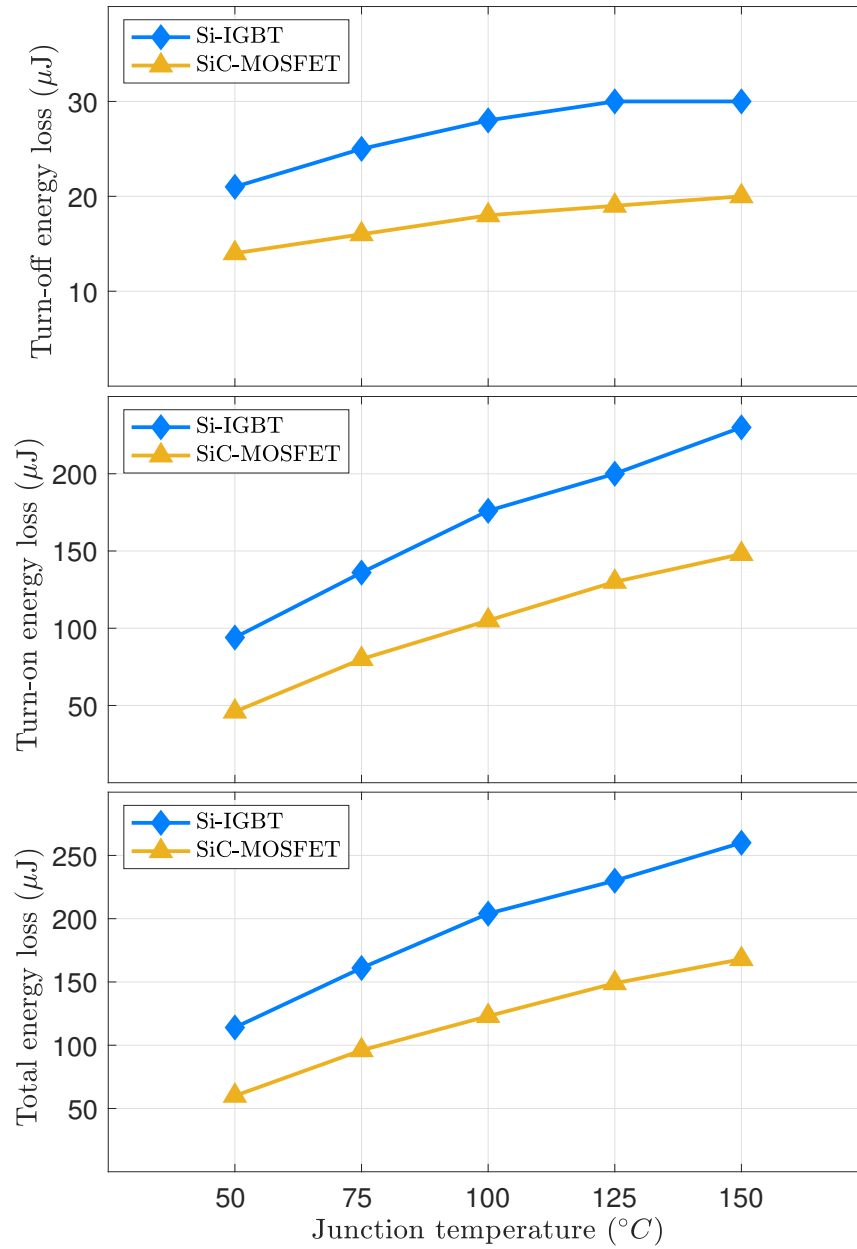
Figure 5.9: Turn-on, turn-off, and total energy losses of Si-IGBT and SiC-MOSFET as the junction temperature increased from 25 to 150°C.
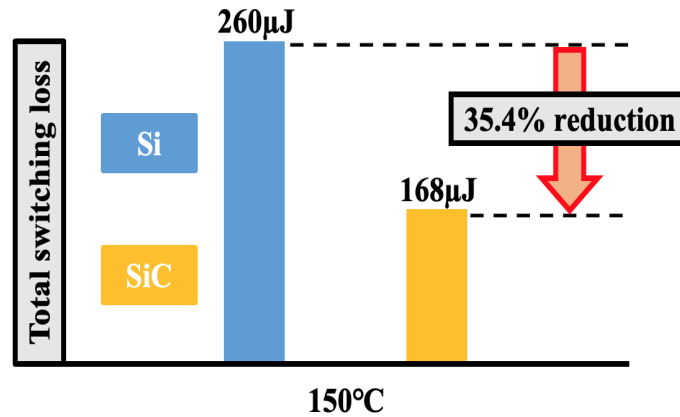
Figure 5.10: Total energy loss of Si-IGBT and SiC-MOSFET at the junction temperature of 150°C.

5.3.4 Various DC-bus Voltages

The total energy losses of Si-IGBT and SiC-MOSFET are analyzed at the switch current of 10 A and operating temperature of 25°C at a high DC-bus voltage. The switching energy losses are measured by integrating the instantaneous power during turn-on and turn-off times [72], as the previously mentioned. Table 5.5 shows a comparison of turn-on and turn-off energy losses as the DC-bus voltage is increased by the high-voltage DC power supply from 200 to 360 V. It is noted that the both energy losses for Si-IGBT and SiC-MOSFET are increased in conjunction with increasing the DC-bus voltage. Figure 5.11 illustrates that the total energy loss for Si and SiC devices is significantly increased, particularly after the DC-bus voltage exceeds 280 V. Nevertheless, the SiC-MOSFET offers a lower total energy loss at different DC-bus voltages. Compared to the Si-IGBT, the SiC-MOSFET has a considerable reduction in the total energy loss by nearly 47% at the DC-bus voltage of 360 V and switch current of 10 A. Therefore, SiC device exhibits improved

switching performance along with highly minimized turn-on and turn-off energy losses at a higher DC-bus voltage.

Table 5.5: Comparison of turn-on and turn-off energy losses between Si-IGBT and SiC-MOSFET at various DC-bus voltages.

DC-bus voltage	Turn-on energy loss (μJ)		Turn-off energy loss (μJ)	
	Si-IGBT	SiC-MOSFET	Si-IGBT	SiC-MOSFET
200 V	43	49	60	21
240 V	50	59	64	22
280 V	57	67	76	25
320 V	70	73	92	29
360 V	102	80	108	32
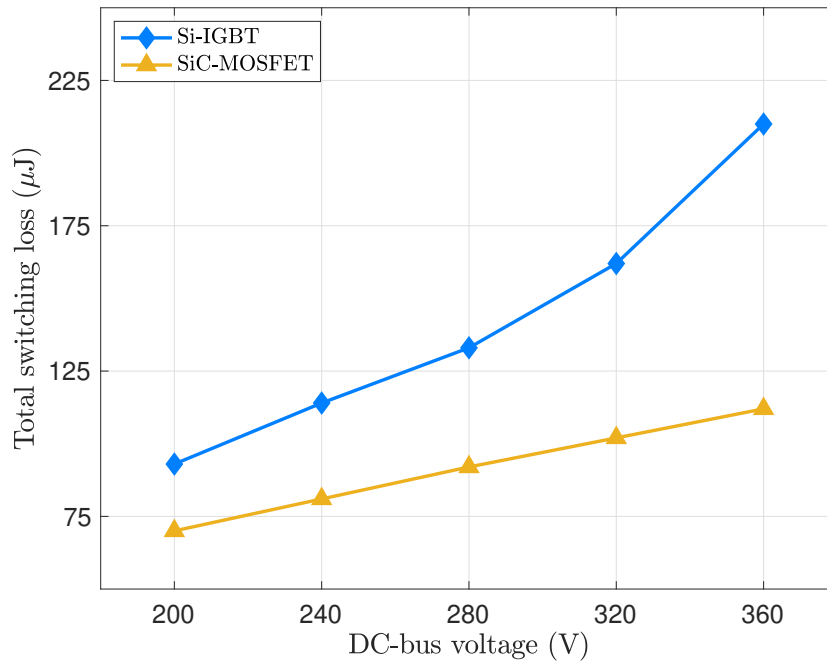
Figure 5.11: Total switching energy loss of Si-IGBT and SiC-MOSFET as the DC-bus voltage increased from 200 to 360 V.

5.4   Summary

The energy loss for Si-IGBT and SiC-MOSFET during turn-on and turn-off events is evaluated through the DPT circuit. The turn-on and turn-off, total energy losses of the Si and SiC semiconductors are investigated at different operating points of a gate resistance value, switch current, junction temperature, and DC-bus voltage because these high operating capabilities are very important factors for power conversion systems. The SiC-MOSFET shows a remarkable reduction in total energy loss compared to the Si-IGBT at harsh operating conditions. The results reveal that the SiC-MOSFET exhibits better switching characteristics along with lower switching energy losses compared to the Si-MOSFET. Thus, SiC power devices substantially enhance the switching performance of the converters used in high-power and high-temperature applications.

Chapter 6

Overview of Bidirectional DC–DC Power Converters

This chapter presents the background description and state-of-the-art of bidirectional DC–DC converters to expound this research and its novelty. It begins with describing bidirectional DC–DC power converters, including isolated and non-isolated bidirectional topologies. Due to appealing advantages and wide implementation of non-isolated bidirectional topologies in medium-voltage applications, this dissertation mainly focuses on the non-isolated converters. Various non-isolated bidirectional DC–DC converters are demonstrated and compared to find an optimal choice for power converters employed in DC microgrids. The operation and analysis of the bidirectional DC–DC power converter are described in this dissertation along with design considerations.

6.1 State-of-the-art of Bidirectional DC–DC Converter Technology

DC microgrids, energy storage elements, automotive applications, and renewable energy systems are essentially required integrating bidirectional power converters in order to ensure the power flow in forward and reverse directions between energy storage elements and DC-buses at different voltage and current levels [132]. Figure 6.1 depicts a typical DC microgrid where bidirectional power electronics are widely implemented [5]. Bidirectional converters play a pivotal role in interfacing DC microgrid, including various distributed energy systems, with utility networks and they control power flow and microgrid operation during the grid-connected mode and islanding mode [5, 133]. These converters are indispensable parts in automotive systems and energy storage devices to provide different voltage ratios between input and output along with improving the power conversion system and the stability of the DC microgrid [5, 134]. In addition, bidirectional power converters are widely incorporated in the most exciting distributed renewable energy systems that are utilized batteries or super-capacitors in order to compensate the variability of alternative energy sources, such as PV and wind, and also to provide a stable and smooth power flow to the load [135, 136]. Therefore, the bidirectional power converters are attracted a great deal of interests in diverse applications due to their remarkable capabilities of grid synchronization, power management and bidirectional power flow operation.

The worldwide development and rapid penetration of renewable energy systems, energy storage devices, electric vehicle applications pose increasing require-
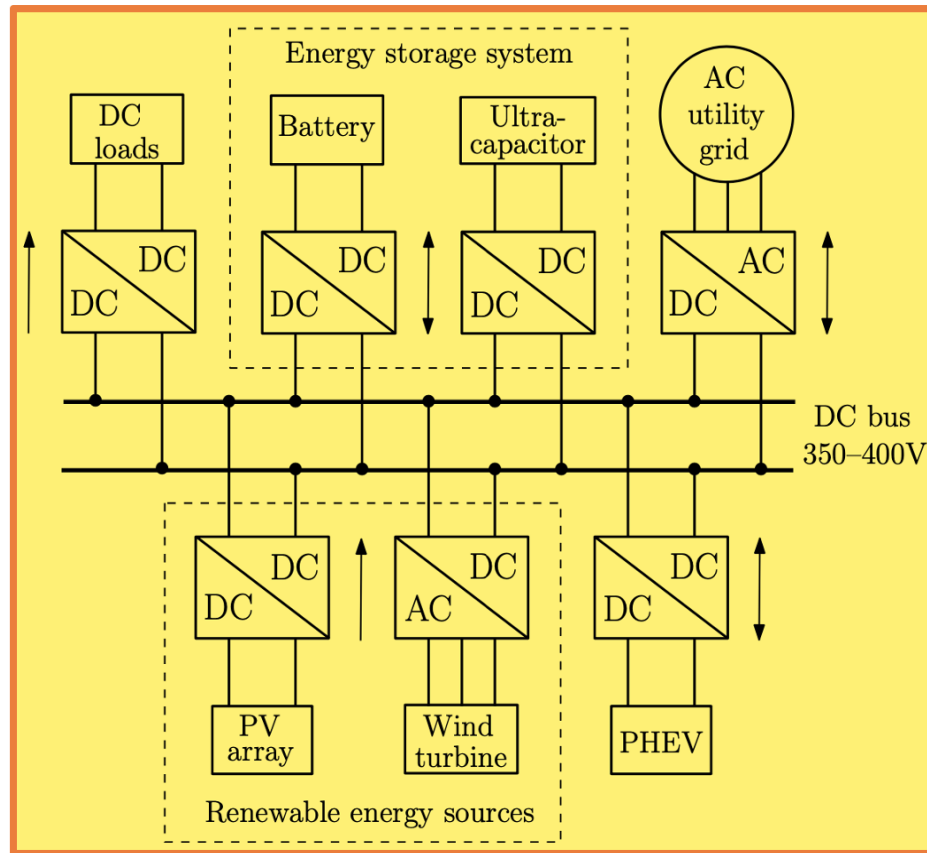
Figure 6.1: A typical DC microgrid system where various bidirectional converters are used [139].

ments and demands for bidirectional DC–DC converters as the majority of these sources are DC power, especially in distribution sectors [137–139]. By connecting different power sources with energy storage elements or DC buses, bidirectional converter topology considerably minimizes the system size and enhances the performance of energy efficiency as it avoids using two individual power converters for forward and reverse power flows [140, 141]. Based on the position of the energy storage devices, the bidirectional DC–DC converter works as either a buck or boost mode, where control operating system is performed to regulate the current or voltage into a desired level [142, 143]. Bidirectional DC–DC converters

are basically divided into two main categories depending on their input circuitry. The first one is a current-fed bidirectional power converter, which has an input inductor acting as a current source at the input circuit [144]. The second one is a voltage-fed bidirectional power converter, which has a capacitor acting as a voltage source at its terminals. Based on the galvanic isolation between the input and output voltage [145], bidirectional DC–DC power converters are classified into two major groups of structures which are non-isolated and isolated converters [5], as shown in Figure 6.2.
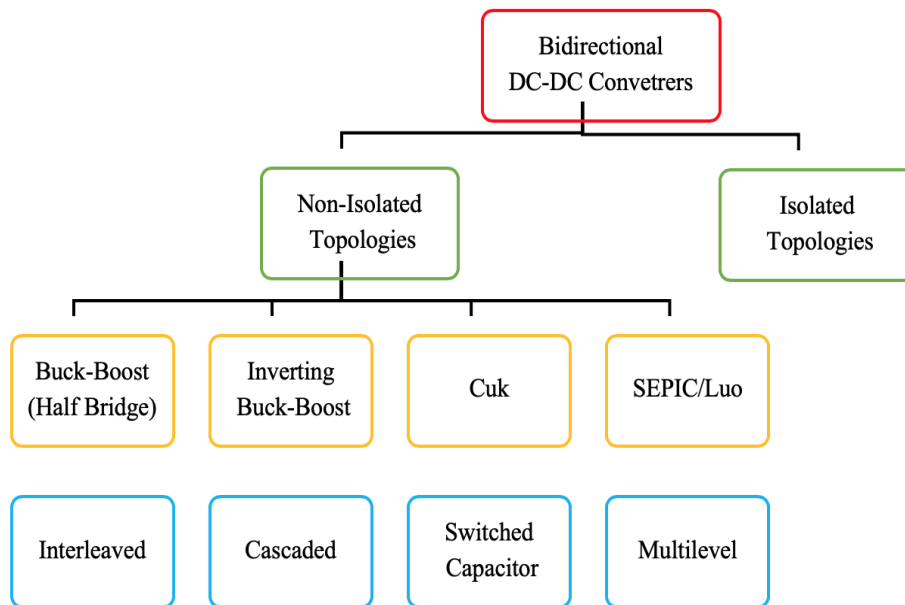
Figure 6.2: Bidirectional DC-DC converter topology classification.

6.1.1   Isolated Bidirectional DC–DC Converters

Electrical galvanic isolation is a significant feature for a wide range of high-switching speed and high-power density applications, especially in grid-tied DC–DC converters, that require a reliable power transfer with major noise and electro-

magnetic interference (EMI) reductions. Based on the safety standard that is applicable a large number of power conversion systems, the voltage level of galvanic isolation between the input and output side of power converters can be accomplished by either a coupled inductor or transformer. The safety factor is considered a major concern in numerous applications such as avionics, military, medical systems containing some sensitive DC loads, which can susceptible to any noise and fault. Voltage matching is also highly required in these applications for designing and optimizing the voltage level between different stages of eclectic power system.
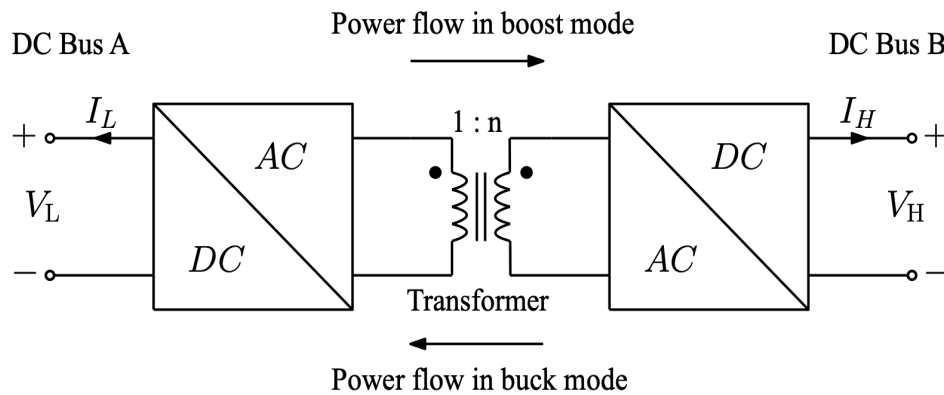
Figure 6.3: Isolated bidirectional DC–DC power flow illustration.

Predominantly, the electrical galvanic isolation is necessary since it offers isolation between the input- and output-side voltage along with a high conversion gain ratio as well as the benefits of implementing multi-input or multi-output converters [145]. However, the main drawbacks of these isolated converters are high weight and cost along with low energy efficiency due to the leakage inductance effects, resulting from the transformer. The power flow of the isolated bidirectional DC–DC power converters is illustrated in Figure 6.3. In this category, the isolated bidirectional converters essentially convert the DC voltage level to AC voltage going through the magnetic component of a transformer to rectify the AC waveform to

DC waveform [145]. Compared to the non-isolated topologies, the isolated converter topologies have commonly higher voltage gain ability.

6.1.2 Non-Isolated Bidirectional DC–DC Converters

Non-isolated, which is known as transformer-less, bidirectional DC–DC converters are increasingly gaining a lot of attention due to the acute need to power electronics with high efficiency and bidirectional power flow capability between two DC buses or energy storage sources [5]. The power flow of the non-isolated bidirectional DC–DC converters is illustrated in Figure 6.4 [5]. Because these converters do not implement electrical galvanic isolation in their configuration, they outstandingly exhibit the appealing advantages of straightforward structure, light weight, increased efficiency, improved power density, reduced size, and minimized cost [5, 27].

Power flow in boost mode
$(I_L < 0, I_H > 0)$

DC Bus A

DC Bus B

I_L

I_H

$+$

DC

$+$

V_L

V_H

DC

$-$

$-$

Power flow in buck mode
$(I_L > 0, I_H < 0)$
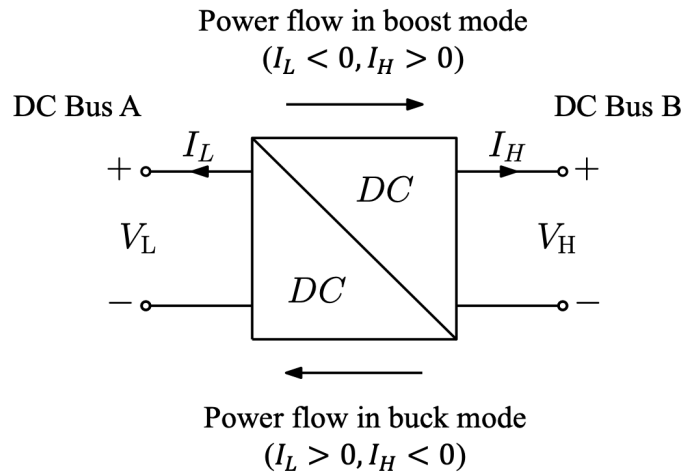
Figure 6.4: Non-isolated bidirectional DC–DC power flow illustration.

Owing to their remarkable advantages, non-isolated bidirectional DC–DC power converters are rapidly used in low-to-medium power applications such as renewable

energy conversion systems, battery energy storages, UPS, fuel cell energy systems, and hybrid electric vehicles (HEV), where the efficiency, size, weight are major concerns. Non-isolated bidirectional DC–DC power converters are categorized into main topologies such as buck-boost (half-bridge) converter, inverting buck-boost converter, Cuk converter, SEPIC/Luo converter, interleaved converter, cascaded converter, switched capacitor converter, and multilevel converter. Table 6.1 presents the key comparison of all non-isolated bidirectional DC–DC power converters. Figure 6.5 depicts the most commonly used bidirectional DC–DC topologies in medium-voltage applications. They are buck-boost (half-bridge) converter, inverting buck-boost converter, interleaved converter, and cascaded converter.
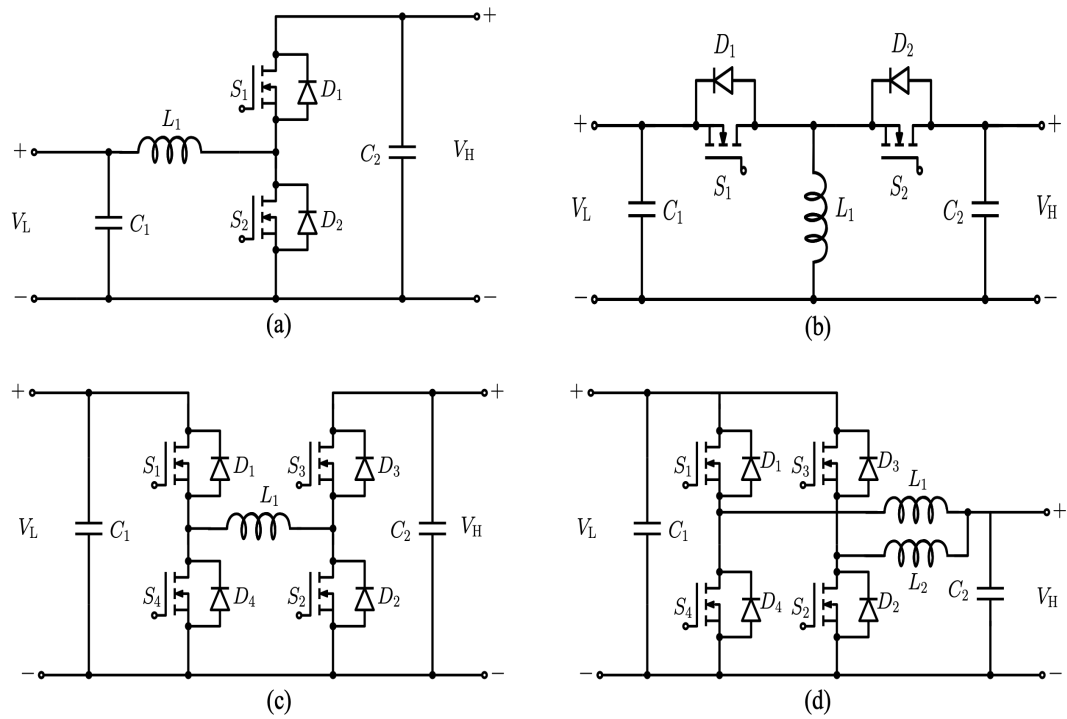
Figure 6.5: Commonly used non-isolated DC–DC bidirectional topologies: (a) basic buck-boost (half-bridge) converter, (b) inverting buck-boost converter, (c) interleaved converter, and (d) cascaded converter.

Table 6.1: Comparison of non-isolated bidirectional DC–DC converters.

Bidirectional topology	V_L/V_H (buck mode)	V_H/V_L (boost mode)	Switch	L	C
1.Basic buck-boost converter	d	$1/(1-d)$	2	1	2
2.Inverting buck-boost converter	$-d/(1-d)$	$-d/(d-d)$	2	1	1
3.Cuk converter	$-d/(1-d)$	$-d/(1-d)$	2	2	3
4.SEPIC/Luo converter	$d/(1-d)$	$d/(1-d)$	2	2	2
5.Interleaved converter	d	$1/(1-d)$	4	2	2
6.Cascaded converter	d	$1/(1-d)$	4	1	2
7.Switched-capacitor converter	1/2	2	4	0	3
8.Multilevel converter	$n/2$	n	$n(n+1)$	0	$n(n+1)/2$

6.2 Converter Operation and Modeling

Fundamentally, the non-isolated bidirectional DC–DC buck-boost converter is derived from the unidirectional counterpart by replacing a diode with a full controllable switch in its structure. In DC microgrid and storage systems, this converter is capable of providing a bidirectional power flow between DC buses and energy storage elements along with a flexible control system for charge and discharge operations [27]. Figure 6.6 depicts the schematic of the non-isolated bidirectional

buck-boost converter, which is connecting a low-side voltage (V_L), such as a bat-teries or super-capacitor, with a high-side voltage (V_H), like DC link or bus. This converter is composed of one inductor (L), two capacitors (C_1, C_2) for low- and high-side voltages, two switching devices (S_1, S_2), and two anti-parallel diodes (D_1, D_2), acting as free-wheeling diodes [5].

The bidirectional converter performs as a buck converter (discharge mode) from the low voltage to high voltage level and it works as a boost converter (charge mode) when operating in the reverse direction [5]. In the bidirectional DC–DC buck-boost converter, the inductor is considered the main energy transfer element, which is accountable for the output current ripple [5]. This converter can step-down or step-up the voltage depending on the status of two power switching devices, such as MOSFETs and IGBTs, combined with anti-parallel diodes, which are acting as freewheeling diodes, respectively [5]. As the bidirectional buck-boost converter is assumed to work in the continuous conduction mode (CCM), the principle opera-tion of the bidirectional buck-boost converter can be demonstrated in the two main modes, as follows:
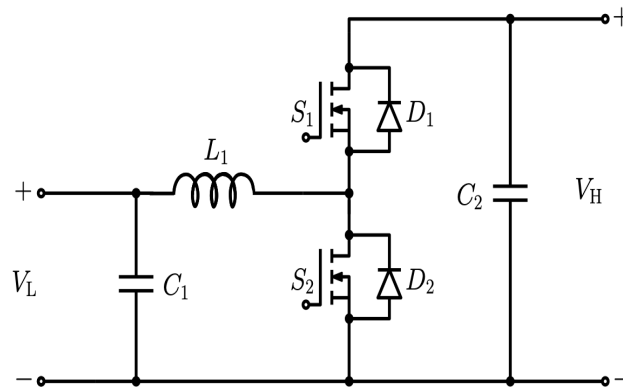
Figure 6.6: Structure of a non-isolated bidirectional DC–DC buck-boost converter.

- **Buck (charge) mode:** The upper S_1 switch and the lower D_2 diode operate as a buck converter with energy flowing from the high-side voltage to the low-side voltage so the battery is charged during regenerative braking period, whereas the lower S_2 switch and upper D_1 diode are turned off all the time. Figure 6.7(a) illustrates the operation of the bidirectional buck-boost converter in the charge mode. The buck mode can be divided into two intervals depending on the conduction of the S_1 switch and D_2 diode. In the first interval, the S_1 switch is turned on while the S_2 switch is turned off and the D_1 and D_2 diodes are reversed. The inductor gets charged up linearly by the high voltage. The low-side capacitor also gets charged, causing that the inductor current is increased linearly with slope. In the second interval, the D_2 diode is conducting while the S_1 and S_2 switches are turned off and the D_1 diode is reversed. The inductor current starts to decrease linearly with slope as it is passing through the freewheeling diode D_2. Therefore, the voltage across the battery is stepped down compared with the high voltage.

- **Boost (discharge) mode:** The lower S_2 switch and upper D_1 diode work as a boost converter with energy flowing from the low-side voltage to the high-side voltage so the battery is discharged during this duration, whereas the upper S_1 switch and lower D_2 diode are turned off all the time. Figure 6.7(b) illustrates the operation of the bidirectional buck-boost converter in the discharge mode. The boost mode can be divided into two intervals depending on the conduction of the S_2 switch and D_1 diode. The operating waveforms for the non-isolated bidirectional DC–DC buck-boost converter in boost mode at CCM are plotted in Figure 6.8. In the first interval, the S_2 switch is turned on while the S_1 switch is turned off and the D_2 diodes is reversed. The lower

voltage battery charges the inductor element and the inductor current is increasing linearly as long as the S_2 switch is conducting. Because the diode D_1 is reversed biased in the discharge mode as well as the switch S_1 is turned off, the current is not passing through the switch S_1. In the second interval, the D_1 diode is conducting while the S_1 and S_2 switches are turned off and the D_2 diode is reversed. The inductor current starts to decrease linearly with slope. As the inductor is discharged, the high-side capacitor begins to be charged by the current discharging from the battery. Thus, the output voltage at the high side is stepped up compared to the low-side voltage.
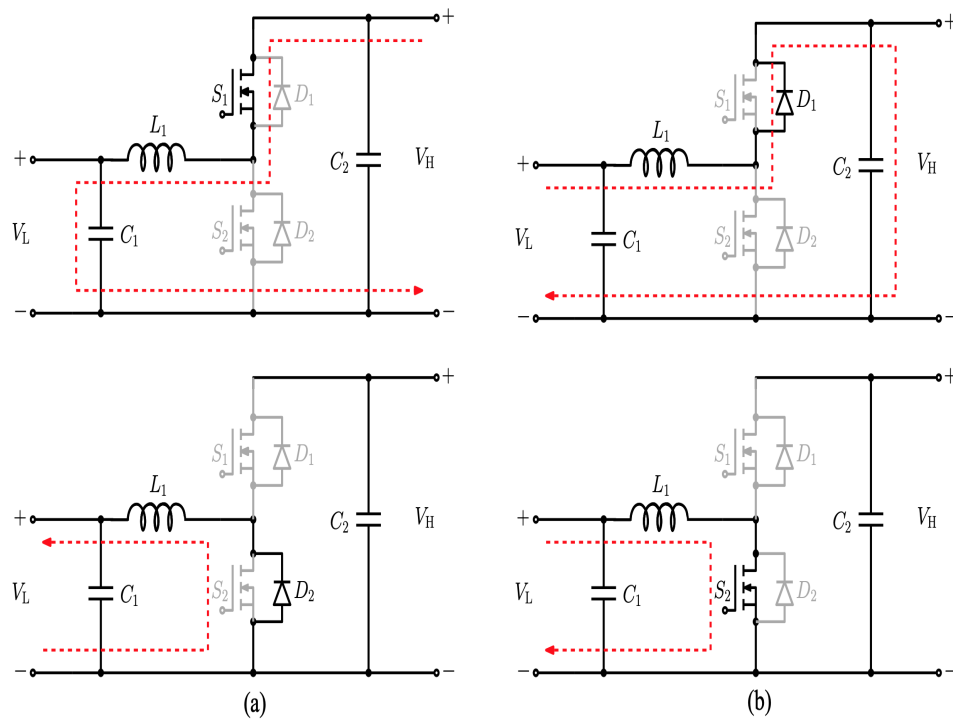
Figure 6.7: Non-isolated bidirectional DC–DC buck-boost topology: (a) buck mode operation and (b) boost mode operation.

The voltage of energy storage element, such as a battery and ultra-capacitor, is lower than the voltage of the DC link or bus. The polarity and output voltage of the
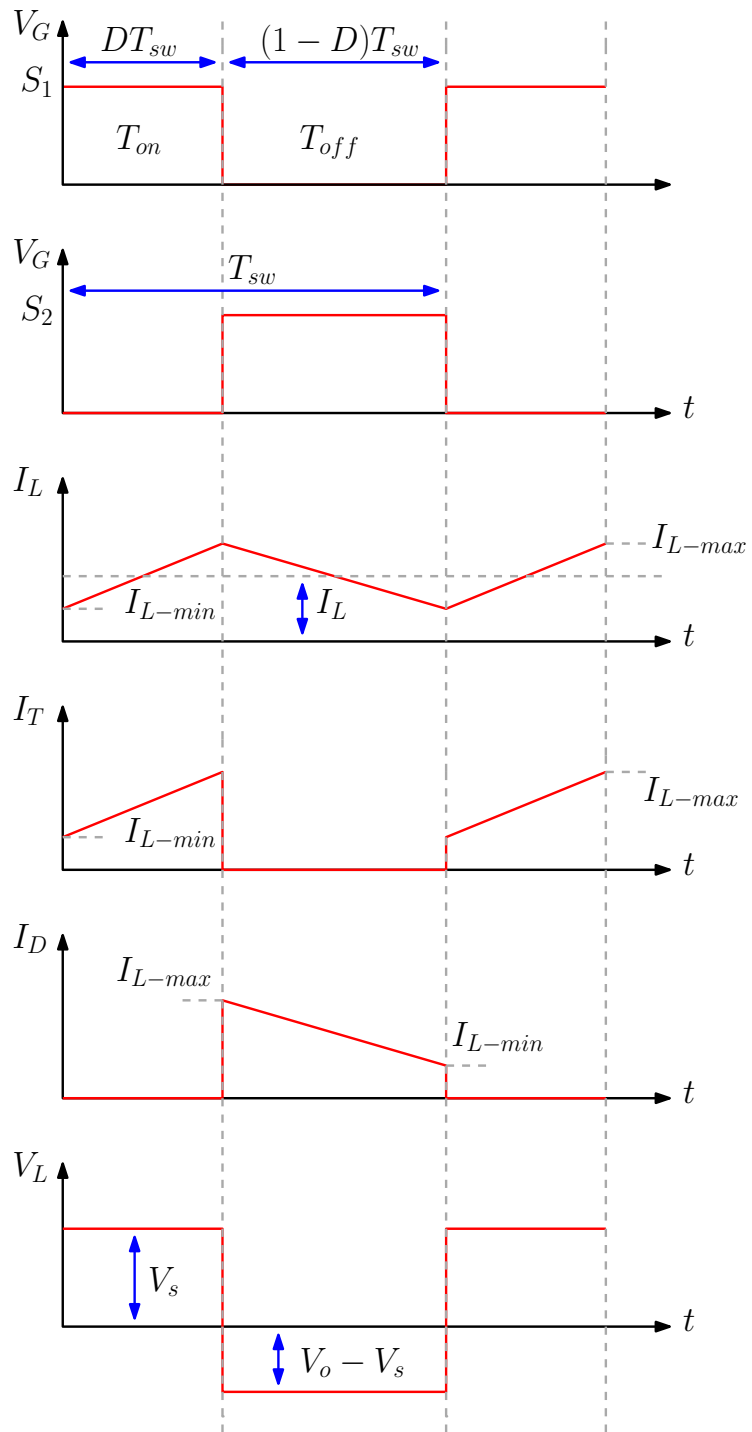
Figure 6.8: Operating waveforms for the non-isolated bidirectional DC–DC buck-boost converter in boost mode at CCM.

energy storage systems set to be the same with respect to the common ground in DC microgrid. The bidirectional buck-boost converter is linked the energy storage device at the low-side voltage with the DC bus at high-side voltage. In the discontinuous conduction mode (DCM), the bidirectional converter is required to operate at high switching frequency with a sufficient filtering capacitor on both sides in order to obtain a smooth output power. The low-side and high-side voltages could be operating at a fixed duty cycle of power switching devices, such as MOSFETs and diodes, assuming that the voltage drop across these devices is neglected. The duty cycle (d) during the switching time (T_{sw}) of bidirectional DC–DC buck-boost converter is presented as follows:

$$d = \frac{t_{on}}{T_{sw}} \tag{6.1}$$

$$(1 - d) = \frac{t_{off}}{T_{sw}} \tag{6.2}$$

$$T_{sw} = t_{on} + t_{off} = \frac{1}{f_{sw}} \tag{6.3}$$

where t_{on} and t_{off} are the time-on and time-off while f_{sw} is the switching frequency.

The analysis of the bidirectional converter is presented in the steady-state operation at the buck and boost modes, considering the average modeling values. The average inductor voltage along with the net change in the inductor current are considered to be zero for periodic operation. In the buck-mode operation, the derivative of the current flowing in the inductor is a positive constant during the first interval as the S_1 switch is turned on, as follows:

$$\frac{\Delta i_L}{\Delta t} = \frac{\Delta i_L}{d\,T_{sw}} = \frac{V_H - V_L}{L} \tag{6.4}$$

where V_L and V_H are the low-side and high-side voltages while Δi_L is the inductor ripple current, which is equal to the low-side current. In the second interval, the derivative of the inductor current is a negative constant as the S1 switch is turned off, as follows:

$$\frac{\Delta i_L}{\Delta t} = \frac{\Delta i_L}{(1 - d)\,T_{sw}} = \frac{-V_L}{L} \tag{6.5}$$

Since the net change in the inductor current is considered to be zero over one period, the relationship between low-side and high-side voltages is described, as follows:

$$(\frac{V_H - V_L}{L})\,d\,T_{sw} + (\frac{-V_L}{L})\,(1 - d)\,T_{sw} = 0 \tag{6.6}$$

$$V_H = \frac{V_L}{d} \tag{6.7}$$

To obtain an efficient power conversion, the duty ratio should remain smaller than the unity. Therefore, the converter in the buck mode is capable of converting an output voltage to equal or less than the input voltage level. In the meantime, the converter in the boost-mode is able to converter an output voltage to equal or larger than the input voltage level. In the boost-mode operation, the derivative of the current passing through the inductor is a positive constant during the first interval as the S_2 switch is turned on, as follows:

$$\frac{\Delta i_L}{\Delta t} = \frac{\Delta i_L}{d\, T_{sw}} = \frac{V_L}{L} \tag{6.8}$$

In the second interval, the derivative of the inductor current is a negative constant as the S_2 switch is turned off, as follows:

$$\frac{\Delta i_L}{\Delta t} = \frac{\Delta i_L}{(1-d)\, T_{sw}} = \frac{V_L - V_H}{L} \tag{6.9}$$

Since the net change in the inductor current is considered to be zero over one period, the relationship between low-side and high-side voltages is described, as follows:

$$(\frac{V_L}{L})\, d\, T_{sw} + (\frac{V_L - V_L}{L})\, (1-d)\, T_{sw} = 0 \tag{6.10}$$

$$V_H = \frac{V_L}{(1-d)} \tag{6.11}$$

Furthermore, the state-space averaging method is applied for the modeling of the bidirectional DC–DC buck-boost converter in the balanced current and small ripple assumptions as well as the dead-time effect and the variation of conduction voltage drop in bidirectional power flow directions are neglected [5]. It is noteworthy that the inductor parasitic resistance (R_{lp}) and on-state resistance ($R_{ds(on)}$) are involved in this model because they exhibit a critical impact on converter performance [5]. As shown in Figure 6.6, there are three energy storage elements, which are inductor, low-side capacitor, and high-side capacitor. The size of the inductor and two capacitors depends on the maximum allowable ripple in the inductor current and the capacitor voltage [5]. The converter can operate either charge or

discharge mode while each mode has always two intervals [5]. In the buck mode, when the S_1 switch is turned on and the S_2 switch is turned off, inductor voltage across the inductor and capacitor currents are illustrated, as follows [5]:

$$L \frac{di_L}{dt} + di_L \left(R_{lp} - R_{ds(on)} \right) = v_{c2} - v_{c1} \tag{6.12}$$

$$C_1 \frac{dv_{c1}}{dt} = i_L - \frac{v_{c1} - V_L}{R_L} \tag{6.13}$$

$$C_2 \frac{dv_{c2}}{dt} = -(i_L + \frac{v_{c2} - V_H}{R_L}) \tag{6.14}$$

Where v_{c1} and v_{c2} are low- and high-side capacitor voltages, R_L and R_H are low- and high-side resistive loads [5]. In the boost mode, when the S_2 switch is turned on and the S_1 switch is turned off, inductor voltage across the inductor and capacitor currents are described, as follows [5]:

$$L \frac{di_L}{dt} + di_L \left(R_{lp} - R_{ds(on)} \right) = -v_{c1} \tag{6.15}$$

$$C_1 \frac{dv_{c1}}{dt} = i_L - \frac{v_{c1} - V_L}{R_H} \tag{6.16}$$

$$C_2 \frac{dv_{c2}}{dt} = -\frac{v_{c2} - V_H}{R_H} \tag{6.17}$$

95

6.3 Converter Design and Considerations

Among various non-isolated bidirectional DC–DC topologies, the bidirectional buck-boost converter is tremendously utilized in DC microgrids, which provides a sustainable approach for implementing renewable energy, automotive, and energy storage applications. This converter contains outstanding advantages of simpler structure, higher efficiency, smaller volume, lighter weight, and lower cost due to the straightforward operation principle and minimum components used in the power converters. In this dissertation, the basic background description and review of the state-of-the-art bidirectional DC–DC power converters are demonstrated firstly to elucidate the scope of this research and its novelty. As the critical challenges of the bidirectional buck-boost converter was previously specified in chapter 1, WBG semiconductor technology is exploited in order to mitigate converter issues related to switching performance and energy efficiency. The improved converter is proposed with the advantages of integrating a new cascode GaN power devices along with SiC-Schottky diodes for high-power and high-frequency bidirectional converter applications.

Table 6.2: Main specifications for the bidirectional DC–DC buck-boost converter.

Converter parameter	Symbol	Value
Rating power	P_r	500 W
High-side (DC bus) voltage	V_H	400 V
Low-side (Battery) voltage	V_L	48 – 96 V
Switching frequency	f_{sw}	40 – 200 kHz
Inductor	L	20 mH
Low-side and high-side capacitors	C_1, C_2	16 μF

Table 6.2 highlights the converter specifications, which are compatible with renewable energy sources and energy storage applications employed in DC microgrid systems [5]. The converter is designed to work in continuous conduction mode in order to investigate the impacts of various semiconductors on the converter performance [5, 27]. The size of reactive components, such as capacitors and inductors, is characterized based on their optimal values determined in the buck-mode and boost-mode operation, taking different switching frequencies into consideration [5].

6.4   Summary

The background description and state-of-the-art of bidirectional DC–DC converters are demonstrated in order to show their important role in power conversion systems, especially in distribution sector. Because of bidirectional converter capabilities, a large number of new applications, such as energy storage elements, UPS, HEV, and renewable energy systems, are increasingly implemented in DC microgrids. The classification of bidirectional DC–DC converter topologies, including isolated and non-isolated bidirectional topologies, is described with their disadvantage and advantage. Due to the widespread integration of non-isolated bidirectional topologies in medium-voltage applications, various non-isolated bidirectional DC–DC converters are focused and compared in this chapter. The operation and modeling of bidirectional DC–DC buck-boost converters are comprehensively presented because of their remarkable benefits among other converters employed in DC microgrids. The converter design and its operating considerations are illustrated to accomplish the experimental results.

Chapter 7

Bidirectional Converter Evaluation Based on WBG Technology

The objective of this chapter is to demonstrate the effects of merging various new semiconductor devices into power converters [5]. The switching performance of cascode GaN-FETs, SiC-MOSFETs, and Si-MOSFETs employed in the bidirectional converter is examined with the same power converter layout [5]. The semiconductor losses, including conduction and switching power losses that occurred in power devices, are analyzed and compared at various operating temperatures and switching frequencies [5]. The overall performance of the GaN-based converter is experimentally evaluated at harsh operating conditions and compared it to Si-based and SiC-based converters in terms of total power loss, overall efficiency, and cost to realize the benefits of using GaN technology [5].

7.1 Converter Performance Evaluation

To evaluate the impacts of using different semiconductor device technologies on power converters in terms of switching performance, total power loss, and energy efficiency, three bidirectional DC–DC buck-boost converters are built and examined: the first one is constructed with traditional Si-MOSFETs and Si-diodes, the second one is constructed with common SiC-MOSFETs and SiC-Schottky diodes, and the third one is constructed with new cascode GaN-FETs and SiC-Schottky diodes [5]. Figure 7.1 shows three bidirectional converters with different power devices. These converters are assessed at various switching frequencies, input voltages, load currents, and output power levels, which are the most crucial operating parameters in power systems [5, 27]. SiC-Schottky diodes (C3D16065D1) are incorporated in WBG-based converters because these diodes have the remarkable advantages of a higher blocking voltage, ultra-faster switching speed, and virtually zero reverse-recovery loss compared to Si-diodes (IDW30C65D1) [5, 27]. The key electrical parameters of different power devices are listed in Table 7.1. These de-
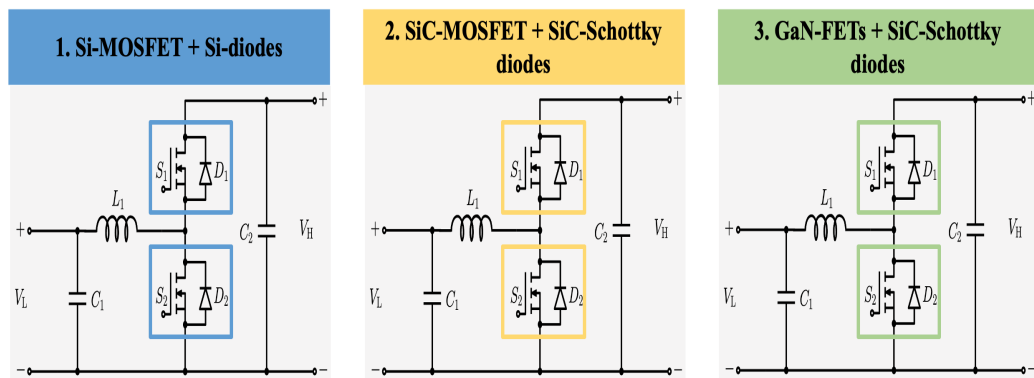
Figure 7.1: Three bidirectional DC–DC buck-boost converters with different semiconductor device technologies.

vices are selected based on their compatibility with converter's operating modes as well as their similarity in electrical characteristics [5, 27].

Table 7.1: Key parameters of power devices integrated into bidirectional converters.

Device semiconductor technology	Transphorm Cascode GaN-FET TP65H035WS	ROHM SiC-MOSFET SCT3060AL	On Semiconductor Si-MOSFET NTHL082N65S3F
V_{ds}	650 V	650 V	650 V
V_{gs}	$\pm$20 V	–4/+22 V	$\pm$30 V
I_d (@ 25°C)	46.5 A	39 A	40 A
$R_{ds(on)}$ (@ 25°C)	35 $m\Omega$	60 $m\Omega$	70 $m\Omega$
T_j (max)	150°C	175°C	150°C
Package	TO-247	TO-247	TO-247

7.2   Simulated Converter Switching Performance

The converter switching performance with different semiconductor devices is captured through the simulation software and evaluated at an input voltage (V_{in}) of 400 V and a load current (I_{load}) of 20 A during turn-on and turn-off events.

7.2.1   Turn-on Switching Waveforms

The turn-on waveforms of Si-MOSFET, SiC-MOSFET and cascode GaN-FET devices integrated into the bidirectional converter are evaluated and compared at the switching frequency (f_{sw}) of 20 kHz [5]. Figure 7.2 illustrates the switching performance of three bidirectional converters during the turn-on transition [5]. It is noticed that the Si-based converter has the largest overshoot, which is 12.88

A, in the current waveform due the high due to the rate of di/dt during the turn-on condition among the other two converters [5]. The current waveform for Si- and GaN-based converters shows a higher oscillation while the SiC-converter has a lower ringing effect because SiC-MOSFETs are ordinarily insensitive to larger gate resistances [5]. The GaN-based converter exhibits a considerably lower turn-on energy loss, which is 310 μJ, while the turn-on energy losses for Si- and SiC-based converters are 359 and 425 μJ, respectively [5].
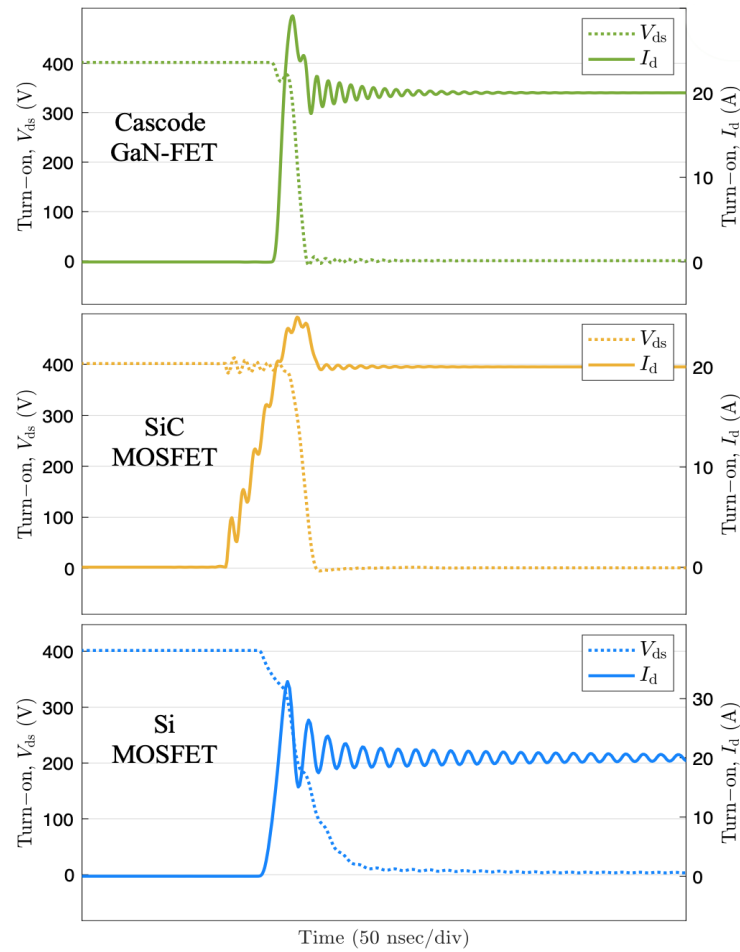
Figure 7.2: Simulated turn-on waveforms of GaN-, SiC-, and Si-based converters at $V_{in} = 400$ V, $I_{load} = 20$ A, $f_{sw} = 20$ kHz, and $T_j = 25°$C.

7.2.2 Turn-off Switching Waveforms

The turn-off waveforms of Si-, SiC-, and GaN-based converters are investigated and compared at the switching frequency is 20 kHz. Figure 7.3 presents the switching performance of each bidirectional converter during the turn-off transition. It is observed that the GaN-based converter shows a slight oscillation occurred in the voltage waveform during the turn-off transition. In contrast, Si- and SiC-based converters contain a majorly severe ringing phenomenon in the voltage waveform due
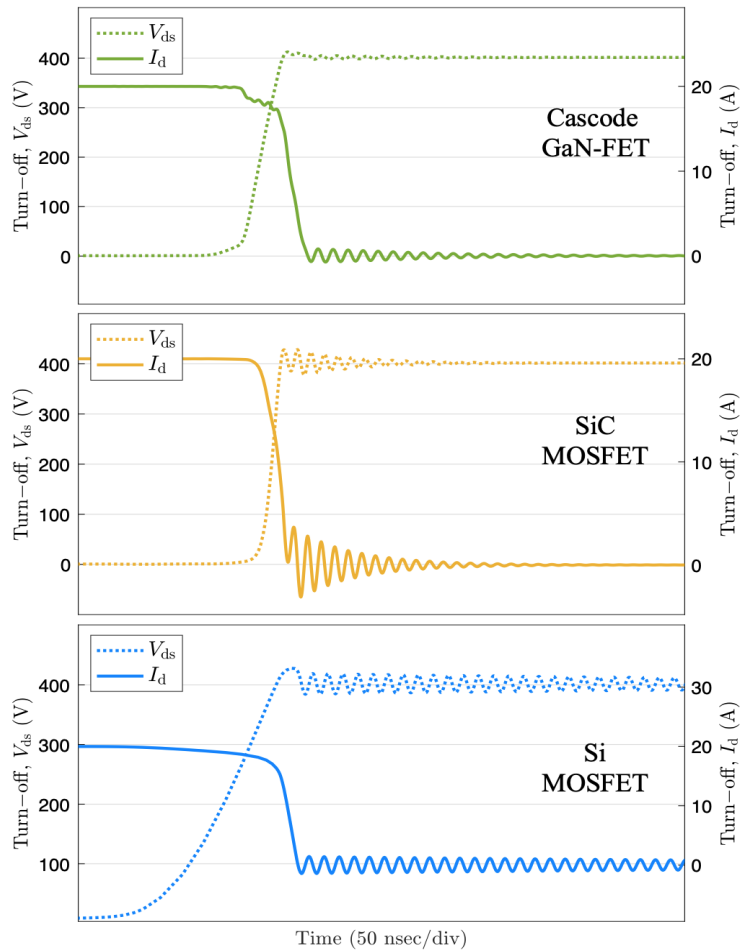
Figure 7.3: Simulated turn-off waveforms of GaN-, SiC-, and Si-based converters at V_{in} = 400 V, I_{load} = 20 A, f_{sw} = 20 kHz, and T_j = 25°C.

the high due the rate of dv/dt during the turn-off event. The turn-off energy losses for GaN- and SiC-based converters are 3.4 and 2.2 μJ, respectively. The Si-based converter has clearly the highest turn-off energy loss, which is 4.1 μJ, compared with the other two converters.

7.3   Experimental Converter Switching Performance

Further detailed investigation and analysis are necessitated for medium-voltage power converter applications in order to demonstrate tradeoffs in switching performance and converter efficiency when substituting GaN devices for Si and SiC counterparts, especially in a cascode configuration [5]. Therefore, a prototype of 500 W bidirectional converter is implemented to validate the impacts of emerging 650/900 V cascode GaN devices on the converter efficiency and performance [5]. Under identical operating conditions, the three bidirectional converters with different power devices are experimentally assessed in terms of current and voltage overshoots, switching times, and switching energy losses during turn-on and turn-off events [5]. The switching performance of each converter highly depends on the gate requirements of power devices; therefore, the investigation on the impact of device's gate characteristics was studied in chapter 2 in order to find the optimal values of gate parameters [5]. The gate-source voltage and gate resistance of each device integrated into the bidirectional converter are listed in Table 7.2, taking the manufacture's datasheet into considerations [5].

Table 7.2: Gate specifications for each device used in bidirectional converters.

Power	Gate resistance (Ω)		Gate-source voltage (V)	
device	Turn-on	Turn-off	Turn-on	Turn-off
Si-MOSFET	20	5	+18	–5
SiC-MOSFET	25	5	+14	–4
Cascode GaN-FET	15	5	+15	–5

7.3.1 Si-based Converter Switching Performance

The switching performance of the bidirectional converter based on the integration of Si-MOSFETs together with Si-diodes is investigated during the turn-on and turn-off events at the input voltage of 360 V, load current of 12 A, and operating temperature of 25°C. Si-MOSFETs are examined with a gate-source voltage of –5 to +18 V for the turn-on and turn-off times while the turn-on and turn-off gate resistance values are set up as 20 and 5 Ω to achieve a smaller overshoot along with a lower oscillation. Figure 7.4 and Figure 7.5 show turn-on and turn-off waveforms of the switch voltage, current, and energy loss for the Si-based converter during turn-on and turn-off events. The Si-based converter shows a high overshoot of 10 A and a distinct ringing in current waveform during the turn-on time because of the high rate of di/dt. In the turn-off time, this converter shows a clear overshoot of 33 V along with a large ringing in the current and voltage waveforms due to the stray inductance, which is decreased by the current commutation loop [27]. Switching times during turn-on and turn-off conditions are 170 and 95 ns, respectively. Therefore, measured turn-on and turn-off energy losses for the Si-based converter are 94 and 30 μJ, respectively.
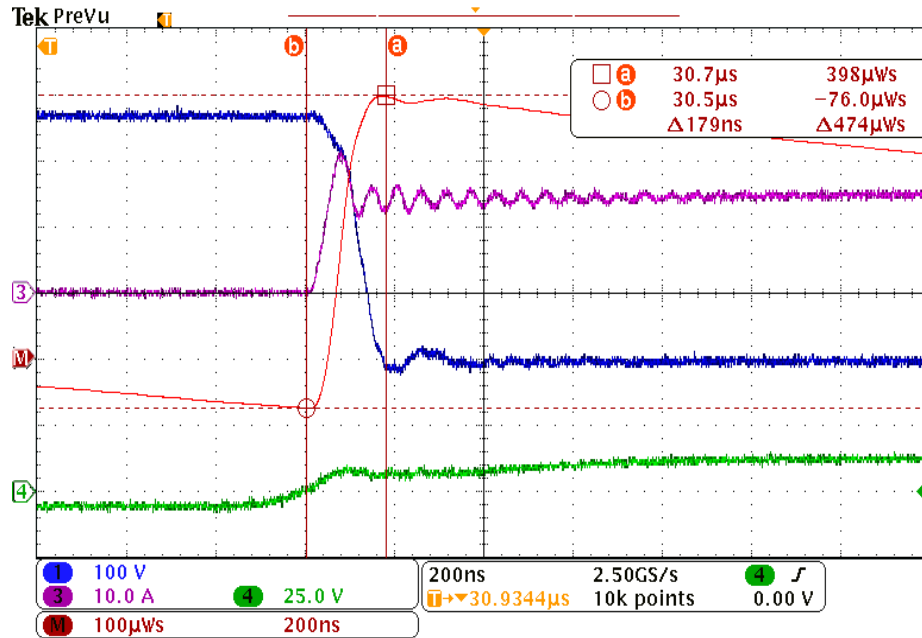
Figure 7.4: Turn-on waveforms of Si-based converter at $V_{gs} = -5/+18$ V, $R_{g(on)} = 20$ Ω, and $R_{g(off)} = 5$ Ω when $V_{in} = 360$ V, $I_{load} = 12$ A, and $T_j = 25°C$.
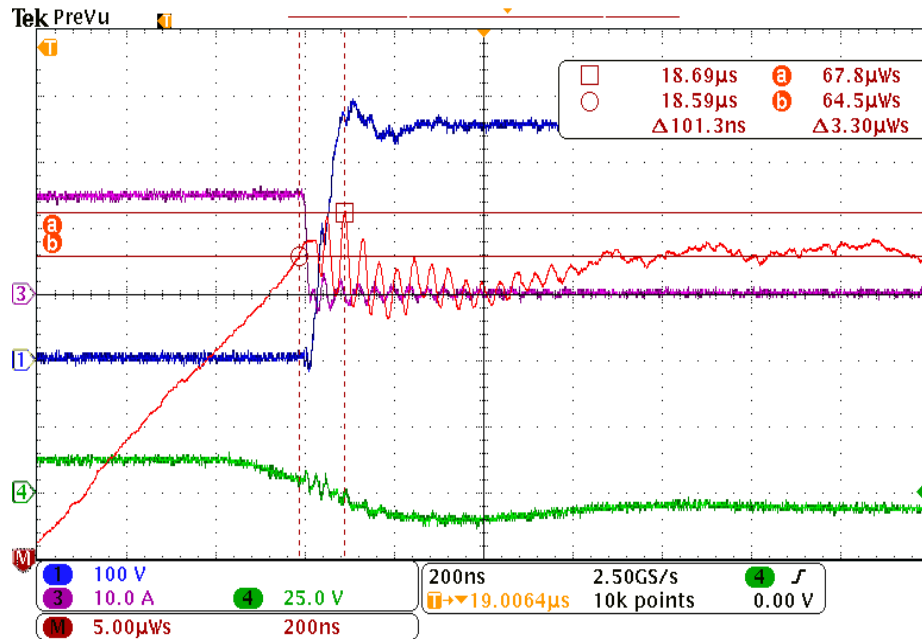
Figure 7.5: Turn-off waveforms of Si-based converter at $V_{gs} = -5/+18$ V, $R_{g(on)} = 20$ Ω, and $R_{g(off)} = 5$ Ω when $V_{in} = 360$ V, $I_{load} = 12$ A, and $T_j = 25°C$.

7.3.2   SiC-based Converter Switching Performance

The converter's switching performance using SiC-MOSFETs combined with SiC-Schottky diodes is evaluated during the turn-on and turn-off events at the input voltage of 360 V, load current of 12 A, and operating temperature of 25°C. SiC-MOSFETs are tested with a gate-source voltage of –4 to +14 V for the turn-on and turn-off times while the turn-on and turn-off gate resistance values are chosen to be 25 and 5 Ω for lowering the overshoot and ringing effects. Figure 7.6 and Figure 7.7 depict turn-on and turn-off waveforms of the switch voltage, current, and energy loss for the SiC-based converter during turn-on and turn-off events. The SiC-based converter shows a high overshoot of 13 A along with a ringing in current waveform during the turn-on event because of the high di/dt rate. From the turn-off transition, the SiC-based converter contains a clear overshoot of 20 V and a small ringing only
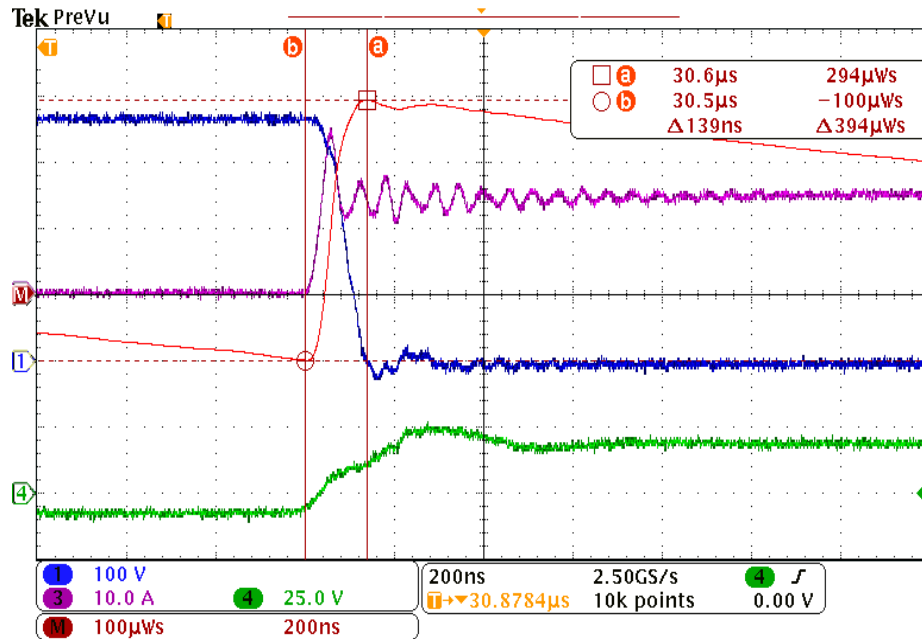
Figure 7.6: Turn-on waveforms of SiC-based converter at V_{gs} = –4/+14 V, $R_{g(on)}$ = 25 Ω, and $R_{g(off)}$ = 5 Ω when V_{in} = 360 V, I_{load} = 12 A, and T_j = 25°C.
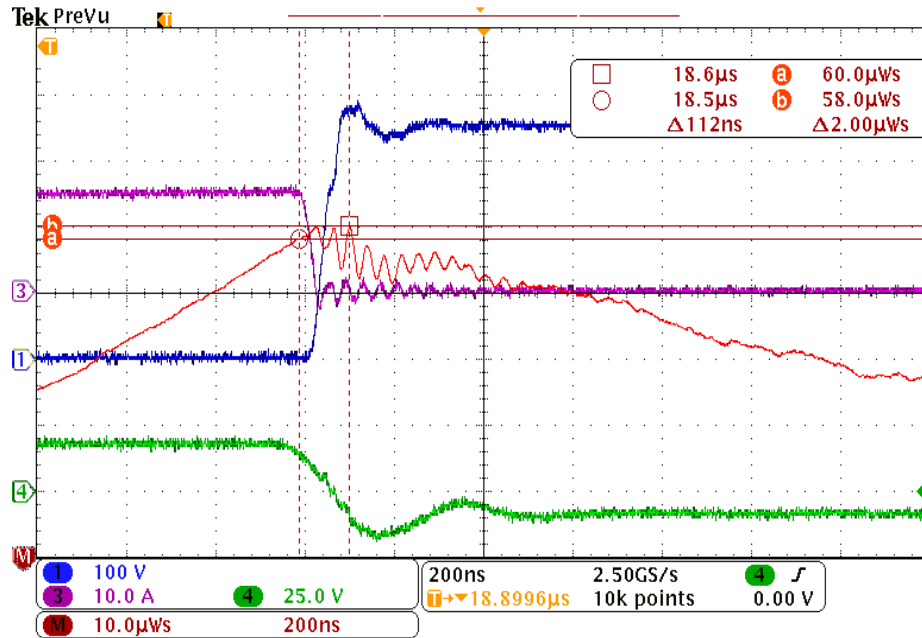
Figure 7.7: Turn-off waveforms of SiC-based converter at $V_{gs} = -4/+14$ V, $R_{g(on)} = 25$ Ω, and $R_{g(off)} = 5$ Ω when $V_{in} = 360$ V, $I_{load} = 12$ A, and $T_j = 25°$C.

in current waveform. Switching times during turn-on and turn-off conditions are 131 and 90 ns, respectively. Thus, measured turn-on and turn-off energy losses for the Si-based converter are 394 and 2 μJ, respectively.

7.3.3   GaN-based Converter Switching Performance

The switching performance of the bidirectional converter utilizing cascode GaN-FETs coupled with SiC-Schottky diodes is assessed during the turn-on and turn-off events at the input voltage of 360 V, load current of 12 A, and operating temperature of 25°C. Cascode GaN-FETs are performed with a gate-source voltage of –5 to +15 V for the turn-on and turn-off times while the turn-on and turn-off gate resistance values are selected as 15 and 5 Ω for improving the switching performance. Figure 7.8 and Figure 7.9 display turn-on and turn-off waveforms of the switch voltage,
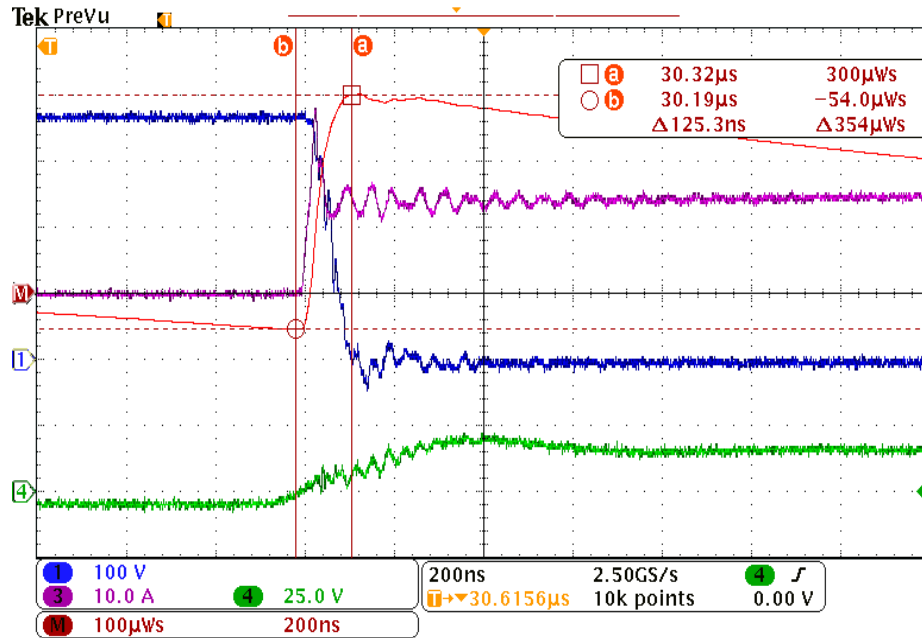
Figure 7.8: Turn-on waveforms of GaN-based converter at V_{gs} = –5/+15 V, $R_{g(on)}$ = 15 Ω, and $R_{g(off)}$ = 5 Ω when V_{in} = 360 V, I_{load} = 12 A, and T_j = 25°C.
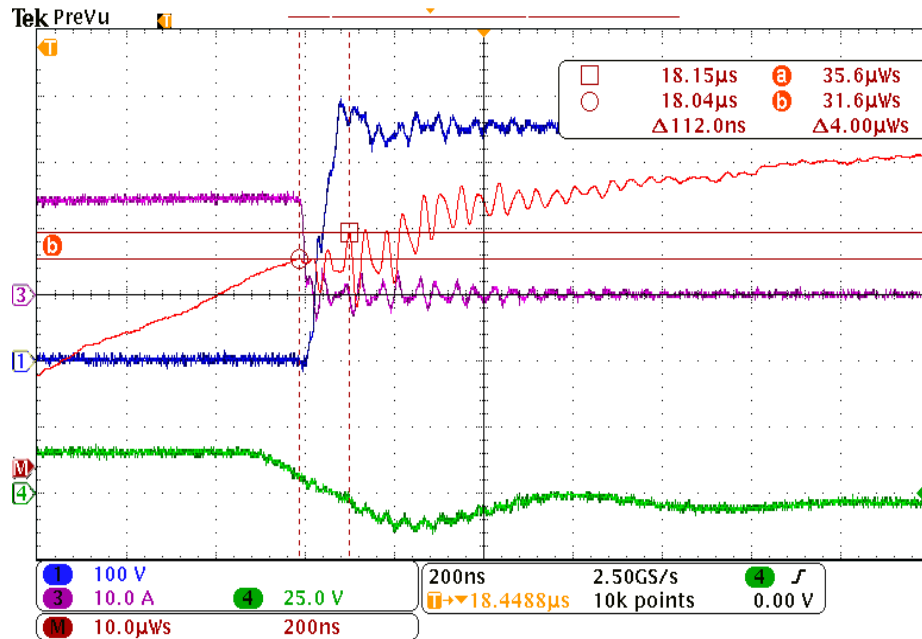
Figure 7.9: Turn-off waveforms of GaN-based converter at V_{gs} = –5/+15 V, $R_{g(on)}$ = 15 Ω, and $R_{g(off)}$ = 5 Ω when V_{in} = 360 V, I_{load} = 12 A, and T_j = 25°C.

current, and energy loss for GaN-based converter during turn-on and turn-off times. The GaN-based converter exhibits a large overshoot of 16 A and a small ringing in voltage and current waveforms during the turn-on event because of the high rate of di/dt. In the turn-off transition, this converter has a clear overshoot of 35 V along with a large ringing in both the voltage and current waveforms due to the high rate of dv/dt. Switching times during turn-on and turn-off conditions are 116 and 99 ns, respectively. Therefore, measured turn-on and turn-off energy losses for the GaN-based converter are 354 and 4 μJ, respectively.

7.4 Converter Power Loss Evaluation

Power loss analysis is one of the important steps to evaluate various semiconductor devices implemented in the bidirectional converter [5]. To find conduction and switching losses of each devices, the on-state resistance is obtained from the device's datasheet while the energy loss is measured through the DPT during the turn-on and turn-off events [5, 72]. Total power loss is calculated by the sum of the switching and conduction losses of each power device along with other loss such as passive and gate-driver losses [5, 72]. It is noteworthy that the duty cycle is considered in the power loss evaluation [5]. Total power loss is represented as:

$$P_{total} = P_{S,sw-on} + P_{S,sw-off} + P_{S,con} + P_{D,con} + P_{ind} + P_{cap} + P_{gate} \quad (7.1)$$

where $P_{S,sw-on}$ and $P_{S,sw-on}$ are turn-on and turn-off switching power losses of each switch while $P_{S,con}$ and $P_{D,con}$ are the conduction loss for the switch and

diode [5]. P_{ind}, P_{cap}, and P_{gate} are the inductor, capacitors, gate-driver losses, respectively [5].
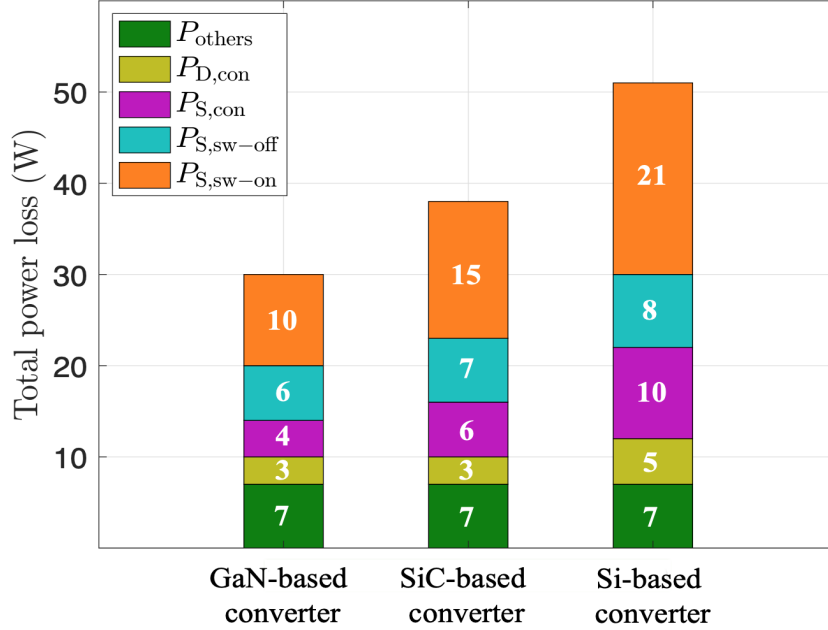
Figure 7.10: Total power loss of each bidirectional converter.

Total loss of Si-MOSFETs/Si-diodes, SiC MOSFETs/SiC-Schottky diodes, and cascode GaN-FETs/SiC-Schottky diodes incorporated into the bidirectional converter is determined when the converter system is performed under the output power of 500 W, a switching frequency of 100 kHz, and an operating temperature of 25°C [5]. Figure 7.10 depicts a comparison of total power loss between Si-based, SiC-based, GaN-based bidirectional converters [5]. Compared to Si-based and SiC-based converters, the GaN-based converter has a substantially lower total power loss because of smaller on-state resistance value and shorter switching times [5]. Table 7.3 presents that total power loss of each bidirectional converter is assessed at two different temperatures. It is clear that the converter using cascode GaN-FETs

combined with SiC-Schottky diodes shows a major reduction in total power loss, leading to increased converter efficiency level even at higher operating temperature.

Table 7.3: Total power loss of each bidirectional converter at different temperatures.

| Operating temperature | Total power loss (W) | | |
	GaN-based converter	SiC-based converter	Si-based converer
$T_1 = 25°C$	30.3	38.4	51.1
$T_2 = 125°C$	35.8	41.2	59.8

7.5   Converter Efficiency Evaluation

This section is presented the efficiency measurement approach along with the converter efficiency evaluation at different operating conditions [5]. Power conversion efficiency is basically the ratio of input and out power measurements [5]. This efficiency is computed by dividing the output power by the input power in watts, while it is commonly presented as a percentage [5]. The method of measuring converter efficiency plays a key role in evaluating the converter performance using various semiconductor devices [5]. To obtain accurate results, the voltage and current should be simultaneously measured at the input-side and output-side of the converter [5]. Among diverse efficiency measurement processes, the power analyzer (P2022A), made by Keysight, significantly provides higher measurement accuracy and flexibility in the converter connection [5]. This power analyzer with precision internal shunt current and high differential voltage probes is used to achieve an accurate measurement efficiency for bidirectional DC–DC converters [5].
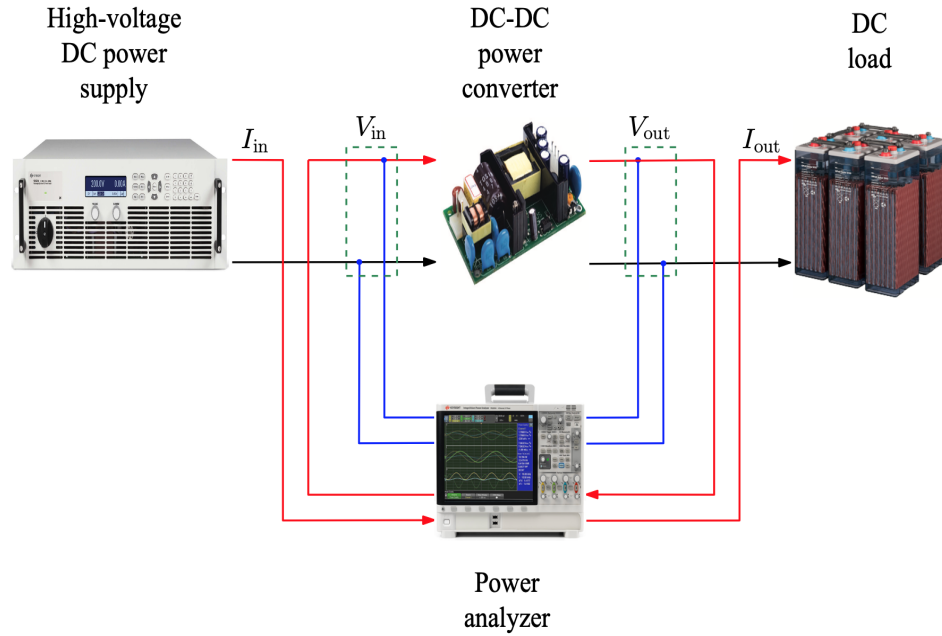
Figure 7.11: Schematic representation of the converter efficiency measurement.

The power analyzer is remarkably operated as an oscilloscope in order to visualize current and voltage along with power waveforms in real-time event, reducing a separated oscilloscope in the measurement s arrangement [5]. At the steady-state period, the voltage and current at the input-side and output-side of converter system are measured at the same time to gain the instantaneous power and overall converter efficiency [5]. Figure 7.11 illustrates a schematic representation of the converter efficiency measurements [5]. Overall converter efficiency (η) is computed by dividing the output power level(P_{out}) by the input power level (P_{in}) , as follows [5] :

$$\eta = \frac{P_{out}}{P_{in}} \cdot 100\% \tag{7.2}$$

In this dissertation, the investigation on effects of integrating different semiconductor device technologies into power converters for energy efficiency is performed at harsh operating conditions [5]. The efficiency of Si-based, SiC-based, and GaN-

based converters is compared and evaluated as increasing of switching frequency, input voltage, and output power level are increased [5].

In diverse applications, there is an acute need for power electronics working at high switching frequencies, which can considerably minimize the size of passive elements and the reduce the volume of cooling systems [5, 27]. Therefore, the Si-based, SiC-based, and GaN-based converters are examined at fast switching speeds [5, 63]. In the examination, the passive components, such as capacitors and inductors, are optimized to handle the increase of a high switching frequency [5]. Figure 7.12 shows the efficiency of the three tested converters as the switching frequency is increased gradually from 40 to 200 kHz at an input voltage of 96 V and an operating temperature of 25°C [5]. As the switching speed is increased, the efficiency of the Si-based converter decreases dramatically due to higher conduction
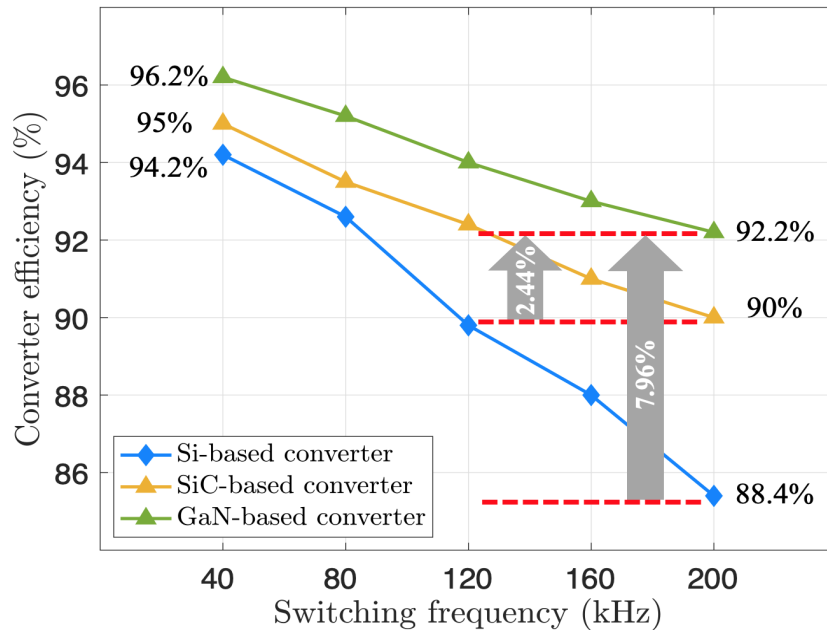
Figure 7.12: Converter efficiency with different semiconductor device technologies as a function of increasing switching frequency from 40 to 200 kHz at an input voltage of 96 V.

and switching power losses while SiC-based and GaN-based converters offer better efficiency level [5, 27]. It is observed the GaN-based converter achieves 92.2% efficiency while the SiC-based converter obtains only 90% efficiency and the Si-based converter can barely reach 88.4% at a switching frequency of 200 kHz [5]. The results show that cascode GaN-FETs along with SiC-Schottky diodes substantially improves the overall converter efficiency by 2.44% compared to the SiC-based converter and by nearly 8% compared to the Si-based converter [5]. Thus, integrating GaN power devices into the bidirectional converter provides beneficial effects in terms of loss reduction and efficiency improvement [5, 27].
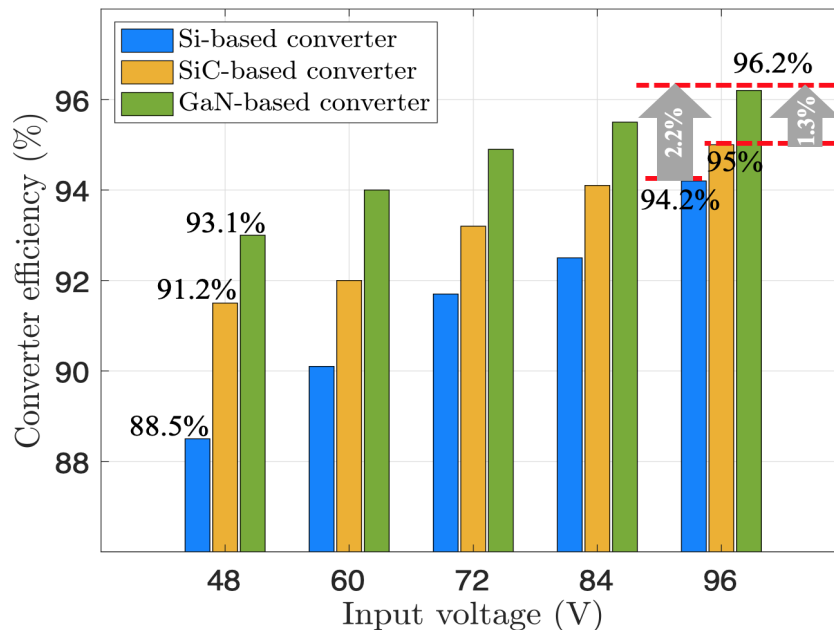
Figure 7.13: Converter efficiency with different power devices as increasing input voltage from 48 to 96 V at a switching frequency of 40 kHz.

The input voltage of the bidirectional converter is a pivotal factor in energy storage and renewable energy applications because the voltage can be changeable based on operating condition of power operation systems for supplying or storing

electric energy [5, 63]. Therefore, the performance of each converter is assessed to measure the energy efficiency over a wide range of input voltages [5]. It is noteworthy that the bidirectional converter is constructed to operate effectively around the designed input voltage [5]. This means that the converter performance obtains peak efficiency at the input voltage of 96 V [5]. As the input voltage is increased from 48 to 96 V, the efficiency of three converters is compared at a switching frequency of 40 kHz [5], as shown in Figure 7.13.

Table 7.4 highlights the efficiency comparison of the three converters at different operating temperatures while the input voltage is 96 V [5]. SiC-based and GaN-based converters provide a higher efficiency level while the Si-based is struggling to reach better efficiency because of its larger conduction and switching losses, especially at higher input voltages [5]. Among three bidirectional converters, the converter using GaN-FETs and SiC-Schottky diodes achieves 96.2% efficiency, which is considerably higher than the efficiency of both Si-based and SiC-based converters [5]. At the input voltage of 96 V, GaN power device technology remarkably enhances converter efficiency by 1.3% compared to the SiC-based converter and by 2.2% compared to the Si-based converter [5]. As a result, the combination of cascode GaN-FETs and SiC-Schottky diodes is enabling power converter to perform efficiently even at higher input voltages [5].

The performance of the Si-based, SiC-based and GaN-based converters is evaluated at a wide range of output power levels, which can play an important role in power conversion systems [5, 27]. The input and output powers of each converter are measured through current and voltage probes to determine their efficiency level, which is computed by the power analyzer at two switching frequencies of 100 and 200 kHz [5]. Here, each bidirectional converter works efficiently around 300 and

Table 7.4: Efficiency comparison for GaN-based, SiC-based, and Si-based converters at different operating temperatures.

Converter Technology	Converter efficiency at		
	50°C	100°C	150°C
GaN-based converter	96%	95.1%	94.3%
SiC-based converter	94.8%	93.2%	92.5%
Si-based converter	93.7%	91.4%	90.1%

400 W, as the designed power rating [5]. Thus, the converter reaches peak efficiency at output power levels of 300 and 400 W [5]. It is clear that converter efficiency with different device technologies at the full-load condition is drastically dropped because of the high current flowing through switching devices, leading to a large conduction loss [5]. The effect of increasing switching frequency on converter efficiency is becoming crucially significant because the turn-on and turn-off energy losses are proportional to the switching speed [5].

Figure 7.14 shows the efficiency comparison of Si-based, SiC-based, and GaN-based converters when the output power gradually increased from 100 to 500 W at two different switching speeds [5]. SiC-based and GaN-based converters offer better efficiency levels throughout different out powers compared to the Si-based converter [5]. After 400 W, the converter efficiency with Si devices drops drastically while the GaN-based converter obtains 94% efficiency, which is higher than the other two converters [5]. Even though the converter works at higher output power levels, the combination of cascode GaN-FETs and SiC-Schottky diodes can still preserve the converter at a higher efficiency level [5]. At the switching frequency of 200 kHz, it is noticed that efficiency of the GaN-based converter is only reduced by 1.1% while efficiency of Si-based and SiC-based converters decreased

116
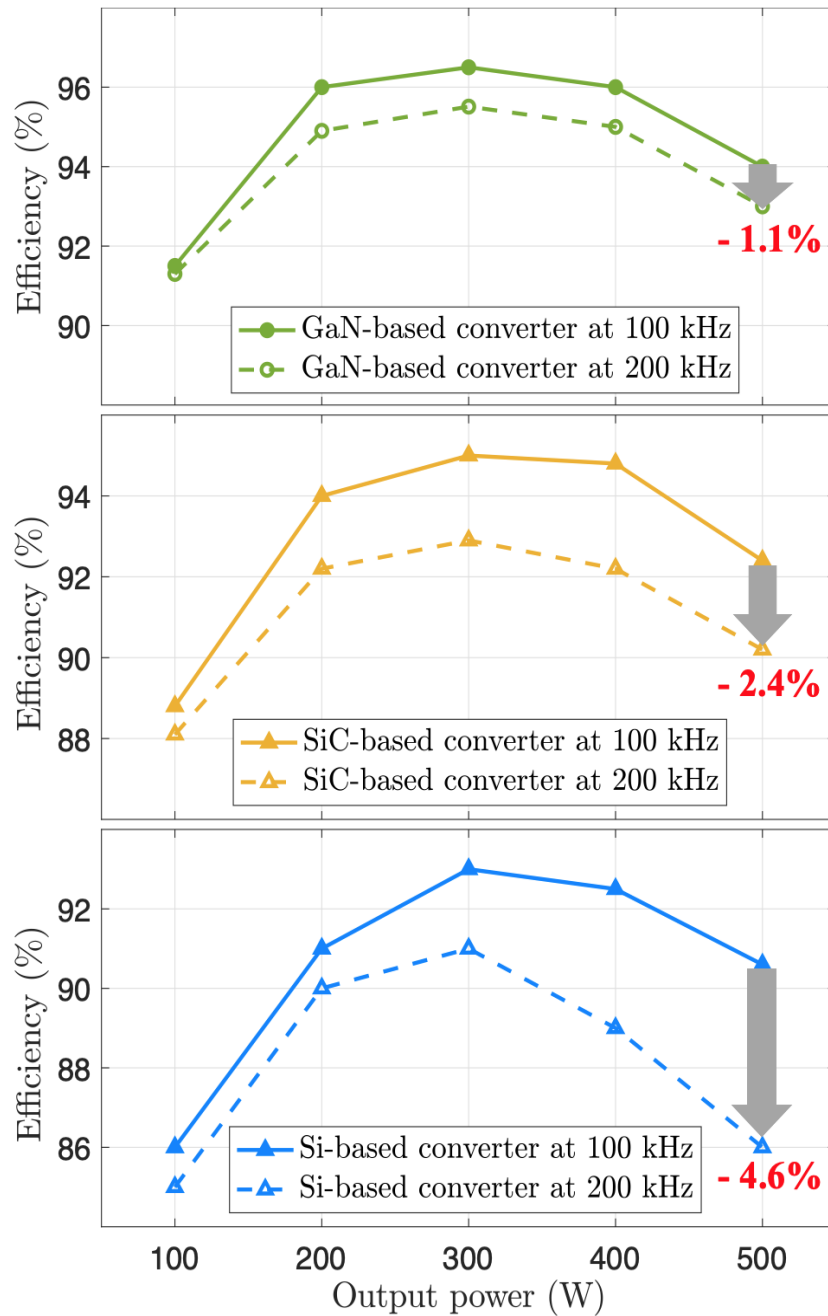
Figure 7.14: Converter efficiency using different semiconductor devices with increasing output power level from 100 to 500 W at two switching frequencies of 100 and 200 kHz.

dramatically by 2.4% and 4.6%, respectively [5]. Therefore, integrating GaN-FETs into the converter can noticeably increase the energy efficiency because of the superior material properties and high operating capabilities of GaN technology [5, 27].

7.6   Market Price Comparison for Power Devices

The cost of power devices is a significant factor in power converter applications; therefore, this section investigates the market price between different semiconductor devices incorporated into the bidirectional DC–DC converters [5]. Si-MOSFETs, SiC-MOSFETs, and cascode GaN-FETs from various semiconductor manufacturers are compared in terms of their price and availability in the market [5]. In this comparison, the current rate, device package, and voltage level are taken into consideration [5]. Figure 7.15 shows the average cost for three different device topologies as a function of increasing rating current and the price is collected from different semiconductor distributors [5]. It is realized that the price of GaN semiconductors is the most expensive devices among device technologies since GaN power devices are relatively new candidates in the market [5]. Based on the main suppliers, such as Digi-key and Mouser, the actual price for power devices used in the three bidirectional converters is listed in Table 7.5 [5]. It is noticed that the price for the first combination of Si-MOSFETs and Si-diodes is $16.64 while the price in the second combination of SiC-MOSFETs and SiC-Schottky diodes is $29.82 and the price for the third combination of cascode GaN-FETs and SiC-Schottky diodes is $45.14 [5]. It looks that the GaN-based converter is costly, which is nearly three times higher than the Si-base converter while the SiC-based converter is expensive, which is approximately two times higher than Si-based converters [5].
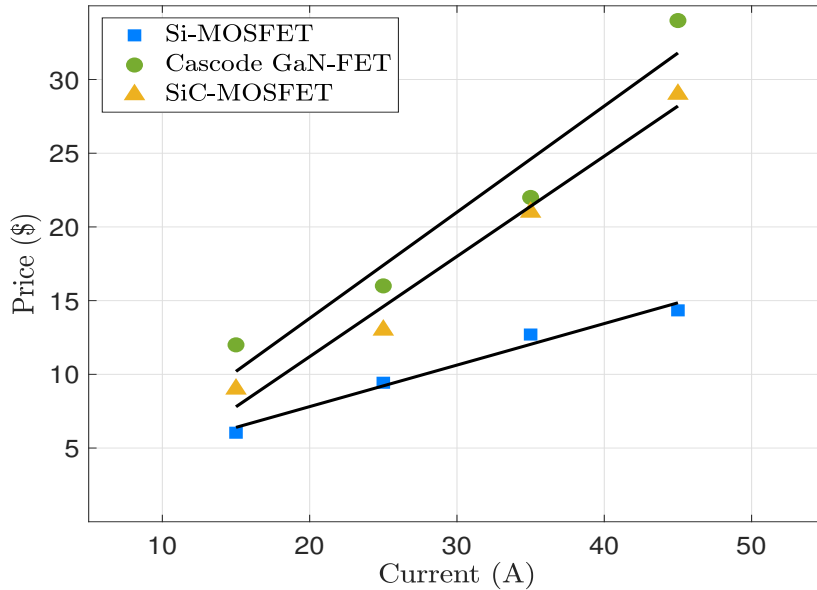
Figure 7.15: Price comparison between Si-MOSFET, SiC-MOSFET, and cascode GaN-FET power devices at various rating currents.

Table 7.5: Price comparison for various power device technologies used in the bidirectional DC–DC converter.

	Bidirectional converter with different power devices		
	Combination (1) (Si-MOSFET/ Si-diode) (NTHL082N65S3F/ IDW30C65D1)	Combination (2) (SiC-MOSFET/ SiC-Schottky diode) (SCT3060AL/ C3D16065D1)	Combination (3) (Cascode GaN-FET/ SiC-Schottky diode) (TP65H035WS/ C3D16065D1)
Switches (S_1, S_2)	$2 \times \$5.51$	$2 \times \$11.26$	$2 \times \$18.92$
Diodes (D_1, D_2)	$2 \times \$2.81$	$2 \times \$3.65$	$2 \times \$3.65$
Total cost	**\$16.64**	**\$29.82**	**\$45.14**

In spite of the fact that the price of GaN power devices is more expensive compared to the Si and SiC counterparts, GaN device technology offers remarkably

more than 40% reduction in switching energy losses, leading to enhance the switching performance of the converter [5]. As mentioned in chapter 2, cascode GaN-FET devices feature high operating capabilities, which are enabling power converters to work effectively at harsh operating conditions of switching frequency, junction temperature, and output power level [5]. Since GaN devices are able to operate at higher switching speeds compared to other device technologies, the size of passive elements as well as the volume of cooling systems used in power converters can be greatly minimized, resulting significant reduction in total power loss and weight of the bidirectional converter [5]. The converter using cascode GaN-FET devices is more robust and efficient than other converters [5], as shown in this chapter. It also exhibits a significantly higher efficiency level with lower converter size even at high operating conditions [5]. As a result, the high price of GaN deices can be reasonably compensated by implementing smaller passive components, such as capacitors and inductors, and lower cooling systems in power converters, which can majorly improve the converter performance as well as increase the energy efficiency [5].

7.7   Summary

In this chapter, the effects of merging various new semiconductor devices into power converters is demonstrated at different operating conditions. To assess the impacts of using different semiconductor device technologies on power converters in terms of switching performance, total loss, and efficiency, three bidirectional DC–DC buck-boost converters are designed: the first one is constructed with traditional Si-MOSFETs and Si-diodes, the second one is constructed with common SiC-MOSFETs and SiC-Schottky diodes, and the third one is constructed with cas-

code GaN-FETs and SiC-Schottky diodes. The switching performance of cascode GaN-FETs, SiC-MOSFETs, and Si-MOSFETs employed in the bidirectional converter is evaluated at the same power converter layout. The GaN-based converter shows an outstanding switching behavior in the current and voltage waveforms because GaN-FETs has substantially lower total energy loss as well as reduced overshoot and ringing effects compared to Si and SiC devices.

In the power loss analysis, losses are occurred in power devices are determined and compared at different operating temperatures and switching frequencies. Among semiconductor devices, cascode GaN-FETs show much lower in conductions and switching losses due to smaller on-state resistance and shorter turn-on and turn-off times. The GaN-based converter is experimentally evaluated at high operating conditions and compared its performance to Si-based and SiC-based converters in terms of total power loss and energy efficiency. Based on the efficiency measurement, the GaN-based converter shows a significantly better efficiency level at higher switching frequency, input voltage, and output power because its reduced total power loss compared to Si-based and SiC-based converters. Although GaN devices are more expensive compared to the Si and SiC counterparts, the high price of GaN-FET deices can be noticeably reduced by containing smaller passive elements and lower cooling systems in power converters, leading to enhance greatly the switching performance and improve energy efficiency of the converter.

Chapter 8

Conclusion and Future Work

The aim of this dissertation was experimentally evaluated the impact of integrating medium-voltage cascode GaN power devices into bidirectional DC–DC power converters that are substantially used in energy storage systems and renewable energy applications [5]. The prime conclusion and future work of the dissertation are summarized as the following aspects.

8.1 Conclusion

As increasing demand for more reliable, efficient, and compact power electronics in diverse applications, most existing converters are hindered by conventional Si-based power devices, which unfortunately are reaching their theoretical and physical limits as there is a very small possibility for further improvements. WBG semiconductors, especially GaN switching devices, show outstanding physical properties as well as they provide great potential for replacing traditional Si devices with WBG technology, pushing the boundaries of semiconductors to han-

dle higher operating conditions of higher switching speeds, output power levels, blocking voltages, and junction temperatures. Therefore, this research was demonstrated tradeoffs in switching performance and converter efficiency when substituting GaN devices for Si and SiC counterparts, particularly in a cascode configuration. It also offered a further detailed investigation and analysis that are necessitated for medium-voltage GaN devices in power converter applications.

In addition, superior material advantages and remarkable benefits of GaN semiconductors was presented in this dissertation while literature review of prior research on GaN power device was conducted. The basic structures and main characteristics of GaN devices were addressed, including vertical and lateral semiconductors and enhancement-mode as well as depletion-mode and enhancement-mode GaN devices. A focused survey of GaN power devices was carried out to find the most compatible GaN devices with high-power and high-switching speed applications. The prime factors that contributed to this survey were commercially available GaN power devices, voltage rating, current rating, and device packaging. It was realized that cascode GaN-FET devices, made by Transphorm, are the most suitable GaN power devices for power converters among various GaN device technologies. These GaN devices feature a cascode structure, which does not require designing a sophisticated gate-driver circuit as well as they exhibit the highest voltage level available in market with TO-247 packaging, which is more desirable for DC converters. Due to high-operating capabilities of GaN technology, GaN-based converters have attracted a great deal of interest in automotive, UPS, energy storage, and renewable energy systems.

In this dissertation, the DPT circuit, including the load inductor, DC capacitor, and gate driver circuit, along with the measurement requirements for the switch-

ing characterization, explained and discussed to study and evaluate the switching behavior of power devices during turn-off and turn-on transitions. From the DPT board, the switching energy losses and the rate of dv/dt and di/dt were obtained. The power dissipation resulted from semiconductor switching devices was analyzed to evaluate the converter performance and efficiency at different operating conditions. The major power consumption can be divided into conduction and switching losses; therefore, these losses for different device technologies investigated and compared at increasing switch current and junction temperature. Compared to different Si and SiC devices, the results showed that cascode GaN-FET devices offered significantly reduced semiconductor losses due to their smaller on-state resistance value and shorter switching times. Gate-source voltage, gate-driver circuit, and gate resistance are considered to be the most crucial factors in how power devices operate and switch efficiently because their switching behavior are depending on these factors. The switching performance of the cascode GaN-FET was mainly assessed at different gate-driver circuit, gate-source voltage, and gate resistance in order to find the optimal values of gate requirements. To achieve better performance for GaN devices, the gate-driver (1EDI60I12AH), made by Infineon, was used while the turn-on and turn-off gate resistance values found to be 15 and 5 Ω as the gate-source voltage was –5/+15.

Furthermore, the dynamic characteristics of Si, SiC, and cascode GaN power devices were examined through the DPT circuit at various gate resistance values, device currents, and DC-bus voltages. The switching performance and energy loss as well as the rate of voltage and current changes over time were studied and analyzed at different operating conditions. The behavior of cascode power devices illustrated an outstanding switching performance among Si and SiC devices in terms

124

of lower ringing and overshooting effects. The turn-on and turn-off, total energy losses for tested power devices were computed and investigated under various operating points of a gate resistance value, switch current, junction temperature, and DC-bus voltage. The results showed that the cascode GaN-FETs provided a significant reduction in total energy loss compared to Si and SiC as a function of increasing operating conditions. Thus, SiC power devices substantially enhance the switching performance of the converters used in high-power and high-temperature applications.

Finally, the impacts of merging various new semiconductor devices on power converter systems were evaluated thorough the experimental converter prototype to validate the benefits of cascode GaN semiconductors for the power converter operation and performance. To assess the effects of using different device technologies on power converters in terms of switching performance, total loss, and efficiency, three bidirectional DC–DC buck-boost converters were designed: the first one is constructed with traditional Si-MOSFETs and Si-diodes, the second one is constructed with common SiC-MOSFETs and SiC-Schottky diodes, and the third one is constructed with new cascode GaN-FETs and SiC-Schottky diodes. The switching performance of cascode GaN-FETs, SiC-MOSFETs, and Si-MOSFETs used in the bidirectional converter was compared at various operating conditions. The GaN-based converter exhibited an improved switching behavior in the voltage and current waveforms because GaN-FETs showed a substantially lower total energy loss as well as reduced overshoot and ringing effects compared to Si and SiC semiconductors. Comprehensive analysis of the power loss and efficiency improvement for Si-based, SiC-based, and GaN-based converters were performed and evaluated as a function of increasing switching speed, working temperature, and output power

125

level. The results revealed that the converter with cascode GaN-FETs features a major reduction in total power losses due to smaller on-state resistance and shorter turn-on and turn-off times. Based on the efficiency measured by the power analyzer, the GaN-based converter showed a significantly better efficiency level at higher switching frequency, input voltage, and output power level compared to Si-based and SiC-based converters. Even though GaN devices are considered to be more expensive compared to Si and SiC counterparts, the high price of cascode GaN-FET deices can be distinctly decreased by having smaller passive components and lower cooling systems, which helped to improve visibly the switching performance and increase the energy efficiency for power converters.

8.2 Future Work

In order to entirely explain the benefits of merging cascode GaN power devices in the non-isolated bidirectional DC–DC converter, future work can be further explored in the following aspects.

- Reliability of GaN device technology is one the main concerns for power converter applications since these devices are relatively new compared to Si and SiC counterparts. To investigate the GaN reliability, cascode GaN-FETs should undergo thermal cycling tests for identifying their material limitations and maximum operating conditions.

- Electromagnetic interference (EMI) is a critical issue in power converter operating at high switching frequency, which can highly cause acute EMI because of high harmonics and very steep edges of voltage waveforms during

126

turn-on and turn-off events. A further investigation on EMI noise and filter design is needed to be addressed at converter and system levels.

- To obtain high energy efficiency and high power density, the power converter should operate at switching speed. However, switching power loss can be considerably large. It is a pivotal aspect to investigate various approaches, such as zero-voltage-switched (ZVS) and zero-current-switched (ZCS) techniques, to mitigate or reduce the switching loss of GaN device at faster speeds.

- Although this dissertation assessed the performance of a non-isolated bidirectional DC–DC converter using various semiconductor devices, the control and protection aspects of the converter are necessary to be experimentally demonstrated at system level with different operating conditions.

- GaN devices show a substantially high operating capabilities for power converters. At high temperatures, it is systematically beneficial to evaluate converter in terms of thermal management, heat sink and cooling system since these factors paly a significant role in determining the size and volume of the power converters as well as obtaining better energy efficiency.

Bibliography

[1] M. Fan, K. Sun, D. Lane, W. Gu, Z. Li, and F. Zhang, "A novel generation rescheduling algorithm to improve power system reliability with high renewable energy penetration," *IEEE Trans. Power Syst.*, vol. 33, no. 3, pp. 3349–3357, May 2018.

[2] C. Ma, F. Gao, G. He, and G. Li, "A voltage detection method for the voltage ride-through operation of renewable energy generation systems under grid voltage distortion conditions," *IEEE Trans. Sustain. Energy*, vol. 6, no. 3, pp. 1131–1139, July 2015.

[3] H. Wu, K. Sun, L. Zhu, and Y. Xing, "An interleaved half-bridge three-port converter with enhanced power transfer cpability using three-leg rectifier for renewable energy applications," *IEEE J. of Emerging and Select. Topics in Power Electron.*, vol. 4, no. 2, pp. 606–616, June 2016.

[4] A. Deihimi and M. E. S. Mahmoodieh, "Analysis and control of battery-integrated dc/dc converters for renewable energy applications," *IET Power Electron.*, vol. 10, no. 14, pp. 1819–1831, 2017.

[5] S. S. Alharbi and M. Matin, "Experimental evaluation of medium-voltage cascode gallium nitride (GaN) devices for bidirectional DC–DC converters," *CES Transactions on Electrical Machines and Systems*, 2020, manuscript submitted for publication.

[6] T. Adefarati and R. C. Bansal, "Integration of renewable distributed generators into the distribution system: a review," *IET Renewable Power Generation*, vol. 10, no. 7, pp. 873–884, February 2016.

[7] F. R. Yu, P. Zhang, W. Xiao, and P. Choudhury, "Communication systems for grid integration of renewable energy resources," *IEEE Network*, vol. 25, no. 5, pp. 22–29, September 2011.

[8] J. M. Guerrero, F. Blaabjerg, T. Zhelev, K. Hemmes, E. Monmasson, S. Jemei, M. P. Comech, R. Granadino, and J. I. Frau, "Distributed generation:

Toward a new energy paradigm," *IEEE Ind. Electron. Magazine*, vol. 4, no. 1, pp. 52–64, March 2010.

[9] M. Garg, R. K. Singh, and R. Mahanty, "Magnetically coupled boost converter with enhanced equivalent series resistance filter capacitor for DC microgrid," *IET Power Electron.*, vol. 9, no. 9, pp. 1943–1951, March 2016.

[10] A. K. Rathore, D. R. Patil, and D. Srinivasan, "Non-isolated bidirectional soft-switching current-fed LCL resonant DC/DC converter to interface energy storage in DC microgrid," *IEEE Trans. on Ind. Appl.*, vol. 52, no. 2, pp. 1711–1722, March 2016.

[11] Y. Xiang, J. Liu, and Y. Liu, "Robust energy management of microgrid with uncertain renewable generation and load," *IEEE Transactions on Smart Grid*, vol. 7, no. 2, pp. 1034–1043, March 2016.

[12] T. Dragičević, X. Lu, J. C. Vasquez, and J. M. Guerrero, "DC microgrids–part I: A review of control strategies and stabilization techniques," *IEEE Transactions on Power Electronics*, vol. 31, no. 7, pp. 4876–4891, 2016.

[13] M. Kwon and S. Choi, "Control scheme for autonomous and smooth mode switching of bidirectional DC-DC converters in a DC microgrid," *IEEE Trans. on Power Electron.*, vol. 33, no. 8, pp. 7094–7104, Aug 2018.

[14] R. Ahmadi and M. Ferdowsi, "Improving the performance of a line regulating converter in a converter-dominated DCmicrogrid system," *IEEE Transactions on Smart Grid*, vol. 5, no. 5, pp. 2553–2563, 2014.

[15] X. Zhao, Y. W. Li, H. Tian, and X. Wu, "Energy management strategy of multiple supercapacitors in a DC microgrid using adaptive virtual impedance," *IEEE Journal of Emerging and Selected Topics in Power Electronics*, vol. 4, no. 4, pp. 1174–1185, 2016.

[16] H. S. B. J. W. K. H. J. J. J. H. Jeong, D. K. Kim, "Autonomous control strategy of DC microgrid for islanding mode using power line communication," *Energies*, vol. 30, no. 11, p. 924, 2018.

[17] V. Nasirian, S. Moayedi, A. Davoudi, and F. L. Lewis, "Distributed cooperative control of DC microgrids," *IEEE Trans. on Power Electron.*, vol. 30, no. 4, pp. 2288–2303, April 2015.

[18] L. Yang, Y. Chen, A. Luo, W. Wu, K. Huai, X. Zhou, L. Zhou, Q. Xu, and J. M. Guerrero, "Second ripple current suppression by two bandpass filters and current sharing method for energy storage converters in DC microgrid,"

IEEE Journal of Emerging and Selected Topics in Power Electronics, vol. 5, no. 3, pp. 1031–1044, 2017.

[19] T. Pavlovic, T. Bjazic, and Z. Ban, "Simplified averaged models of DC–DC power converters suitable for controller design and microgrid simulation," *IEEE Transactions on Power Electronics*, vol. 28, no. 7, pp. 3266–3275, 2013.

[20] M. Baranwal, A. Askarian, S. Salapaka, and M. Salapaka, "A distributed architecture for robust and optimal control of DC microgrids," *IEEE Transactions on Industrial Electronics*, vol. 66, no. 4, pp. 3082–3092, 2019.

[21] S. F. Rafique and Z. Jianhua, "Energy management system, generation and demand predictors: a review," *IET Generation, Transmission Distribution*, vol. 12, no. 3, pp. 519–530, 2018.

[22] F. Blaabjerg, Y. Yang, D. Yang, and X. Wang, "Distributed power-generation systems and protection," *Proceedings of the IEEE*, vol. 105, no. 7, pp. 1311–1331, July 2017.

[23] V. Kalkhambkar, R. Kumar, and R. Bhakar, "Joint optimal allocation methodology for renewable distributed generation and energy storage for economic benefits," *IET Renewable Power Generation*, vol. 10, no. 9, pp. 1422–1429, 2016.

[24] Y. Tang, J. Zhong, and J. Liu, "A generation adjustment methodology considering fluctuations of loads and renewable energy sources," *IEEE Trans. Power Syst.*, vol. 31, no. 1, pp. 125–132, Jan 2016.

[25] N. Kawakami, S. Ota, H. Kon, S. Konno, H. Akagi, H. Kobayashi, and N. Okada, "Development of a 500-KW modular multilevel cascade converter for battery energy storage systems," *IEEE Trans. Ind. Appl.*, vol. 50, no. 6, pp. 3902–3910, Nov 2014.

[26] W. Xiao, M. S. E. Moursi, O. Khan, and D. Infield, "Review of grid-tied converter topologies used in photovoltaic systems," *IET Renewable Power Generation*, vol. 10, no. 10, pp. 1543–1551, 2016.

[27] S. S. Alharbi, S. S. Alharbi, and M. Matin, "The benefits of using cascode GaN power devices in a bidirectional DC-DC buck/boost converter," in *2018 IEEE International Power Modulator and High Voltage Conference (IPMHVC)*, 2018, pp. 166–171.

[28] M. H. Nehrir, C. Wang, K. Strunz, H. Aki, R. Ramakumar, J. Bing, Z. Miao, and Z. Salameh, "A review of hybrid renewable/alternative energy systems for electric power generation: configurations, control, and applications," *IEEE Trans. Sustain. Energy*, vol. 2, no. 4, pp. 392–403, Oct 2011.

[29] H. Zhou, T. Bhattacharya, D. Tran, T. S. T. Siew, and A. M. Khambadkone, "Composite energy storage system involving battery and ultracapacitor with dynamic energy management in microgrid applications," *IEEE Trans. Power Electron.*, vol. 26, no. 3, pp. 923–930, March 2011.

[30] S. Lakshminarayana, T. Q. S. Quek, and H. V. Poor, "Cooperation and storage tradeoffs in power grids with renewable energy resources," *IEEE J. on Select. Areas in Commun.*, vol. 32, no. 7, pp. 1386–1397, July 2014.

[31] K. Sun, L. Zhang, Y. Xing, and J. M. Guerrero, "A distributed control strategy based on DC bus signaling for modular photovoltaic generation systems with battery energy storage," *IEEE Trans. on Power Electron.*, vol. 26, no. 10, pp. 3032–3045, Oct 2011.

[32] O. Cornea, G. Andreescu, N. Muntean, and D. Hulea, "Bidirectional power flow control in a DC microgrid through a switched-capacitor cell hybrid DC–DC converter," *IEEE Transactions on Industrial Electronics*, vol. 64, no. 4, pp. 3012–3022, 2017.

[33] N. R. Tummuru, M. K. Mishra, and S. Srinivas, "Dynamic energy management of renewable grid integrated hybrid energy storage system," *IEEE Transactions on Ind. Electron.*, vol. 62, no. 12, pp. 7728–7737, Dec 2015.

[34] K. Tytelmaier, O. Husev, O. Veligorskyi, and R. Yershov, "A review of non-isolated bidirectional dc-dc converters for energy storage systems," in *2016 II International Young Scientists Forum on Applied Physics and Engineering (YSF)*, 2016, pp. 22–28.

[35] T. Dragičević, X. Lu, J. C. Vasquez, and J. M. Guerrero, "DC microgrids– part II: a review of power architectures, applications, and standardization issues," *IEEE Trans. on Power Electron.*, vol. 31, no. 5, pp. 3528–3549, May 2016.

[36] M. Farrokhabadi, B. V. Solanki, C. A. Canizares, K. Bhattacharya, S. Koenig, P. S. Sauter, T. Leibfried, and S. Hohmann, "Energy storage in microgrids: compensating for generation and demand fluctuations while providing ancillary services," *IEEE Power and Energy Mag.*, vol. 15, no. 5, pp. 81–91, Sept 2017.

[37] M. Zeraati, M. E. H. Golshan, and J. Guerrero, "Distributed control of battery energy storage systems for voltage regulation in distribution networks with high PV penetration," *IEEE Trans. Smart Grid*, pp. 1–1, 2016.

[38] P. Shanthi, G. Uma, and M. S. Keerthana, "Effective power transfer scheme for a grid connected hybrid wind/photovoltaic system," *IET Renewable Power Generation*, vol. 11, no. 7, pp. 1005–1017, 2017.

[39] L. Nousiainen, J. Puukko, A. Mäki, T. Messo, J. Huusari, J. Jokipii, J. Viinamäki, D. T. Lobera, S. Valkealahti, and T. Suntio, "Photovoltaic generator as an input source for power electronic converters," *IEEE Trans. on Power Electron.*, vol. 28, no. 6, pp. 3028–3038, June 2013.

[40] K. Tytelmaier, O. Husev, O. Veligorskyi, and R. Yershov, "A review of non-isolated bidirectional dc-dc converters for energy storage systems," in *2016 II Int. Young Scientists Forum on pl. Physics and Eng. (YSF)*, Oct 2016, pp. 22–28.

[41] C. Chakraborty, H. H. C. Iu, and D. D.-C. Lu, "Power converters, control, and energy management for distributed generation," *IEEE Trans. Ind. Electron.*, vol. 62, no. 7, pp. 4466–4470, July 2015.

[42] Y. Shan, J. Hu, Z. Li, and J. M. Guerrero, "A model predictive control for renewable energy based AC microgrids without any PID regulators," *IEEE Trans. Power Electron.*, pp. 1–1, 2018.

[43] C. c. Lin, L. s. Yang, and G. W. Wu, "Study of a non-isolated bidirectional DC-DC converter," *IET Power Electron.*, vol. 6, no. 1, pp. 30–37, Jan 2013.

[44] F. Wang, Z. Zhang, T. Ericsen, R. Raju, R. Burgos, and D. Boroyevich, "Advances in power conversion and drives for shipboard systems," *Proc. of the IEEE*, vol. 103, no. 12, pp. 2285–2311, Dec 2015.

[45] A. Ajami, H. Ardi, and A. Farakhor, "A novel high step-up DC/DC converter based on integrating coupled inductor and switched-capacitor techniques for renewable energy applications," *IEEE Trans. on Power Electron.*, vol. 30, no. 8, pp. 4255–4263, Aug 2015.

[46] S. Du, B. Wu, K. Tian, D. Xu, and N. R. Zargari, "A novel medium-voltage modular multilevel DC-DC converter," *IEEE Trans. on Ind. Electron.*, vol. 63, no. 12, pp. 7939–7949, Dec 2016.

[47] Y. Du, X. Zhou, S. Bai, S. Lukic, and A. Huang, "Review of non-isolated bi-directional DC-DC converters for plug-in hybrid electric vehicle charge

station application at municipal parking decks," in *2010 Twenty-Fifth Annual IEEE Applied Power Electronics Conference and Exposition (APEC)*, 2010, pp. 1145–1151.

[48] Y. Du, S. Lukic, B. Jacobson, and A. Huang, "Review of high power isolated bi-directional DC-DC converters for PHEV/EV DC charging infrastructure," in *2011 IEEE Energy Conversion Congress and Exposition*, 2011, pp. 553–560.

[49] J. M. Guerrero, P. C. Loh, T. Lee, and M. Chandorkar, "Advanced control architectures for intelligent microgrids—part II: power quality, energy storage, and CC/DC microgrids," *IEEE Transactions on Industrial Electronics*, vol. 60, no. 4, pp. 1263–1270, 2013.

[50] M. Forouzesh, Y. P. Siwakoti, S. A. Gorji, F. Blaabjerg, and B. Lehman, "Step-up DC–DC converters: a comprehensive review of voltage-boosting techniques, topologies, and applications," *IEEE Trans. on Power Electron.*, vol. 32, no. 12, pp. 9143–9178, Dec 2017.

[51] X. She, A. Q. Huang, and R. Burgos, "Review of solid-state transformer technologies and their application in power distribution systems," *IEEE J. of Emerging and Select. Topics in Power Electron.*, vol. 1, no. 3, pp. 186–198, Sept 2013.

[52] M. Das and V. Agarwal, "Design and analysis of a high-efficiency DC–DC converter with soft switching capability for renewable energy applications requiring high voltage gain," *IEEE Trans. on Ind. Electron.*, vol. 63, no. 5, pp. 2936–2944, May 2016.

[53] S. Kouro, J. I. Leon, D. Vinnikov, and L. G. Franquelo, "Grid-connected photovoltaic systems: an overview of recent research and emerging PV converter technology," *IEEE Ind. Electron. Maga.*, vol. 9, no. 1, pp. 47–61, March 2015.

[54] D. Han, J. Noppakunkajorn, and B. Sarlioglu, "Comprehensive efficiency, weight, and volume comparison of SiC- and Si-based bidirectional DC–DC converters for hybrid electric vehicles," *IEEE Trans. on Veh. Technol.*, vol. 63, no. 7, pp. 3001–3010, Sept 2014.

[55] A. Marzoughi, A. Romero, R. Burgos, and D. Boroyevich, "Comparing the state-of-the-art SiC MOSFETs: test results reveal characteristics of four major manufacturers? 900-v and 1.2-kv SiC devices," *IEEE Power Electron. Mag.*, vol. 4, no. 2, pp. 36–45, June 2017.

[56] A. Anthon, Z. Zhang, M. A. E. Andersen, D. G. Holmes, B. McGrath, and C. A. Teixeira, "The benefits of SiC MOSFETs in a T-Type inverter for grid-tie applications," *IEEE Trans. on Power Electron.*, vol. 32, no. 4, pp. 2808–2821, April 2017.

[57] D. Han, J. Noppakunkajorn, and B. Sarlioglu, "Comprehensive efficiency, weight, and volume comparison of SiC- and Si-based bidirectional DC–DC converters for hybrid electric vehicles," *IEEE Trans. on Veh. Technology*, vol. 63, no. 7, pp. 3001–3010, Sept 2014.

[58] S. S. Alharbi, S. S. Alharbi, A. M. S. Al-bayati, and M. Matin, "A highly efficient non-isolated DC-DC buck-boost converter with a cascode GaN-FET and SiC-Schottky diode," in *2017 IEEE Conf. on Technol. for Sustainability (SusTech)*, Nov 2017, pp. 1–6.

[59] H. A. Mantooth, K. Peng, E. Santi, and J. L. Hudgins, "Modeling of wide bandgap power semiconductor devices–part I," *IEEE Trans. on Electron Devices*, vol. 62, no. 2, pp. 423–433, Feb 2015.

[60] J. C. Balda and A. Mantooth, "Power-semiconductor devices and components for new power converter developments: a key enabler for ultrahigh efficiency power electronics," *IEEE Power Electron. Magazine*, vol. 3, no. 2, pp. 53–56, June 2016.

[61] T. P. Chow, I. Omura, M. Higashiwaki, H. Kawarada, and V. Pala, "smart power devices and ICs using GaAs and wide and extreme bandgap semiconductors," *IEEE Trans. Electron Devices*, vol. 64, no. 3, pp. 856–873, March 2017.

[62] K. Shenai, "Future prospects of widebandgap (WBG) semiconductor power switching devices," *IEEE Trans. on Electron Devices*, vol. 62, no. 2, pp. 248–257, Feb 2015.

[63] S. S. Alharbi, S. S. Alharbi, and M. Matin, "An improved interleaved DC-DC SEPIC converter based on SiC-Cascode power devices for renewable energy applications," in *2018 IEEE International Conference on Electro/Information Technology (EIT)*, 2018, pp. 0487–0492.

[64] T. P. Chow, "Wide bandgap semiconductor power devices for energy efficient systems," in *2015 IEEE 3rd Workshop on Wide Bandgap Power Devices and Applications (WiPDA)*, Nov 2015, pp. 402–405.

[65] N. Kaminski, "State of the art and the future of wide band-gap devices," in *2009 13th European Conference on Power Electronics and Applications*, Sep. 2009, pp. 1–9.

[66] K. Shenai and A. Chattopadhyay, "Optimization of high-voltage wide bandgap semiconductor power diodes," *IEEE Trans. on Electron Devices*, vol. 62, no. 2, pp. 359–365, Feb 2015.

[67] J. Jordán, V. Esteve, E. Sanchis-Kilders, E. J. Dede, E. Maset, J. B. Ejea, and A. Ferreres, "A comparative performance study of a 1200 V Si and SiC MOSFET intrinsic diode on an induction heating inverter," *IEEE Trans. on Power Electron.*, vol. 29, no. 5, pp. 2550–2562, May 2014.

[68] Q. Yan, X. Yuan, Y. Geng, A. Charalambous, and X. Wu, "Performance evaluation of split output converters with SiC MOSFETs and SiC schottky diodes," *IEEE Trans. on Power Electron.*, vol. 32, no. 1, pp. 406–422, Jan 2017.

[69] A. Trentin, L. Empringham, L. de Lillo, P. Zanchetta, P. Wheeler, and J. Clare, "Experimental efficiency comparison between a direct matrix converter and an indirect matrix converter using both Si IGBTs and SiC mosfets," *IEEE Transactions on Industry Applications*, vol. 52, no. 5, pp. 4135–4145, 2016.

[70] G. R. C. Mouli, J. H. Schijffelen, P. Bauer, and M. Zeman, "Design and comparison of a 10-kW interleaved boost converter for PV application using Si and SiC devices," *IEEE Journal of Emerging and Selected Topics in Power Electron.*, vol. 5, no. 2, pp. 610–623, June 2017.

[71] J. He, T. Zhao, X. Jing, and N. A. O. Demerdash, "Application of wide bandgap devices in renewable energy systems- benefits and challenges," in *2014 Int. Conf. on Renewable Energy Research and Applicat. (ICRERA)*, Oct 2014, pp. 749–754.

[72] S. S. Alharbi, S. S. Alharbi, A. M. S. Al-bayati, and M. Matin, "Design and performance evaluation of a DC-DC buck-boost converter with cascode GaN FET, SiC JFET, and Si IGBT power devices," in *2017 North Amer. Power Symp. (NAPS)*, Sept 2017, pp. 1–6.

[73] K. Shenai, "Wide bandgap (WBG) semiconductor power converters for DC microgrid applications," in *2015 IEEE First International Conference on DC Microgrids (ICDCM)*, June 2015, pp. 263–268.

[74] Y. Wang, B. Chen, Y. Hou, Z. Meng, and Y. Yang, "Analysis and design of a 1-MHz bidirectional multi-CLLC resonant DC-DC converter with GaN devices," *IEEE Transactions on Industrial Electronics*, vol. 67, no. 2, pp. 1425–1434, Feb 2020.

[75] F. Xue, R. Yu, and A. Q. Huang, "A 98.3% efficient GaN isolated bidirectional DC–DC converter for DC microgrid energy storage system applications," *IEEE Transactions on Industrial Electronics*, vol. 64, no. 11, pp. 9094–9103, Nov 2017.

[76] F. C. Lee and Q. Li, "High-frequency integrated point-of-load converters: overview," *IEEE Transactions on Power Electronics*, vol. 28, no. 9, pp. 4127–4136, Sep. 2013.

[77] Y. Guan, Y. Wang, D. Xu, and W. Wang, "A 1 MHz half-bridge resonant DC/DC converter based on GaN FETs and planar magnetics," *IEEE Trans. on Power Electron.*, vol. 32, no. 4, pp. 2876–2891, April 2017.

[78] P. M. Roschatt, S. Pickering, and R. A. McMahon, "Bootstrap voltage and dead time behavior in GaN DC–DC buck converter with a negative gate voltage," *IEEE Trans. on Power Electron.*, vol. 31, no. 10, pp. 7161–7170, Oct 2016.

[79] K. Shah and K. Shenai, "Simple and accurate circuit simulation model for gallium nitride power transistors," *IEEE Trans. on Electron Devices*, vol. 59, no. 10, pp. 2735–2741, Oct 2012.

[80] X. Ding, Y. Zhou, and J. Cheng, "A review of gallium nitride power device and its applications in motor drive," *CES Transactions on Electrical Machines and Systems*, vol. 3, no. 1, pp. 54–64, 2019.

[81] A. Marzoughi, R. Burgos, and D. Boroyevich, "Characterization and performance evaluation of the state-of-the-art 3.3 kV 30 a full-SiC MOSFETs," *IEEE Transactions on Industry Applications*, vol. 55, no. 1, pp. 575–583, Jan 2019.

[82] J. Millán, P. Godignon, X. Perpiñà, A. Pérez-Tomás, and J. Rebollo, "A survey of wide bandgap power semiconductor devices," *IEEE Transactions on Power Electronics*, vol. 29, no. 5, pp. 2155–2163, May 2014.

[83] C. M. DiMarino, R. Burgos, and B. Dushan, "High-temperature silicon carbide: characterization of state-of-the-art silicon carbide power transistors," *IEEE Industrial Electronics Magazine*, vol. 9, no. 3, pp. 19–30, 2015.

[84] E. A. Jones, F. F. Wang, and D. Costinett, "Review of commercial GaN power devices and GaN-based converter design challenges," *IEEE Journal of Emerging and Selected Topics in Power Electronics*, vol. 4, no. 3, pp. 707–719, Sep. 2016.

[85] S. Sandler, "Faster-switching GaN : presenting a number of interesting measurement challenges," *IEEE Power Electronics Magazine*, vol. 2, no. 2, pp. 24–31, June 2015.

[86] C. Mueth and R. K. Lal, "Utilizing modern design methodologies for wide-bandgap power electronics: predictive simulation techniques to save time and money," *IEEE Power Electronics Magazine*, vol. 4, no. 2, pp. 46–55, June 2017.

[87] A. Bindra, "Wide-bandgap-based power devices: reshaping the power electronics landscape," *IEEE Power Electronics Magazine*, vol. 2, no. 1, pp. 42–47, March 2015.

[88] A. Q. Huang, "Power semiconductor devices for smart grid and renewable energy systems," *Proceedings of the IEEE*, vol. 105, no. 11, pp. 2019–2047, Nov 2017.

[89] J. Glaser, "How GaN power transistors drive high-performance lidar: generating ultrafast pulsed power with GaN FETs," *IEEE Power Electronics Magazine*, vol. 4, no. 1, pp. 25–35, March 2017.

[90] R. J. Kaplar, J. C. Neely, D. L. Huber, and L. J. Rashkin, "Generation-after-next power electronics: ultrawide-bandgap devices, high-temperature packaging, and magnetic nanocomposite materials," *IEEE Power Electronics Magazine*, vol. 4, no. 1, pp. 36–42, March 2017.

[91] A. Bindra, "APEC guides engineers to latest advances in power devices, components, and packaging: high-voltage gallium nitride transistors and the new generation of digital controllers," *IEEE Power Electronics Magazine*, vol. 2, no. 2, pp. 48–53, June 2015.

[92] C. Liu, A. Salih, B. Padmanabhan, W. Jeon, P. Moens, M. Tack, and E. De Backer, "Breakthroughs for 650-V GaN power devices: stable high-temperature operations and avalanche capability," *IEEE Power Electronics Magazine*, vol. 2, no. 3, pp. 44–50, Sep. 2015.

[93] W. Zhang, X. Huang, Z. Liu, F. C. Lee, S. She, W. Du, and Q. Li, "A new package of high-voltage cascode gallium nitride device for megahertz operation," *IEEE Transactions on Power Electronics*, vol. 31, no. 2, pp. 1344–1353, Feb 2016.

[94] E. Gurpinar, Y. Yang, F. Iannuzzo, A. Castellazzi, and F. Blaabjerg, "Reliability-driven assessment of GaN HEMTs and Si IGBTs in 3L-ANPC PV inverters," *IEEE Journal of Emerging and Selected Topics in Power Electronics*, vol. 4, no. 3, pp. 956–969, Sep. 2016.

[95] A. S. Abdelrahman, Z. Erdem, Y. Attia, and M. Z. Youssef, "Wide bandgap devices in electric vehicle converters: A performance survey," *Canadian Journal of Electrical and Computer Engineering*, vol. 41, no. 1, pp. 45–54, winter 2018.

[96] E. Gurpinar and A. Castellazzi, "Single-phase T-type inverter performance benchmark using Si IGBTs, SiC MOSFETs, and GaN HEMTs," *IEEE Transactions on Power Electronics*, vol. 31, no. 10, pp. 7148–7160, Oct 2016.

[97] G. Zulauf, S. Park, W. Liang, K. N. Surakitbovorn, and J. Rivas-Davila, "COSS losses in 600 V GaN power semiconductors in soft-switched, high- and very-high-frequency power converters," *IEEE Transactions on Power Electronics*, vol. 33, no. 12, pp. 10 748–10 763, Dec 2018.

[98] R. Yan, J. Xi, and L. He, "A 2–10 MHz GaN HEMTs half-bridge driver with bandgap reference comparator clamping and dual level shifters for automotive applications," *IEEE Transactions on Industrial Electronics*, vol. 67, no. 2, pp. 1446–1454, Feb 2020.

[99] D. M. Rhodes, S. D. Chowdhury, S. Yea, J. Guerrero, and N. Bushnell, "Characterization of electroless nickel plated materials during high temperature solder processing," *IEEE Transactions on Semiconductor Manufacturing*, vol. 32, no. 4, pp. 381–386, Nov 2019.

[100] J. Ren, C. W. Tang, H. Feng, H. Jiang, W. Yang, X. Zhou, K. M. Lau, and J. K. O. Sin, "A novel 700 V monolithically integrated Si-GaN cascoded field effect transistor," *IEEE Electron Device Letters*, vol. 39, no. 3, pp. 394–396, March 2018.

[101] W. Qian, X. Zhang, Y. Fu, J. Lu, and H. Bai, "Applying normally-off GaN HEMTs for coreless high-frequency wireless chargers," *CES Transactions on Electrical Machines and Systems*, vol. 1, no. 4, pp. 418–427, December 2017.

[102] K. J. Chen, O. Häberlen, A. Lidow, C. l. Tsai, T. Ueda, Y. Uemoto, and Y. Wu, "GaN-on-Si power technology: devices and applications," *IEEE Transactions on Electron Devices*, vol. 64, no. 3, pp. 779–795, March 2017.

[103] Z. Wang, F. Qi, and Y. Wu, "High efficient single-phase transformerless PV inverter using GaN HEMTs and Si MOSFETs," in *2019 IEEE Applied Power Electronics Conference and Exposition (APEC)*, March 2019, pp. 3189–3194.

[104] Y. . Wu, J. Gritters, L. Shen, R. P. Smith, J. McKay, R. Barr, and R. Birkhahn, "Performance and robustness of first generation 600-V GaN-on-Si power transistors," in *The 1st IEEE Workshop on Wide Bandgap Power Devices and Applications*, Oct 2013, pp. 6–10.

[105] W. Zhang, F. Wang, D. J. Costinett, L. M. Tolbert, and B. J. Blalock, "Investigation of gallium nitride devices in high-frequency LLC resonant converters," *IEEE Transactions on Power Electronics*, vol. 32, no. 1, pp. 571–583, Jan 2017.

[106] W. Zhang, Z. Xu, Z. Zhang, F. Wang, L. M. Tolbert, and B. J. Blalock, "Evaluation of 600 V cascode GaN HEMT in device characterization and all-GaN-based LLC resonant converter," in *2013 IEEE Energy Conversion Congress and Exposition*, Sep. 2013, pp. 3571–3578.

[107] X. Huang, Z. Liu, Q. Li, and F. C. Lee, "Evaluation and application of 600 V GaN HEMT in cascode structure," *IEEE Transactions on Power Electronics*, vol. 29, no. 5, pp. 2453–2461, May 2014.

[108] C. Li, D. Jiao, M. J. Scott, C. Yao, L. Fu, X. Lu, T. Chen, J. Li, and J. Wang, "A 2 KW gallium nitride based switched capacitor three-port inverter," in *The 1st IEEE Workshop on Wide Bandgap Power Devices and Applications*, Oct 2013, pp. 119–124.

[109] X. Huang, F. C. Lee, Q. Li, and W. Du, "High-frequency high-efficiency GaN-based interleaved CRM bidirectional buck/boost converter with inverse coupled inductor," *IEEE Transactions on Power Electronics*, vol. 31, no. 6, pp. 4343–4352, June 2016.

[110] X. Huang, W. Du, F. C. Lee, Q. Li, and Z. Liu, "Avoiding Si MOSFET avalanche and achieving zero-voltage switching for cascode GaN devices," *IEEE Transactions on Power Electronics*, vol. 31, no. 1, pp. 593–600, Jan 2016.

[111] W. Qian, J. Lu, H. Bai, and S. Averitt, "Hard-switching 650-V GaN HEMTs in an 800-V DC-grid system with no-diode-clamping active-balancing three-level topology," *IEEE Journal of Emerging and Selected Topics in Power Electronics*, vol. 7, no. 2, pp. 1060–1070, 2019.

[112] E. Gurpinar and A. Castellazzi, "Tradeoff study of heat sink and output filter volume in a GaN HEMT based single-phase inverter," *IEEE Transactions on Power Electronics*, vol. 33, no. 6, pp. 5226–5239, 2018.

[113] D. Ji, W. Li, and S. Chowdhury, "A study on the impact of channel mobility on switching performance of vertical GaN MSFETs," *IEEE Transactions on Electron Devices*, vol. 65, no. 10, pp. 4271–4275, 2018.

[114] X. Huang, W. Du, F. C. Lee, Q. Li, and W. Zhang, "Avoiding divergent oscillation of a cascode GaN device under high-current turn-off condition," *IEEE Transactions on Power Electronics*, vol. 32, no. 1, pp. 593–601, 2017.

[115] S. Perkins, A. Arvanitopoulos, K. N. Gyftakis, and N. Lophitis, "A comprehensive comparison of the static performance of commercial GaN-on-Si devices," in *2017 IEEE 5th Workshop on Wide Bandgap Power Devices and Applications (WiPDA)*, 2017, pp. 177–184.

[116] D. Kinzer and S. Oliver, "Monolithic HV GaN power ICs: performance and application," *IEEE Power Electron. Mag.*, vol. 3, no. 3, pp. 14–21, Sept 2016.

[117] C. D. Santi, M. Meneghini, G. Meneghesso, and E. Zanoni, "Review of dynamic effects and reliability of depletion and enhancement GaN HEMTs for power switching applications," *IET Power Electron.*, vol. 11, no. 4, pp. 668–674, (2018).

[118] Transphorm, "Cascode vs. e-mode," 2018. [Online]. Available: https://www.transphormusa.com/en/document/transphorm-vs-emode.shtml

[119] X. Wang, S. Huang, Y. Zheng, K. Wei, X. Chen, H. Zhang, and X. Liu, "Effect of GaN channel layer thickness on DC and RF performance of GaN HEMTs with composite AlGaN/GaN buffer," *IEEE Transactions on Electron Devices*, vol. 61, no. 5, pp. 1341–1346, May 2014.

[120] M. Vasić, D. Diaz, O. Garcia, P. Alou, J. A. Oliver, and J. A. Cobos, "Optimal design of envelope amplifier based on linear-assisted buck converter," in *2012 Twenty-Seventh Annual IEEE Applied Power Electronics Conference and Exposition (APEC)*, Feb 2012, pp. 836–843.

[121] K. Shenai, "Wide bandgap (WBG) semiconductor power converters for DC microgrid applications," in *2015 IEEE First International Conference on DC Microgrids (ICDCM)*, 2015, pp. 263–268.

[122] F. Roccaforte, G. Greco, P. Fiorenza, and F. Iucolano, "An overview of normally-off GaN-based high electron mobility transistors," *Energies*, no. 12, p. 1599, 2019,.

[123] A. A. Hussein, N. Kutkut, Z. J. Shen, and I. Batarseh, "Distributed battery micro-storage systems design and operation in a deregulated electricity market," *IEEE Trans. Sustain. Energy*, vol. 3, no. 3, pp. 545–556, July 2012.

[124] Y. Développement, "Power GaN 2017: Epitaxy, devices, applications, and technology trends 2017," 2017. [Online]. Available: https://www.systemplus.fr/wp-content/uploads/2018/04/Yole_YDPE17044_Power-GaN2017_Flyer-1.pdf

[125] C. N. M. Ho, H. Breuninger, S. Pettersson, G. Escobar, and F. Canales, "A comparative performance study of an interleaved boost converter using commercial Si and SiC diodes for PV applications," *IEEE Trans.on Power Electron.*, vol. 28, no. 1, pp. 289–299, Jan 2013.

[126] A. León-Masich, H. Valderrama-Blavi, J. M. Bosque-Moncusí, and L. Martínez-Salamero, "Efficiency comparison between Si and SiC-based implementations in a high gain DC-DC boost converter," *IET Power Electron.*, vol. 8, no. 6, pp. 869–878, 2015.

[127] L. Wu and M. Saeedifard, "A simple behavioral electro-thermal model of GaN FETs for SPICE circuit simulation," *IEEE Journal of Emerging and Selected Topics in Power Electron.*, vol. 4, no. 3, pp. 730–737, Sept 2016.

[128] H. Mirzaee, A. De, A. Tripathi, and S. Bhattacharya, "Design comparison of high-power medium-voltage converters based on a 6.5-kv Si-IGBT/Si-PiN diode, a 6.5-kv Si-IGBT/SiC-JBS diode, and a 10-kv SiC MOSFET/SiC-JBS diode," *IEEE Trans. on Ind. Applicat.*, vol. 50, no. 4, pp. 2728–2740, July 2014.

[129] S. Jahdi, O. Alatise, J. A. O. Gonzalez, R. Bonyadi, L. Ran, and P. Mawby, "Temperature and switching rate dependence of crosstalk in Si-IGBT and SiC power modules," *IEEE Trans. on Ind. Electron.*, vol. 63, no. 2, pp. 849–863, Feb 2016.

[130] X. Song, A. Q. Huang, S. Sen, L. Zhang, P. Liu, and X. Ni, "15-kV/40-A FREEDM supercascode: a cost-effective SiC high-voltage and high-frequency power switch," *IEEE Trans. on Ind. Applicat.*, vol. 53, no. 6, pp. 5715–5727, Nov 2017.

[131] Z. Wang, X. Shi, Y. Xue, L. M. Tolbert, F. Wang, and B. J. Blalock, "Design and performance evaluation of overcurrent protection schemes for silicon carbide (SiC) power MOSFETs," *IEEE Trans. on Ind. Electron.*, vol. 61, no. 10, pp. 5570–5581, Oct 2014.

[132] B. K. Bose, "Power electronics, smart grid, and renewable energy systems," *Proc. of the IEEE*, vol. 105, no. 11, pp. 2011–2018, Nov 2017.

[133] Q. Xu, N. Vafamand, L. Chen, T. Dragičević, L. Xie, and F. Blaabjerg, "Review on advanced control technologies for bidirectional DC/DC converters in DC microgrids," *IEEE Journal of Emerging and Selected Topics in Power Electronics*, pp. 1–1, 2020.

[134] J. M. Guerrero, P. C. Loh, T. Lee, and M. Chandorkar, "Advanced control architectures for intelligent microgrids–part II: Power quality, energy storage, and AC/DC microgrids," *IEEE Transactions on Industrial Electronics*, vol. 60, no. 4, pp. 1263–1270, 2013.

[135] M. O. Badawy, M. N. Arafat, A. Ahmed, S. Anwar, Y. Sozer, P. Yi, and J. A. De Abreu-Garcia, "Design and implementation of a 75-kW mobile charging system for electric vehicles," *IEEE Transactions on Industry Applications*, vol. 52, no. 1, pp. 369–377, 2016.

[136] A. A. Khan, Honnyong Cha, and H. F. Ahmed, "A family of high efficiency bidirectional DC-DC converters using switching cell structure," in *2016 IEEE 8th International Power Electronics and Motion Control Conference (IPEMC-ECCE Asia)*, 2016, pp. 1177–1183.

[137] S. Dusmez, A. Hasanzadeh, and A. Khaligh, "Comparative analysis of bidirectional three-level DC-DC converter for automotive applications," *IEEE Transactions on Industrial Electronics*, vol. 62, no. 5, pp. 3305–3315, 2015.

[138] Y. P. Siwakoti, F. Z. Peng, F. Blaabjerg, P. C. Loh, and G. E. Town, "Impedance-source networks for electric power conversion part I: A topological review," *IEEE Transactions on Power Electronics*, vol. 30, no. 2, pp. 699–716, 2015.

[139] A. M. S. A.-b. Y. A. T. S. S. Alharbi, S. S. Alharbi and M. Matin, "Impact of cascode gan power devices on a bidirectional DC-DC buck/boost converter in DC microgrids," in *Proceedings of the SPIE*, vol. 10754, 2018.

[140] A. Agarwal, K. Deekshitha, S. Singh, and D. Fulwani, "Sliding mode control of a bidirectional DC/DC converter with constant power load," in *2015 IEEE First International Conference on DC Microgrids (ICDCM)*, 2015, pp. 287–292.

[141] K. Kruse, M. Elbo, and Z. Zhang, "GaN-based high efficiency bidirectional DC-DC converter with 10 MHz switching frequency," in *2017 IEEE Applied Power Electronics Conference and Exposition (APEC)*, 2017, pp. 273–278.

[142] M. A. Khan, A. Ahmed, I. Husain, Y. Sozer, and M. Badawy, "Performance analysis of bidirectional DC-DC converters for electric vehicles,"

IEEE Transactions on Industry Applications, vol. 51, no. 4, pp. 3442–3452, 2015.

[143] C. Young, Y. Cheng, B. Peng, S. Chi, and Z. Yang, "Design and implementation of a high-efficiency bidirectional DC-DC converter," in *2015 IEEE 2nd International Future Energy Electronics Conference (IFEEC)*, 2015, pp. 1–5.

[144] M. Forouzesh, Y. P. Siwakoti, S. A. Gorji, F. Blaabjerg, and B. Lehman, "A survey on voltage boosting techniques for step-up DC-DC converters," in *2016 IEEE Energy Conversion Congress and Exposition (ECCE)*, 2016, pp. 1–8.

[145] S. A. Gorji, H. G. Sahebi, M. Ektesabi, and A. B. Rad, "Topologies and control schemes of bidirectional DC-DC power converters: An overview," *IEEE Access*, vol. 7, pp. 117 997–118 019, 2019.